Membrane fusion of vesicles of oligomerisable lipids

Ravoo, Bart Jan

Membrane Fusion of Vesicles of Oligomerisable Lipids

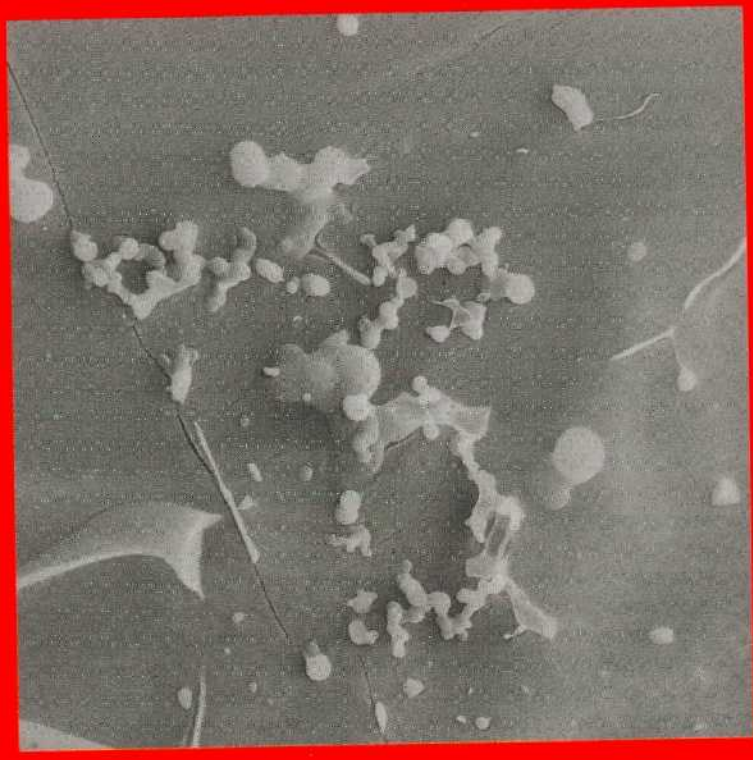

Bart Jan Ravoo

Membrane Fusion of Vesicles of Oligomerisable Lipids

The front cover shows vesicles of DDPBNS that aggregate and fuse in the presence of calcium chloride. Magnification ca. 10000 x. Cryo-scanning electron microscopy by Mr. I. Stokroos.

RIJKSUNIVERSITEIT GRONINGEN

Membrane Fusion of Vesicles of Oligomerisable Lipids

Proefschrift

ter verkrijging van het doctoraat in de
Wiskunde en Natuurwetenschappen
aan de Rijksuniversiteit Groningen
op gezag van de
Rector Magnificus, dr. D.F.J. Bosscher,
in het openbaar te verdedigen op
vrijdag 6 november 1998
om 16.15 uur

door

Bart Jan Ravoo

geboren op 31 augustus 1970
te Enschede

Promotor: Prof. dr. J.B.F.N. Engberts

Referent: Dr. W.D. Weringa

ISBN 90-367-0992-x

Dankwoord

Dit proefschrift vormt de afsluiting van een periode van zeven jaar waarin ik in de groep van Jan Engberts gewerkt heb. En steeds met veel plezier. Ik ben Jan Engberts veel dank verschuldigd voor het enthousiasme, de openheid, de professionaliteit en de humor waarmee hij het onderzoek begeleid heeft. Terugkijkend denk ik dat we met een gevaarlijke dosis vooringenomenheid aan dit onderzoek zijn begonnen, maar dat we die gaandeweg achter ons hebben gelaten. Ik heb daar ontzettend veel van geleerd. Ik dank ook Wilke Weringa, die met Groningse nuchterheid de puntjes op de i zette.
Een constante steun was de grote collegialiteit in de werkgroep. Ik dank met name mijn (ex-) zaalgenoten Anno Wagenaar, Lisette Streefland, Rixt Buwalda en Irene van der Woude, maar zeker ook de heren Otto en Kevelam op het waterlab, en Arthur Meekel. Ik kijk met heel veel voldoening terug op de samenwerking met Jan Kevelam: verbazingwekkend was het hoe een 'Friday afternoon experiment' volledig uit de hand liep, en uiteindelijk, doch niet zonder het vergieten van veel bloed, zweet en tranen, tot een fraaie publicatie leidde.
Hulde ook aan de elektronenmicroscopisten Jan van Breemen en Marc Stuart voor hun deskundigheid en creativiteit, die zij geduldig ter beschikking stelden van mijn onwillige vesicles. Vele illusies armer, maar wel een stuk wijzer verliet ik keer op keer hun fraaie lab, mijn Waterloo. Je remercie également Alain Brisson pour l'hospitalité dans son laboratoire et les discussions de mon travail.
I am indebted to Mike Blandamer and Barbara Briggs at Leicester University for their help in the DSC analyses described in this thesis. Part of the work was carried out during a visit to Leicester. The discussions we had in Groningen, in Leicester and in cyber space have found their place throughout the thesis. Finally, Mike Blandamer is acknowledged for his swift correction of the manuscript as a member of the reading committee.
Ik bedank Dick Hoekstra voor zijn kritische blik op alles wat uit een organisch lab komt, de gastvrijheid in zijn lab, de stimulerende congresbezoeken in Noordwijkerhout en Salamanca (die onder zijn beschermheerschap stonden), en zijn commentaar als lid van de leescommissie.
Bij deze een late pluim voor mijn 'voorgangers' Leo Rupert en Tino Fonteijn, wier werk mij zeer heeft geinspireerd. Nog vele anderen hebben bijgedragen aan het tot stand komen van dit proefschrift. Ik heb ze allemaal met naam en toenaam vermeld in de dankwoorden aan het einde van ieder hoofdstuk. Tevens een woord van dank aan het GBB, dat middels financiële ondersteuning een aantal buitenlandse excursies mogelijk maakte.
Tenslotte zitten er in dit proefschrift ook vele kilometers, die niet volledig tot hun recht zijn gekomen. I spent an unforgettable spring at the Technion in Haifa, Israel, preparing cryo-EM samples of fusing vesicles. Despite the expert help of Dganit Danino and Ishi Talmon, and despite the heart warming care of many others at the Technion as well as the Weizmann Institute, all we observed in the microscope were mysterious flat objects. It is obvious from Chapter 5 that we know a lot more now. Het cowboys-en-indianen-spel aan de Universiteit van Amsterdam, waarbij ik met Jos Grimbergen en Gerrit Brakenhoff met een laser op reuzenvesicles jaagde, is helaas niet in dit proefschrift terechtgekomen. Ietse Stokroos (van het Laboratorium voor Celbiologie en Medische Elektronenmicroscopie) haalde met zijn fraaie cryo-SEM plaatjes wel de voorkant van dit proefschrift, maar ook deze spectaculaire techniek heeft aan de essentie van dit werk niet bij kunnen dragen, en is daarom verder niet beschreven.

Verscholen achter dit geanimeerde promotie-onderzoek ligt een uiterst turbulente periode in het leven van de promovendus. Ik ben trots op de steun van mijn familie, van mijn vrienden, en van mijn lief. Ik draag dit boek op aan mijn ouders, als bescheiden blijk van erkenning voor al het goede dat jullie mij meegegeven hebben.

Table of contents

Chapter 1

Membrane fusion: an introduction

Fusion of lipid bilayer membranes is a ubiquitous event in all eukaryotic cells. In vivo membrane fusion is controled by an intricate protein machinery. The complexities of biological membrane fusion have been successfully mimicked in model membrane systems of increasing sophistication, and the techniques to investigate membrane fusion have advanced along. Although biological membrane fusion is a protein-mediated process, the molecular mechanism of membrane fusion appears to be a delicate lipid rearrangement, best described by the 'stalk-pore' model. This thesis aims to further support the current model of membrane fusion by providing an avenue towards ultrastructural characterisation of membrane fusion intermediates, by extending the model to calcium-induced membrane fusion and by analysing the thermodynamics of membrane fusion.

1.1 Biological membrane fusion events

The formation of phospholipid bilayer membranes which seclude and compartmentalise all eukaryotic cells has often been referred to as a prerequisite for the evolution of cell life.[1, 2] In analogy, transport over the membrane is an equally essential mode of communication between the various compartments in the cell, as well as with the extracellular world. Along with protein-mediated translocation, membrane fusion provides the main gateway across the bilayer membrane for a myriad of compounds. Whereas the channels formed by proteins generally provide exclusive entry or exit pathways for one type of small solutes such as an ion or a molecule, membrane fusion provides a fast means of shuttling over large numbers of molecules at once, their size and number being limited only by the size of the enclosing bilayer compartment.

Membrane fusion can be defined as the process in which two lipid bilayer membranes come together, join at a molecular level, and merge. In many fusion events two fusing membrane enclosed compartments coalesce, leading to mixing of the lipids in the membrane via lateral diffusion (Figure 1.1). The fusing compartments can either be separate or one compartment can be contained in the other. Alternatively, fusion occurs between two domains of a single membrane and leads to formation of two membrane enclosed compartments (Figure 1.1). The two membrane compartments formed during fusion can be either separate or one membrane compartment can be inside the other. 'Symmetric' or 'homotypic' fusion refers to fusion between membranes of identical composition. 'Asymmetric' or 'heterotypic' fusion is fusion between membranes having different composition. Membrane fusion is a ubiquitous event in all eukaryotic cells, and several membrane fusion events that occur *in vivo* are briefly introduced in this section. The section is intended to illustrate the importance of membrane fusion in cells, but it is by no means a comprehensive survey of cell biological phenomena mediated by fusion.

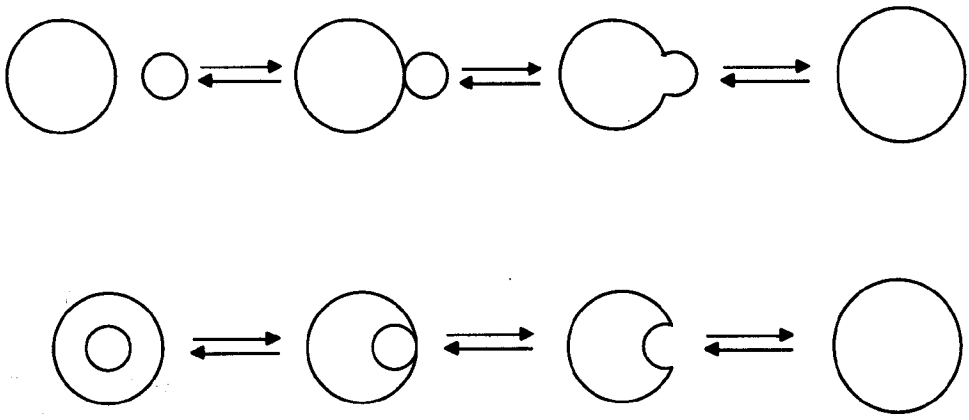

Figure 1.1 Classification of all possible membrane fusion events. Membrane fusion can occur between two membrane enclosed compartments which form one continuous membrane (left to right). Alternatively, one membrane can fuse with itself and forms two separate membrane enclosed compartments (right to left). (Adapted from ref. 28).

Endocytosis Endocytosis provides the major route of uptake of extracellular material by most cells.[3,4,5] This fusion event involves a local invagination of the cellular membrane, which consequently fuses with itself and thus encapsulates some extracellular material in an inside-out bilayer, called an endosome. Endosomes are usually not larger than 200 nm and this poses a limit to the size of material that can be taken up through endocytosis. Endosomes can fuse with various intracellular vesicles and thus build up lysosomes, which process the material that was delivered by the endosome via various biochemical pathways. It is believed that phospholipids that constitute the endosomal membranes are recycled by a budding process (*vide infra*), in which small vesicles are formed that fuse with the cell membrane. Endocytotic uptake is sometimes designated as phagocytosis (eating, for large solutes; *e.g.* liver cells can 'eat' entire microorganisms) or pinocytosis (drinking, for small solutes).

Exocytosis Exocytosis is an important route for secretion of material from cells.[6] Small vesicles that are formed in various organelles fuse with the cell membrane and release their contents into the extracellular medium. Exocytosis is the cornerstone of synaptic *neurotransmission*,[7] the most important signal transmitting system in many organisms. Calcium-triggered fusion of synaptic vesicles filled with neurotransmitters with the presynaptic membrane leads to a quick release of neurotransmitters, which bind to receptor proteins in the postsynaptic membrane. In this way, messages are transmitted through the nervous system of many organisms.

Intracellular fusion Many intracellular transport processes involve membrane fusion.[8] Transport vesicles are formed by budding in many organelles. The organelle membrane locally buds outward, then fuses with itself and pinches off a small vesicle that encapsulates part of the contents of the parent-compartment. Vesicles formed by budding can release their contents via exocytosis. Alternatively, they may fuse with other organelle membranes, thus providing a means of intracellular transport. Extensive budding and fusion occurs between stacks of the Golgi apparatus.

Cell fusion The most compelling example of cell-cell fusion is fertilisation, *i.e.* fusion of an egg and a sperm cell, which demands highly specific membrane fusion of egg and sperm cell membranes.[9,10] Each egg cell can only fuse once, with only one sperm cell. Fusion of cells and fusion of cell nuclei can occur in certain yeasts. Mating yeast cells fuse, and consequently their nuclei fuse. The cell nucleus is protected by the nuclear envelope, which comprises two bilayer membranes. In most eukaryotes, the nuclear envelope is disassembled during replication of genetic material. However, in some yeasts nuclear fusion is mediated by membrane fusion.[11] It is not known whether during nuclear fusion the double membrane fuses concertedly, or in a two-step process.

Cytokinesis Cytokinesis (cell division or fission)[12] is the final step in the life-cycle of a cell. If cells replicate, their membrane must ultimately split into two parts. In the course of cell division, the cell membrane is pinched onto itself by means of a complicated macromolecular machinery. Next, the membrane fuses with itself, and two new cells result. In a morphological sense, cell division can be viewed as a dramatic form of budding, but its biological mechanism is quite different.

Viral infection Viruses depend on cells for their replication. All enveloped viruses may be considered as potent fusing devices, streamlined in the course of evolution to introduce their genetic material into the cell via fusion with its membrane.[13,14] In many cases fusion occurs only after endocytosis of the entire virion (Figure 1.3). After delivery of the nucleocapsid (which contains the genetic material of the virus), the virus exploits the cell machinery of its host to reproduce itself. Finally, the virus leaves the cell via a budding process, in which the new nucleocapsid is coated with the host cell's membrane. The detrimental effects of viral infection are obvious and have been recognised since long. The remarkable fusion capacities of viruses can also be applied for the benefit of living organisms: virus-mediated fusion is currently considered a potential means of introduction of genetic material to cure genetic diseases or defects.[15]

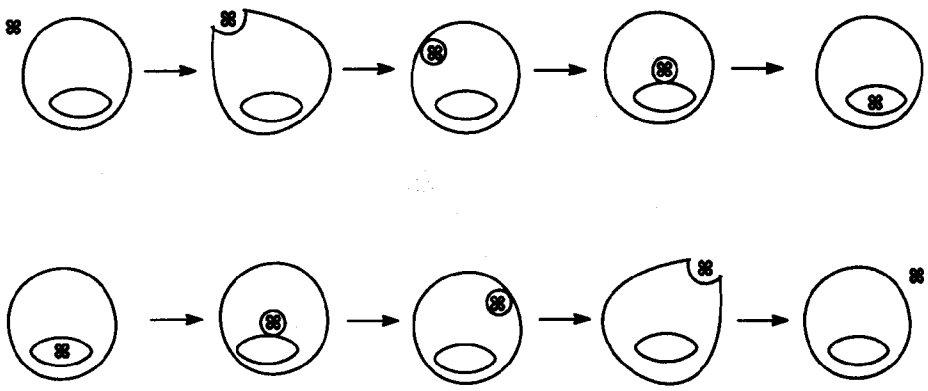

Figure 1.2 Cartoon of various cell biological processes mediated by membrane fusion. Top: extracellular material is taken up by endocytosis, and the endosome fuses with an intracellular vesicle. Bottom: a transport vesicle is formed by budding from an organelle, and releases its contents through exocytosis (alternatively, it may fuse intracellularly).

1.2 The protein machinery of *in vivo* membrane fusion

Biological membrane fusion can certainly not be viewed as a process that solely involves a rearrangement of phospholipid bilayers: in all fusion events, an intricate protein machinery is involved. This protein machinery targets and triggers membrane fusion. Regulated expression of key elements provides a subtle timing of fusion. Interestingly, many of the biological membrane fusion events described above are controlled by a similar set of proteins. Moreover, members of the protein machinery are intimately related and have been conserved in the course of evolution. Publications on this hot topic appear frequently in prominent journals such as *Nature, Science* and *Cell*, and the main findings are reviewed regularly.[16, 17, 18]

The first element in the protein machinery that was discovered is the N-ethylmaleimide Sensitive Fusion protein (NSF) that is involved in attachment and/or fusion of transport vesicles with the target membrane in the Golgi complex.[19, 20] N-ethylmaleimide treatment of this protein inhibits fusion of the transport vesicles with the Golgi membrane. NSF plays a central role in many other vesicular transport processes. NSF function is ATP-dependent. However, NSF cannot bind to membranes directly, and NSF binding is mediated by a set of Soluble NSF Attachment Proteins (SNAPs), which have been identified in many fusion events.[21] NSF and SNAPs do not interact in solution, unless a conformational change is induced in one of the SNAPs. SNAP receptors (SNAREs) on the membrane bind SNAPs[22] and force them into the appropriate conformation allowing for binding of NSF. SNAREs are complexes of membrane-inserted or membrane-bound proteins that can be either vesicle-associated (v-SNAREs) or target membrane-associated (t-SNAREs). Similar SNAREs have been identified in a variety of membrane fusion processes, including neurotransmission.[23] It has been suggested that SNAREs form functional oligomers of defined stoichiometry, and that this complex formation is regulated by another class of proteins, named Rab proteins.[24] Rab function is GTP dependent.[25]

The role of NSF, SNAPs, SNAREs and Rabs in controlling membrane fusion has been framed in the *SNARE hypothesis* proposed by Rothman and coworkers (Figure 1.4).[16] They assume that each cellular membrane carries SNAREs, which serve as address markers. Complex assembly of v-SNAREs at transport vesicles and t-SNAREs at target membranes is regulated by Rab proteins. The SNARE complex recruits SNAPs and NSF from the cytosol to execute fusion of the vesicular and the target membrane. Fusion is ATP dependent, and the fusion machinery is disassembled after completion of fusion.

However, it should be stressed that it is still unclear at a molecular level how these protein complexes mediate membrane fusion. Many proteins involved in the membrane fusion machinery remain unidentified, and their structure and interactions are unknown. Recently, an analogous but more complex version of the SNARE hypothesis has been put forward for nuclear envelope fusion (karyogamy) in yeast, which does not depend on NSF or SNAPs.[26] In addition, it has been shown that SNARE complexes *per se* are sufficient to induce membrane fusion, and that NSF and SNAPs may perhaps mediate complex disassembly and 'recycling' of the membrane fusion machinery, rather than fusion itself.[27] The most recent studies revert to the use of liposomes as model systems, indicating the complexity of *in vivo* fusion. According to an expert in the field, 'at this time it is important to rule nothing out, and to be circumspect when ruling anything in'.[18]

In the course of evolution, enveloped viruses have developed an entirely different protein machinery of membrane fusion. Enveloped viruses follow two different strategies in order to enter their host cell.[13, 14, 28] In the simplest case, a viral surface protein binds to a receptor site (often gangliosides) at the host cell membrane. Receptor binding activates eiher this protein, or a second protein with which it is tightly associated, for fusion. For instance, binding can induce a conformational change that leads to anchoring of a 'fusion peptide' into the target membrane. Examples of viruses that infect cells in this way are the human immunodeficiency virus (HIV), Herpes virus, and paramyxoviruses such as Sendai (see Chapter 7). In a more complex strategy, a viral surface protein binds to receptor sites at the cell surface and the virion is endocytosed. Subsequently, as the pH in the endosome drops, a conformational change occurs in the same or another viral surface protein, which makes the protein fusogenic. The best documented example of this entry route is infection by the Influenza virus. The structure of the fusion protein of this virus (hemagglutinin, HA) has been elucidated.[29] Although viral fusion proteins are capable of dramatic conformational changes under fusogenic conditions, the molecular mechanism by which they induce membrane fusion remains elusive.[30] In addition, several viral fusion proteins must associate into oligomers prior to induction of fusion, but the mechanism of association is not understood.

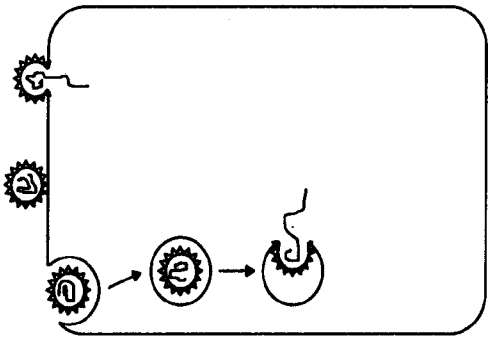

Figure 1.3 Schematic illustration of the two possible ways of infection of cells by enveloped viruses. The virus either fuses directly with the cell membrane (at neutral pH), or it is taken up by endocytosis and fuses only after the pH in the endosome has dropped.

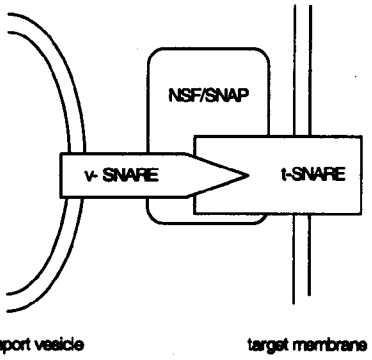

Figure 1.4 The SNARE hypothesis of protein mediated membrane fusion. See text for details.

1.3 Liposomes as membrane fusion model systems

As a result of the enormous complexity of most biological membrane fusion events, and of the lack of powerful *in vivo* analytical techniques, current understanding of membrane fusion has been derived from experiments using models of biological membranes. Since Bangham's preparation of the first liposomes in 1964,[31] model membrane systems have obtained a degree of sophistication that brings them close to the level of complexity of *in vivo* fusion. Simultaneously, techniques for analysing membrane fusion have advanced such that biological membrane fusion events can be monitored.[32]

Liposomes The model membrane system that has found most widespread application is the liposome, a lipid bilayer vesicle enclosing an aqueous compartment. Liposomes can be prepared from a wide range of natural and synthetic lipids and many techniques are available for preparing unilamellar vesicles of a defined size,[33] to enclose water-soluble solutes in the aqueous compartment[34] or to absorb apolar solutes inside the bilayer, and to reconstitute proteins in or at the membrane.[35, 36] Since the discovery of vesicles composed of synthetic amphiphiles,[37] the possibilities for structural variation of lipid and/or amphiphile membrane components has become limitless and the field of membrane mimetic chemistry is flourishing.[38, 39, 40] Fascinating results have been obtained with giant synthetic liposomes which mimic morphological transformation of the cell[41, 42] and with liposomes carrying 'steric shields' of poly(ethylene glycols) or poly(saccharides) which increase colloidal stability and circulation times for *in vivo* medical applications.[43] Concerning membrane fusion, most of the early work was devoted to calcium-induced fusion of liposomes containing negatively charged lipids.[44] Soon after, it was discovered that liposomes fuse equally well with enveloped viruses,[45, 46, 47] and can also engage in asymmetric fusion with purely synthetic membranes.[48, 49] Simultaneously, liposome fusion induced by poly(ethylene glycol) was investigated.[50] Many recently published papers describe viral fusion proteins, reconstituted in or anchored to liposomes, and a large variety of other fusogenic peptides and proteins that are able to induce liposome fusion.[51, 52, 53]

Lipid mixing techniques Since the early 1980's, many techniques have been developed to monitor lipid mixing in the course of membrane fusion. All are based on fluorescence spectroscopy of either hydrophobic or amphiphilic probes that are added to the membrane in small quantities (less than 4 mol%). Fusion of labeled and unlabeled membranes results in probe dilution (Figure 1.5), which results in a proportional change of fluorescence due to a reduction of energy transfer to an acceptor molecule, or relief of self-quenching, or a reduction of eximer concentration.

The resonance energy transfer (RET) assay uses the efficiency of resonance energy transfer between nitrobenzoxadiazole (NBD) and rhodamine (Rh), normally present as derivatives of phosphatidylethanolamine.[54] Within a certain concentration range, the energy transfer of NBD to Rh is linearly dependent on the membrane surface density of the two lipid probes, and any dilution of the probes will cause a proportional decrease of energy transfer, resulting in an increase of NBD fluorescence. Therefore, lipid mixing during membrane fusion can be monitored either as an increase of NBD fluorescence, or as an increase of the NBD to Rh fluorescence ratio.

Alternatively, membranes may be labeled with *n*-octadecyl rhodamine B chloride (R18) at a self-quenching concentration.[55] In the course of fusion of labeled and unlabeled membranes, R18 is diluted and self-quenching is relieved, resulting in an increase of R18 fluorescence. An important advantage of the R18 method is the ease of labeling of biological membranes such as viruses and erythrocytes. However, R18 is a detergent rather than a lipid, and there have been reports of exchange of the probe under non-fusogenic conditions.[56, 57] A related assay is the measurement of the life time of fluorescence of various lipid-associated probes, which is strongly dependent on its membrane surface density.[58]

Finally, pyrene and phospholipid derivatives of pyrene have frequently been used as a probe for lipid mixing.[56, 59] At high concentration in the membrane, pyrene forms eximers upon excitation, rather than monomers. During fusion of labeled and unlabeled membranes, the decrease of the eximer to monomer fluorescence ratio is a measure of lipid mixing.

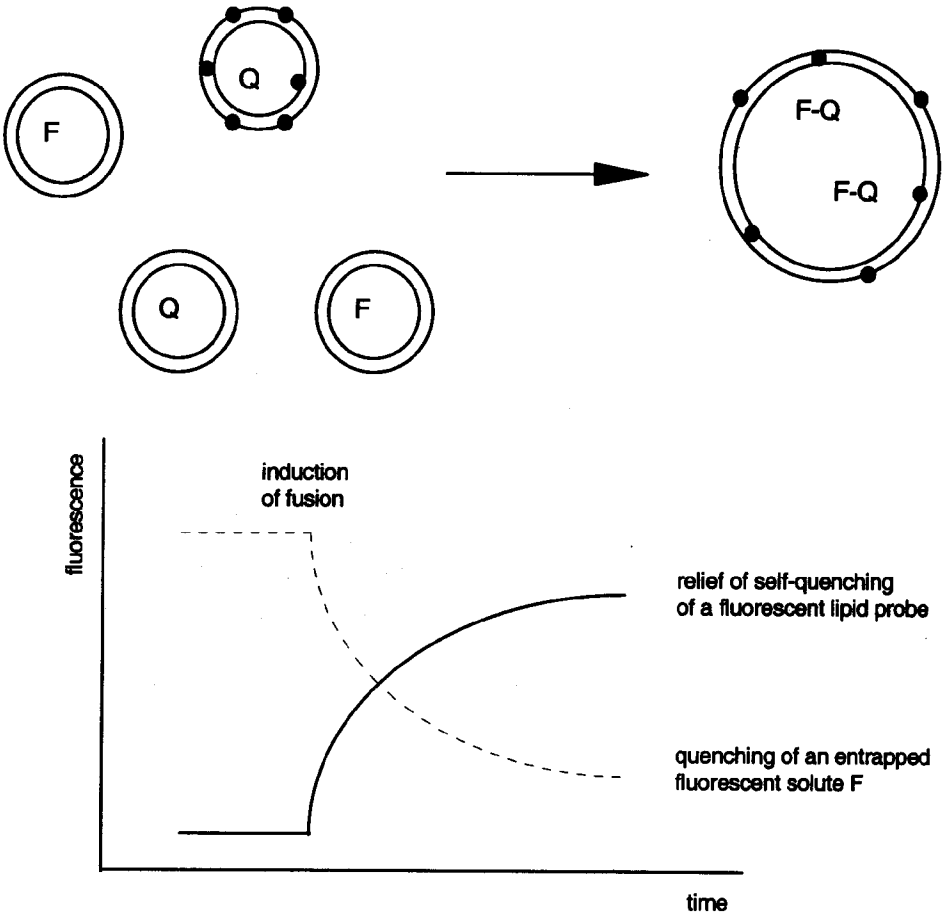

Figure 1.5 Outline of a lipid and contents mixing assay to monitor the rate and extent of liposome fusion.

Contents mixing techniques Contents mixing is the ultimate consequence of fusion of two membrane-enclosed compartments. Most contents mixing assays exploit the drastic change in fluorescence which occurs upon mixing of the contents of the aqueous compartments of two populations of liposomes (or viruses, organelles, etc.). One population may contain a water-soluble fluorophore, and the other a water-soluble quencher (Figure 1.5), or alternatively, two solutes may come together and form a fluorescent complex. Examples are the ANTS/DPX assay[60] and the terbium(III)/dipicolinic acid assay,[61] respectively. A source of concern in all such assays is the need to discriminate between contents mixing and contents leakage prior to, during, or after fusion.

Ultrastructural techniques Microscopy has provided detailed information about a variety of membrane fusion processes. Negative staining, freeze-fracture, and cryogenic electron microscopy have revealed the structure of many membranous structures in great detail, and have advanced to a resolution that allows observation of interactions of unilamellar lipid bilayers. Some of the most interesting results on membrane fusion are briefly reviewed in Section 5.1. However, potential artifacts induced by sample preparation, staining and vitrification procedures have to be taken into account. Morover, electron microscopy only provides static images. At a simpler level, electron microscopy can provide accurate size distributions of liposomes and virions, and evidence an increase of size due to aggregation and fusion. These data can also be obtained using light scattering techniques.[62] Fluorescence microscopy of large membrane structures (> 1 micron) allows real-time imaging of fusion using the fluorescent techniques discussed above. Many cellular fusion events have been investigated with this method.[63, 64]

Membrane capacitance and conductance measurements The electrical capacitance of a membrane is linearly related to its surface area.[65] Depending on the membrane composition, the specific membrane capacitance is *ca.* 10^{-6} F/cm^2. The capacitance of a cell membrane ranges from 10^{-12} to 10^{-9} F (depending on cell size), and that of a vesicle is *ca.* 10^{-15} F. Membrane area increase as a result of membrane fusion can be very accurately detected as an increase in membrane capacitance, and many cellular fusion events have been studied in this way.[63, 66] Membrane conductance measurement is less straightforward, but can provide crucial insight into the rate and extent of pore formation in fusing membranes.[66, 67] However, these techniques are limited to giant liposomes (or cells) which can be aspired to a micropipette ('patch-clamped') and to planar bilayer membranes, and do not apply to liposome-liposome fusion.

1.4 A molecular mechanism of membrane fusion

Aggregation (close approach) of two bilayers is a prerequisite for membrane fusion. Since lipid bilayers repel each other due to a combination of repulsive electrostatic, hydration and entropic interactions,[68, 69, 70, 71, 72] aggregation is by no means a trivial condition for fusion.

It is assumed that *in vivo* two bilayers are brought into close contact because anchoring proteins pull them together. All viral fusion proteins contain a transmembrane region that provides a firm anchor in the viral membrane, and contain a 'fusion peptide' that is assumed to insert into the target membrane.[28] Cellular fusion protein complexes always contain both a parent and a target membrane-anchored domain.[16] The high affinity of the specific protein-protein and protein-receptor complexes can overcome the bilayer repulsion. Probably, conformational changes in the protein complex enable the establishment of molecular contact between two adjacent bilayers. In several viral fusion events, the fusion proteins require a pre-association into oligomers, indicating that only one fusion protein (or protein complex) may be insufficient to induce membrane aggregation.

For bilayers containing anionic lipids, divalent calcium ions can be very efficient fusogenic agents.[44, 73] Ca^{2+} binds to the negatively charged phosphate moieties in the lipid head groups, reducing electrostatic repulsion, and removing large amounts of hydration water. Complexation of Ca^{2+} to phosphatidylserine yields an essentially anhydrous complex. In this way, binding of Ca^{2+} induces local hydrophobic domains at the bilayer surface.[74, 75] Furthermore, although at low Ca^{2+} concentration 'cis' (intravesicular) binding prevails, at sufficiently high concentrations of Ca^{2+} 'trans' (intervesicular) binding occurs, which leads to an additional bridging interaction between membranes, bringing them into molecular contact. Many other divalent and trivalent metal ions also induce aggregation of bilayers containing negatively charged lipids.

Alternatively, bilayers can be brought into contact by polymer depletion interaction.[50, 76] High concentrations of hydrophilic polymer (usually poly(ethylene glycol)) deplete the membrane surface of hydration water, and literally push the membranes together because they take up so much space themselves.[77] In some cases, the effect of different fusogenic agents combine in a cooperative manner.[78, 79]

Apart from bringing the bilayers together, effective fusogenic agents must induce local perturbations in the structure of the opposed bilayers in order to permit the establishment of non-bilayer intermediate structures leading to membrane fusion. Proteins can easily cause large local perturbations by insertion of a 'fusion peptide' into a target membrane and/or conformational changes upon insertion.[30] Depending on the membrane lipid composition, Ca^{2+} may induce domain formation[74, 80] or phase transitions of the liquid crystalline bilayer to either a gel-like lamellar state or an inverted hexagonal state,[44, 81, 82, 83] both of which can result in local differences in lateral compressibility and packing defects. This makes Ca^{2+} unique compared to most other metal ions, which can induce bilayer aggregation, but not fusion. A local perturbation of the outer leaflets *must* be induced in order to trigger membrane fusion induced by poly(ethylene glycol).[50, 75]

Regarding the molecular rearrangements that occur when two bilayer membranes merge into one, views have converged on a generally accepted model. The model is normally referred

to as the (modified) stalk-pore theory of membrane fusion and has been proposed by Markin, Kozlov and Borovjagin[84] and developed by Chernomordik[85, 86] and Siegel.[87, 88] The primary objective of the model (Figure 1.6) is to provide a rearrangement of lipid molecules that allows for membrane fusion with minimal contact between the hydrophobic bilayer interior and the aqueous environment. The main parameters in the model are the curvature stress induced by bending the bilayer leaflets and the packing stress induced by the formation of hydrophobic 'interstices' or 'voids' in the fusing membranes.

According to the stalk-pore hypothesis, close approach of two bilayers is followed by the transient establishment of a stalk-like structure in which the adjacent (contact or 'cis') bilayer leaflets have merged, but the distal (non-adjacent or 'trans') leaflets remain intact. The driving force for stalk formation is strong Van der Waals interaction between two adjacent bilayers. The Gibbs energy cost of stalk formation largely resides in the required bending of the bilayer leaflets, and in the creation of hydrophobic voids at both ends of the stalk. Consequently, the stalk should expand into a hemifusion intermediate in which the two fusing compartments are separated by one mutual bilayer membrane, the 'trans monolayer contact' (if it is small) or 'bilayer diaphragm' (if it is larger), consisting of the distal bilayer leaflets of the fusing membranes. The formation and size of the hemifusion intermediate are subject to debate. Chernomordik *c.s.*[84] have

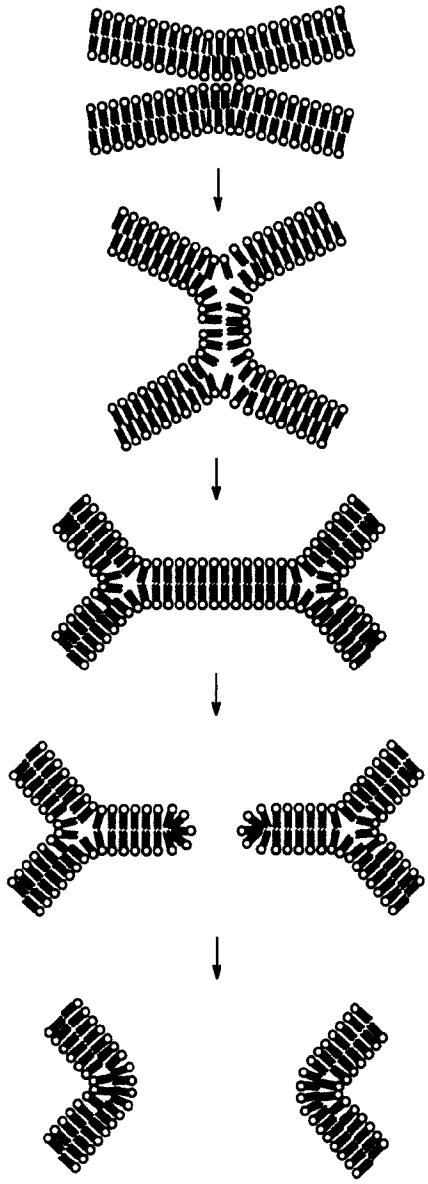

Figure 1.6 Bilayer membrane fusion according to the stalk-pore model. Adjacent bilayers establish a local contact site, a narrow stalk is formed, and the contact monolayers merge into a hemifusion diaphragm. Next, a pore is formed in the hemifusion diaphragm, and full fusion is achieved.

argued that it may be relatively stable and can persist at a longer time scale, and achieve a significant diameter. Siegel[86] has claimed that the intermediate is unstable due to the hydrophobic interstices at the edges, and believes no diaphragm of significant size is formed. In any case, either directly upon formation, or as the diaphragm widens, a minute hole forms in the diaphragm, leading to formation of a fusion pore of limited size. Pore formation is thought to be reversible up to a certain size, beyond which the pore irreversibly opens and full fusion is achieved. The reason of this reversibility is uncertain, but may reside in the Gibbs energy cost of the highly positive curvature along the edges of the pore. Perhaps full fusion can only occur once the diameter of the fusion pore reaches the size of the bilayer diaphragm, so that both the packing stress of the hydrophobic voids at the diaphragm edge and the curvature stress at the edge of the pore are relieved. Siegel[86] argued that this combination of packing and curvature stress prevents formation of large bilayer diaphragms, and that pore formation would immediately follow establisment of a trans monolayer contact.

In sum, the modified stalk-pore model implies that bilayer membrane fusion is a cascade of sequential events. Stalk formation and hemifusion should result in mixing of lipid molecules in the outer bilayer leaflets of fusing membranes. Fusion pore formation should be reversible, and should be accompanied by mixing of lipids in the inner bilayer leaflets as well as the aqueous contents of the fusing membrane compartments. In addition, all stages of the fusion process should be extremely sensitive to modification of the spontaneous curvature of bilayer leaflets. This model of membrane fusion is supported by fluorescence and membrane capacitance and conductance measurements of a variety of bilayer membrane systems.

Recently, Lee and Lentz[75] elegantly demonstrated the sequence and time scale of outer bilayer leaflet mixing, inner bilayer leaflet mixing, and contents mixing (first of small, later of bigger solutes, indicating growing pore size) during poly(ethylene glycol)-induced fusion of small unilamellar lipid vesicles. Hemifusion of membrane-enclosed compartments should result in outer leaflet lipid mixing in the absence of contents mixing, and this has been reported in several systems.[75, 89, 90, 91] Two different forms of hemifusion have been inferred from a combination of lipid mixing and pore formation measurements. In 'unrestricted hemifusion', which has been observed for purely lipidic systems, the outer bilayer leaflets merge in the absence of any significant contents mixing or pore formation.'Restricted hemifusion' has been proposed to explain a very low extent of lipid mixing in influenza virus hemagglutinin-mediated fusion even when a substantial fusion pore has already formed.[67] Possibly, a fence of hemagglutinin molecules obstructs free lipid flow through the pore. Reversible pore formation has been observed directly as a flickering of membrane conductance in various fusion processes.[66, 92, 93, 94]

Chernomordik *c.s.*[89, 95, 96] and others[90] reported the sensitivity of the kinetics of formation of various intermediate states in bilayer fusion to changes in the spontaneous curvature of either of the two bilayer leaflets. Many lipids do not have a perfectly cylindrical morphology, and consequently they tend to induce curvature of the membrane leaflets. Lipids with positive curvature tend to form micelles, and lipids with negative curvature tend to form inverted phases. In accordance with the stalk-pore model, stalk formation and hemifusion (observed as exclusive outer leaflet lipid mixing) is promoted by lipids with negative spontaneous curvature in the outer leaflet of membranes, and both are inhibited by lipids with positive spontaneous

curvature. Inversely, pore formation and completion of fusion (observed as inner leaflet lipid and contents mixing, as well as membrane pore conductance) are strongly inhibited by lipids with negative curvature in the inner leaflet of the membrane, and promoted by lipids with positive curvature. In addition, small amounts of hexadecane promote bilayer fusion. Presumably, the alkane fills hydrophobic voids that occur during stalk formation, and thus lowers the Gibbs energy of activation of the fusion process.[97]

However, ultrastructural evidence for the model is scarce and scattered. No stalk-like connection between two membranes has been unambiguously observed. The first indications for formation of hemifused membranes came from freeze-fracture and thin-section electron microscopy of zoospores.[98] 'Point defects' and 'lipidic intramembranous particles', indicative of primary contact sites of adjacent bilayers that may be on the verge of fusion were observed in freeze-fracture electron microscopy of concentrated lipid suspensions containing substantial amounts of phosphatidylethanolamine.[99, 100] Probably, these structures are small fusion pores. These phenomena are associated with the onset of lamellar to inverted hexagonal phase transitions, which have also been characterised in cryo-electron microscopy of unilamellar liposome solutions.[101, 102, 103] Very recently, structural features of Influenza virus-liposome fusion were revealed in freeze-fracture electron microscopy of pelleted virus-liposome mixtures.[104] Most of the studies mentioned above suffered from the inherent transient nature of the fusion event: all intermediate stages of membrane fusion have limited life-times, they are localised events that occur infrequently, and observations are essentially a matter of 'lucky shots'. Important results are reviewed in Section 5.1.

In addition, the stalk-pore model of membrane fusion is based on considerations of hydrophobic attractions and curvature stress, but does not take into account electrostatic interactions and (de)hydration effects.[86] Therefore, it is not certain that this model provides an accurate description of calcium-induced bilayer fusion. Calcium-induced fusion of small vesicles of phosphatidylserine occurs via a so-called rupture-reseal mechanism in which the small vesicles initially fuse into large lamellar sheets which role up into multilamellar spiral lipid cylinders ('cochleate cylinders') that rearrange into large unilamellar vesicles only upon removal of calcium ions by EDTA.[105] Vesicles rapidly loose their contents in the course of these rearrangements. Calcium-induced fusion of di-*n*-dodecylphosphate (a synthetic lipid) proceeds in a comparable way: small vesicles fuse into large flat vesicles, which rearrange into tubular calcium-lipid lamellar crystals.[106, 107, 108] However, for vesicles of many other negatively charged lipids, and for mixtures of negatively charged and other lipids, there is ample evidence for the occurrence of non-leaky fusion of small vesicles into large vesicles.[109, 110] The molecular mechanisms proposed for such 'tight' calcium-induced fusion processes are similar to the stalk-pore hypothesis.[73]

A fundamental perspective of membrane fusion that has clearly remained underdeveloped both theoretically and experimentally is a thermodynamic consideration of the process. The stalk-pore model is partly based on calculations of the Gibbs energy of formation of hypothetical fusion intermediates from planar lipid bilayers.[86] Thus, the model provides some insight into the activation parameters of membrane fusion, albeit *in vacuo*, but it does not elucidate the thermodynamic driving force(s) of membrane fusion. Papahadjopoulos and coworkers[111] reported the experimental enthalpy of the reaction between phosphatidylserine

liposomes and calcium ions, but the heat effect is a combined result of calcium-lipid binding, phase transformations in the bilayer, and liposome aggregation and fusion. Recently, a microcalorimetric analysis of fusion between liposomes and Influenza virus indicated a rather strongly endothermic enthalpy of fusion.[112] Unfortunately, analysis of the experimental data is quite complicated. Moreover, the authors confuse reaction enthalpies and Gibbs energies of activation, and do not elaborate on the potential entropic driving force for the endothermic process, or on the role of specific protein-lipid interactions.

In sum, it may be concluded that there is evidence that the lipid rearrangements occurring in bilayers in most membrane fusion events are similar. Many experimental observations support the stalk-pore model of membrane fusion. Although biological membrane fusion is triggered and controlled by a protein machinery, ultimately fusion is a universal lipid rearrangement. However, there is little ultrastructural evidence for the model, and parameters that have so far been ignored include electrostatic interactions and (de)hydration effects, which should certainly be taken into account in membrane fusion processes involving charged lipids and/or fusogenic agents (be they proteins or metal ions). Finally, there is no conclusive experimental evidence concerning the thermodynamics of membrane fusion.

1.5 Scope of this thesis

This thesis describes a study of bilayer membrane fusion using novel synthetic lipid molecules as a tool for providing structural, kinetic and thermodynamic information. *Chapter 1* set the stage by introducing the main biological fusion events and by briefly reviewing current understanding of these complicated processes. Also, this chapter advocates the use of sophisticated membrane model systems to improve our insight into fusion of bilayer membranes. *Chapter 2* describes the synthesis of a novel class of phospholipid analogues containing a bifunctional *beta*-nitrostyrene (BNS) group. These lipids form unilamellar vesicles which were characterised by electron microscopy, differential scanning microcalorimetry and light scattering. The chapter presents a method for preparing vesicles in which either both or only the inner bilayer leaflet are photopolymerised into linear lipid oligomers. In addition, a kinetic model for surface-specific reactions of vesicular bilayers is presented. *Chapter 3* presents a characterisation of vesicles of oligomerised lipids. Differential scanning microcalorimetry, monolayer studies, ^{31}P-NMR spectroscopy, contents leakage and solubilisation by detergent provide insight into the molecular packing, the molecular mobility, and the permeability of bilayers of lipid oligomers in comparison to bilayers of lipid monomers. *Chapter 4* describes a study of calcium-induced fusion of unilamellar vesicles of oligomerisable lipids. Fusion was studied using lipid mixing, light scattering, and electron microscopy. Oligomerisation of either both or only the inner bilayer leaflet has a strongly inhibiting effect. Implications for the molecular mechanism of bilayer fusion are discussed in conjunction with the results described in Chapter 3. *Chapter 5* presents an electron microscopic study of the structures resulting from calcium-induced fusion of lipid vesicles containing an oligomerised inner bilayer leaflet. *Chapter 6* reports an investigation of the thermodynamics of calcium-induced vesicle fusion employing titration microcalorimetry. Using the oligomerisable lipid vesicles, and applying a hydrophobically-modified polymer that prevents vesicle aggregation, the fusion process was dissected into successive steps of Ca^{2+}

binding, vesicle aggregation and bilayer fusion. The enthalpy of each of these processes was measured, and a molecular interpretation is suggested. *Chapter 7* describes a study of the fusion of vesicles of oligomersable lipids and Sendai virus. Lipid mixing assays and electron microscopy show that fusion mediated by the spike proteins of Sendai is strongly inhibited by lipid oligomerisation. Titration microcalorimetry was used to assess the enthalpy associated with fusion of Sendai and lipid vesicles, and a molecular interpretation of the thermodynamic results is discussed. Finally, *Chapter 8* is an epilogue which places the observations described in this thesis in perspective and suggests further possibilities for investigations of membrane fusion events using oligomerisable BNS lipids as a tool.

1.6 References

(1) Deamer, D.W.; Harang Mahon, E.; Bosco, G. Self-assembly and function of primitive membrane structures. In: Early life on earth. Nobel Symposium 84 (Bengtson, S., Ed.). Columbia U.P., New York, 1994.

(2) Deamer, D.W. The first living systems: a bioenergetic perspective. *Microbiol. Mol. Biol. Rev.* 1997, 62, 239-261.

(3) Pastan, I.; Willingham, M.C. (Eds.) Endocytosis. Plenum Press, New York, 1985.

(4) Riezman, H.; Woodman, P.G.; Van Meer, G.; Marsh, M. Molecular mechanisms of endocytosis. *Cell* 1997, 91, 731-738.

(5) Robinson, M.S.; Watts, C.; Zerial, M. Membrane dynamics in endocytosis. *Cell* 1996, 84, 13-21.

(6) Burgoyne, R.D.; Morgan, A. Regulated exocytosis. *Biochem. J.* 1993, 293, 305-316.

(7) Paras, H.; Paras, I. Neurotransmitter release at fast synapses. *J. Membr. Biol.* 1994, 142, 267-280.

(8) Wilson, D.W.; Whiteheart, S.W.; Orci, L.; Rothman, J.E. Intracellular membrane fusion. *Trends Biochem. Sci.* 1991, 16, 334-337.

(9) Myles, D.G. Molecular mechanisms of sperm-egg membrane binding and fusion in mammals. *Dev. Biol.* 1993, 158, 35-45.

(10) Snell, W.J.; White, J.M. The molecules of mammalian fertilization. *Cell* 1996, 85, 629-637.

(11) Rose, M.D. Nuclear fusion in the yeast Saccharomyces Cerevisiae. *Ann. Rev. Cell Dev. Biol.* 1996, 12, 663-695.

(12) Fishkind, D.J.; Wang, Y. New horizons for cytokinesis. *Curr. Opin. Cell Biol.* 1995, 7, 23-31.

(13) Kielian, M.; Jungerwirth, S. Mechanisms of enveloped virus entry into cells. *Mol. Biol. Med.* 1993, 7, 17-31.

(14) Hernandez, L.D.; Hoffman, L.R.; Wolfsberg, T.G.; White, J.M. Virus-cell and cell-cell fusion. *Ann. Rev. Cell Dev. Biol.* 1996, 12, 627-661.

(15) Robbins, P.D.; Tahara, H.; Ghivizzani, S.C. Viral vectors for gene therapy. *Trends Biotechnol.* 1998, 16, 35-40.

(16) Rothman, J.E. The protein machinery of vesicle budding and fusion. *Protein Science* 1996, 5, 185-194.

(17) Hay, J.C.; Scheller, R.H. SNAREs and NSF in targeted membrane fusion. *Curr. Opin. Cell Biol.* 1997, 9, 505-512.

(18) Woodman, P.G. The roles of NSF, SNAPs and SNAREs during membrane fusion. *Biochim. Biophys. Acta* 1997, 1357, 155-172.

(19) Balch, W.E.; Glick, B.S.; Rothman, J.E. Sequential intermediates in the pathway of intercompartimental transport in a cell-free system. *Cell* 1984, 39, 525-536.

(20) Glick, B.S.; Rothman, J.E. Possible role for fatty acyl-coenzyme A in intracellular protein transport. *Nature* 1987, 326, 309-312.

(21) Clary, D.O.; Griff, I.C.; Rothman, J.E. SNAPs, a family of NSF attachment proteins involved in intracellular membrane fusion in animals and yeast. *Cell* 1990, 61, 709-721.

(22) Söllner, T.; Whiteheart, S.W.; Brunner, M.; Erdjument-Bromage, H.; Geromanos, S.; Tempst, P.; Rothman, J.E. SNAP receptors implicated in vesicle targeting and fusion. *Nature* 1993, 362, 318-324.

(23) Südhof, T.C.; De Camilli, P.; Niemann, H.; Jahn, R. Membrane fusion machinery: insights from synaptic proteins. *Cell* 1993, 75, 1-4.

(24) Søgaard, M.; Tani, K.; Ye, R.R.; Geromanos, S.; Tempst, P.; Kirchhausen, T.; Rothman, J.E.; Söllner, T. A Rab protein is required for the assembly of SNARE complexes in the docking of transport vesicles. *Cell* 1994, 78, 937-948.

(25) Rybin, V.; Ullrich, O.; Rubino, M.; Alexandrov, K.; Simon, I.; Seabra, M.C.; Goody, R.; Zerial, M. GTPase activity of Rab5 acts as a timer for endocytotic membrane fusion. *Nature* 1996, 383, 266-269.

(26) Latterich, M.; Frölich, K.U.; Schekman, R. Membrane fusion and the cell cycle: Cdc48p participates in the fusion of ER membranes. *Cell* 1995, 82, 885-893.

(27) Weber, T.; Zemelman, B.V.; McNew, J.A.; Westermann, B.; Gmachl, M.; Parlati, F.; Söllner, T.H.; Rothman, J.E. SNAREpins: minimal machinery for membrane fusion. *Cell* 1998, 92, 611-620.

(28) White, J.; Kielian, M.; Helenius, A. Membrane fusion proteins of enveloped animal viruses. *Q. Rev. Biophys.* 1983, 16, 151-195.

(29) Bullough, P.A.; Hughson, F.M.; Shekel, J.J.; Wiley, D.C. Structure of influenza hemagglutinin at the pH of membrane fusion. *Nature* 1994, 371, 37-43.

(30) Hughson, F.M. Molecular mechanisms of protein-mediated membrane fusion. *Curr. Opin. Struct. Biol.* 1995, 5, 507-513.

(31) Bangham, A.D.; Horne, R.W. Negative staining of phospholipids and their structural modification by surface-active agents as observed in the electron microscope. *J. Mol. Biol.* 1964, 8, 660-668.

(32) Düzgünes, N. (Ed.) Membrane fusion techniques. *Methods Enzymol.* 1993, 220 and 221.

(33) Woodle, M.C.; Papahadjopoulos, D. Liposome preparation and size characterization. *Methods Enzymol.* 1989, 171, 193-217.

(34) Szoka, F.; Papahadjopoulos, D. Procedure for preparation of liposomes with large internal aqueous space and high capture by reverse-phase evaporation. *Proc. Natl. Acad. Sci. USA* 1978, 75, 4194-4198.

(35) Eytan, G.D. Use of liposomes for reconstitution of biological functions. *Biochim. Biophys. Acta* 1982, 694, 185-202.

(36) Rigaud, J.L.; Pitard, B.; Levy, D. Reconstitution of membrane proteins into liposomes: application to energy transducing membrane proteins. *Biochim. Biophys. Acta* 1995, 1231, 223-246.

(37) Kunitake, T.; Okahata, Y. A totally synthetic bilayer membrane. *J. Am. Chem. Soc.* 1977, 99, 3860-3681.

(38) Fendler, J.H. Membrane mimetic chemistry. Wiley, New York, 1982.

(39) Kunitake, T. Synthetic bilayer membranes: molecular design, self-organization, and application. *Angew. Chem., Int. Ed. Engl.* 1992, 31, 709-726.

(40) Engberts, J.B.F.N.; Hoekstra, D. Vesicle-forming synthetic amphiphiles. *Biochim. Biophys. Acta* 1995, 1241, 323-340.

(41) Sackmann, E.; Duwe, H.P.; Engelhardt, H. Membrane binding elasticity and its role for shape fluctuations and shape transformations of cells and vesicles. *Faraday Discuss. Chem. Soc.* 1986, 81, 281-290.

(42) Menger, F.M.; Gabrielson, K.D. Cytomimetic organic chemistry: early developments. *Angew. Chem., Int. Ed. Engl.* 1995,34, 2091-2106.

(43) Lasic, D.D. Sterically stabilized vesicles. *Angew. Chem., Int. Ed. Engl.* 1994, 33, 1685-1698.

(44) Papahadjopoulos, D. Calcium-induced phase changes and fusion in natural and model membranes. *Cell Surf. Rev.* 1978, 5, 766-790.

(45) Stegmann, T.; Hoekstra, D.; Scherphof, G.; Wilschut, J. Kinetics of pH-dependent fusion between influenza virus and liposomes. *Biochemistry* 1985, 24, 3107-3113.

(46) Klappe, K.; Wilschut, J.; Nir, S.; Hoekstra, D. Parameters affecting fusion between Sendai virus and liposomes. Role of viral proteins, liposome composition, and pH. *Biochemistry* 1986, 25, 8252-8260.

(47) Bron, R.; Wahlberg, J.M.; Garoff, H.; Wilschut, J. Membrane fusion of Semliki Forest virus in a model system: correlation between fusion kinetics and structural changes in the envelope glycoprotein. *EMBO J.* 1993, 12, 693-701.

(48) Fonteijn, T.A.A.; Hoekstra, D.; Engberts, J.B.F.N. Specific asymmetric fusion between artificial and biological model membranes. *J. Am. Chem. Soc.* 1990, 112, 8870-8872.

(49) Fonteijn, T.A.A.; Engberts, J.B.F.N.; Nir, S.; Hoekstra, D. Asymmetric fusion between synthetic di-n-dodecylphosphate vesicles and virus membranes. *Biochim. Biophys. Acta* 1992, 1110, 185-192.

(50) Lentz, B.R. Polymer-induced membrane fusion: potential mechanism and relation to cell fusion events. *Chem. Phys. Lipids* 1994, 73, 91-106.

(51) Colotto, A.; Martin, I.; Ruysschaert, J.M.; Sen, A.; Hui, S.W.; Epand, R.M. Structural study of the interaction between the SIV fusion peptide and model membranes. *Biochemistry* 1996, 35, 980-989.

(52) Pécheur, E.I.; Hoekstra, D.; Sainte-Marie, J.; Maurin, L.; Bienvenüe, A.; Philippot, J.R. Membrane anchorage brings about fusogenic properties in a short synthetic peptide. *Biochemistry* 1997, 36, 3773-3781.

(53) Durrell, S.R.; Martin, I.; Ruysschaert, J.M.; Shai, Y.; Blumenthal, R. What studies of fusion peptides tell us about viral envelope glycoprotein-mediated membrane fusion. *Mol. Membr. Biol.* 1997, 14, 97-112.

(54) Struck, D.K.; Hoekstra, D.; Pagano, R.E. Use of resonance energy transfer to monitor membrane fusion. *Biochemistry* 1981, 20, 4093-4099.

(55) Hoekstra, D.; De Boer, T.; Klappe, K.; Wilschut, J. Fluorescence method for measuring the kinetics of fusion between biological membranes. *Biochemistry* 1984, 23, 5675-5681.

(56) Stegmann, T.; Schoen, P.; Bron, R.; Wey, J.; Bartoldus, I.; Ortiz, A.; Nieva, J.L.; Wilschut, J. Evaluation of viral membrane fusion assays. Comparison of the octadecylrhodamine assay with

the pyrene eximer assay. *Biochemistry* 1993, 32, 11330-11337.

(57) Stegmann, T.; Orsel, J.G.; Jamieson, J.D.; Padfield, P.J. Limitations of the octadecylrhodamine dequenching assay for membrane fusion. *Biochem. J.* 1995, 307, 875-876.

(58) Burgess, S.W.; Lentz, B.R. Fluorescence lifetime measurements to monitor membrane lipid mixing. *Methods Enzymol.* 1993, 220, 42-50.

(59) Pal, Y.; Barenholz, Y.; Wagner, R.R. Pyrene phospholipid as a biological fluorescent probe for studying the fusion of virus membrane with liposomes. *Biochemistry* 1988, 27, 30-36.

(60) Düzgünes, N.; Wilschut, J. Fusion assays monitoring intermixing of aqueous contents. *Methods Enzymol.* 1993, 220, 3-14.

(61) Wilschut, J.; Düzgünes, N.; Fraley, R.; Papahadjopoulos, D. Studies on the mechanism of membrane fusion: kinetics of calcium ion induced fusion of phosphatidylserine vesicles followed by a new assay for mixing of aqueous vesicle contents. *Biochemistry* 1980, 19, 6011-6021.

(62) Ruf, H.; Georgalis, Y.; Grell, E. Dynamic laser light scattering to determine size distributions of vesicles. *Methods Enzymol.* 1989, 172, 364-390.

(63) Smith, C.B.; Betz, W.J. Simultaneous independent measurement of endocytosis and exocytosis. *Nature* 1996, 380, 531-534.

(64) Munoz-Barroso, I.; Durell, S.; Sakaguchi, K.; Appella, E.; Blumenthal, R. Dilation of the human immunodeficiency virus-1 envelope glycoprotein fusion pore revealed by the inhibitory action of a synthetic peptide from gp41. *J. Cell Biol.* 1998, 140, 315-323.

(65) Kado, R.T. Membrane area and electrical capacitance. *Methods Enzymol.* 1993, 221, 273-302.

(66) Monck, J.R.; Fernandez, J.M. The exocytotic fusion pore. *J. Cell Biol.* 1992, 119, 1395-1404.

(67) Tse, F.W.; Iwata, A.; Almers, W. Membrane flux through the lipid pore formed by a fusogenic viral envelope protein during cell fusion. *J. Cell Biol.* 1993, 121, 543-552.

(68) Israelachvili, J.N. Intermolecular surface forces. Academic Press, New York, 1992.

(69) Rand, R.P.; Parsegian, V.A. Hydration forces between phospholipid bilayers. *Biochim. Biophys. Acta* 1989, 988, 351-376.

(70) Perera, L.; Essmann, U.; Berkowitz, M.L. Role of water in the hydration force acting between lipid bilayers. *Langmuir* 1996, 12, 2625-2629.

(71) Israelachvili, J.; Wennerström, H. Role of hydration and water structure in biological and colloidal interactions. *Nature* 1996, 379, 219-225.

(72) Israelachvili, J.N.; Wennerström, H. Entropic forces between amphiphilic surfaces in liquids. *J. Phys. Chem.* 1992, 96, 520-531.

(73) Papahadjopoulos, D.; Nir, S.; Düzgünez, N. Molecular mechanisms of calcium-induced membrane fusion. *J. Bioenerg. Biomembr.* 1990, 22, 157-179.

(74) Ohki, S. A mechanism of divalent ion-induced phosphatidylserine membrane fusion. *Biochim. Biophys. Acta* 1982, 689, 1-11.

(75) Leckband, D.E.; Helm, C.A.; Israelachvili, J. Role of calcium in the adhesion and fusion of bilayers. *Biochemistry* 1993, 32, 1127-1140.

(76) Lee, J.; Lentz, B.R. Evolution of lipidic structures during model membrane fusion and the relation of this process to cell membrane fusion. *Biochemistry* 1997, 36, 6251-6259.

(77) Kuhl, T. Guo, Y.; Alderfer, J.L.; Berman, A.D.; Leckband, D.; Israelachvili, J.; Hui, S.W. Direct measurement of polyethylene glycol induced depletion attraction between lipid bilayers.

Langmuir 1996, 12, 3003-3014.

(78) Rupert, L.A.M.; Engberts, J.B.F.N.; Hoekstra, D. Effect of poly(ethylene glycol) on the Ca^{2+}-induced fusion of didodecyl phosphate vesicles. *Biochemistry* 1988, 27, 8232-8239.

(79) Herrmann, A.; Claque, M.J.; Blumenthal, R. Enhancement of viral fusion by nonadsorbing polymers. *Biophys. J.* 1993, 65, 528-534.

(80) Haverstick, D.M.; Glaser, M. Visualisation of Ca^{2+}-induced phospholipid domains. *Proc. Natl. Acad. Sci. USA* 1987, 84, 4475-4479.

(81) Cullis, P.R.; De Kruijff, B. Lipid polymorphism and the functional roles of lipids in biological membranes. *Biochim. Biophys. Acta* 1979, 559, 399-420.

(82) Verkleij, A.J.; De Maagd, R.; Leunissen-Bijvelt, J.; De Kruiff, B. Divalent cations and chlorpromazine can induce non-bilayer structures in phosphatidic acid-containing model membranes. *Biochim. Biophys. Acta* 1982, 684, 255-262.

(83) Hong, K.; Baldwin, P.A.; Allen, T.M.; Papahadjopoulos, D. Fluorometric detection of the bilayer-to-hexagonal phase transition in liposomes. *Biochemistry* 1988, 27, 3947-3955.

(84) Markin, V.S.; Kozlov, M.M.; Borovjagin, V.L. On the theory of membrane fusion. The stalk mechanism. *Gen. Physiol. Biophys.* 1984, 5, 361-377.

(85) Chernomordik, L.V.; Melikyan, G.B.; Chizmadzhev, Y.A. Biomembrane fusion: a new concept derived from model studies using two interacting planar lipid membranes. *Biochim. Biophys. Acta* 1987, 906, 309-352.

(86) Chernomordik, L.V.; Zimmerberg, J. Bending membranes to the task: structural intermediates in bilayer fusion. *Curr. Opin. Struct. Biol.* 1995, 5, 541-547.

(87) Siegel, D.P. Energetics of intermediates in membrane fusion: comparison of stalk and inverted micellar intermediate mechanisms. *Biophys. J.* 1993, 65, 2124-2140.

(88) Siegel, D.P.; Epand, R.M. The mechanism of lamellar-to-inverted hexagonal phase transitions in phosphatidylethanolamine: implications for membrane fusion mechanisms. *Biophys. J.* 1997, 73, 3089-3111.

(89) Kemble, G.W.; Danieli, T.; White, J.M. Lipid-anchored Influenza hemagglutinin promotes hemifusion, not complete fusion. *Cell* 1994, 76, 383-394.

(90) Chernomordik, L.V.; Vogel, S.S.; Sokoloff, A.; Onaran, H.O.; Leikina, E.A.; Zimmerberg, J. Lysolipids reversibly inhibit Ca^{2+}-, GTP-, and pH-dependent fusion of biological membranes. *FEBS Letters* 1993, 318, 71-76.

(91) Melikyan, G.B.; Brener, S.A.; Ok, D.C.; Cohen, F.S. Inner but not outer membrane leaflets control the transition from glycosylphosphatidylinositol-anchored influenza hemagglutinin-induced hemifusion to full fusion. *J. Cell Biol.* 1997, 136, 995-1005.

(92) Nanavati, C.; Markin, V.S.; Oberhauser, A.F.; Fernandez, J.M. The exocytotic fusion pore modelled as a lipidic pore. *Biophys. J.* 1992, 63, 1118-1132.

(93) Monck, J.R.; Fernandez, J.M. The fusion pore and mechanisms of biological membrane fusion. *Curr. Opin. Cell Biol.* 1996, 8, 524-533.

(94) Chanturiya, A.; Chernomordik, L.V.; Zimmerberg, J. Flickering fusion pores comparable with initial exocytotic pores occur in protein-free phospholipid bilayers. *Proc. Natl. Acad. Sci. USA* 1997, 94, 14423-14428.

(95) Chernomordik, L.V.; Chanturiya, A.; Green, J.; Zimmerberg, J. The hemifusion intermediate and its conversion to complete fusion: regulation by membrane composition. *Biophys. J.* 1995, 69, 922-929.

(96) Chernomordik, L.V.; Kozlov, M.M.; Zimmerberg, J. Lipids in biological membrane fusion. *J. Membrane Biol.* 1995, 146, 1-14.

(97) Walter, A.; Yeagle, P.L.; Siegel, D.P. Diacylglycerol and hexadecane increase divalent metal-induced lipid mixing rates between phosphatidylserine large unilamellar vesicles. *Biophys. J.* 1994, 66, 366-376.

(98) Pinto da Silva, P.; Noguira, M.L. Membrane fusion during secretion. *J. Cell Biol.* 1977, 73, 161-181.

(99) Hui, S.W.; Stewart, T.P.; Boni, L.T. Membrane fusion through point defects in bilayers. *Science* 1981, 212, 921-923.

(100) Verkleij, A.J. Lipidic intramembranous particles. *Biochim. Biophys. Acta* 1984, 779, 43-63.

(101) Siegel, D.P.; Burns, J.L.; Chestnut, M.H.; Talmon, Y. Intermediates in membrane fusion and bilayer/nonbilayer phase transitions imaged by time-resolved cryo-transmission electron microscopy. *Biophys. J.* 1989, 56, 161-169.

(102) Siegel, D.P.; Green, W.J.; Talmon, Y. The mechanism of lamellar-to-inverted-hexagonal phase transitions: a study using temperature-jump cryo-electron microscopy. *Biophys. J.* 1994, 66, 402-414.

(103) Frederik, P.M.; Stuart, M.C.A.; Verkleij, A.J. Intermediary structures during membrane fusion as observed by cryo-electron microscopy. *Biochim. Biophys. Acta* 1989, 979, 275-278.

(104) Kanaseki, T.; Kawasaki, K.; Murata, M.; Ikeuchi, Y.; Ohnishi, S. Structural features of membrane fusion between influenza virus and liposome as revealed by quick-freezing electron microscopy. *J. Cell Biol.* 1997, 137, 1041-1056.

(105) Papahadjopoulos, D.; Vail, W.J.; Jacobson, K.; Poste, G. Cochleate lipid cylinders: formation by fusion of unilamellar lipid vesicles. *Biochim. Biophys. Acta* 1975, 394, 483-491.

(106) Rupert, L.A.M.; van Breemen, J.F.L.; van Bruggen, E.F.J.; Engberts, J.B.F.N.; Hoekstra, D. Calcium-induced fusion of didodecylphosphate vesicles: the lamellar to hexagonal II (H_{II}) phase transition. *J. Membr. Biol.* 1987, 95, 255-263.

(107) Streefland, L.; Yuan, F.; Rand, P.; Hoekstra, D.; Engberts, J.B.F.N. X-ray structure of the Ca^{2+} and Na^{+} salts of (asymmetric) di-n-alkyl phosphates formed from the corresponding vesicles in water. *Langmuir* 1992, 8, 1715-1717.

(108) Fonteijn, T.A.A.; Hoekstra, D.; Engberts, J.B.F.N. Vesicle formation of di-n-alkyl phosphates: liquid crystalline behavior, myelinization, counterion influence, and stability. *Langmuir* 1992, 8, 2437-2447.

(109) Wilschut, J.; Düzgünez, N.; Hong, K.; Hoekstra, D.; Papahadjopoulos, D. Retention of aqueous contents during divalent cation-induced fusion of phospholipid vesicles. *Biophys. Biochim. Acta* 1983, 734, 309-318.

(110) Hui, S.W.; Nir, S.; Stewart, T.P.; Boni, L.T.; Huang, S.K. Kinetic measurements of fusion of phosphatidylserine containing vesicles by electron microscopy and fluorometry. *Biochim. Biophys. Acta* 1988, 941, 130-140.

(111) Rehfeld, S.J.; Düzgünez, N.; Newton, C.; Papahadjopoulos, D.; Eatough, D.J. The exothermic reaction of calcium with unilamellar phosphatidylserine vesicles. *FEBS Letters* 1981, 123, 249-251.

(112) Nebel, S.; Bartoldus, I.; Stegmann, T. Calorimetric detection of influenza virus induced membrane fusion. *Biochemistry* 1995, 34, 5705-5711.

Chapter 2

Design and preparation of unilamellar lipid vesicles with oligomerised bilayer leaflets[I]

Four new phospholipid derivatives containing a beta-nitrostyrene unit linked to the phosphate head group have been synthesised. Vesicles of these lipids were characterised using transmission electron microscopy, quasi-elastic light scattering and differential scanning calorimetry. The beta-nitrostyrene units can be polymerised yielding vesicles with oligo(styrene)-lipid bilayer leaflets. Furthermore, at pH 11.5 and at temperatures below the main phase transition temperature of the bilayer, the beta-nitrostyrene unit can be cleaved specifically exo-vesicularly. The cleavage process was analysed in terms of a kinetic model providing independent rates of hydrolysis and flip-flop. Exo-vesicular cleavage followed by polymerisation of the remaining endo-vesicular beta-nitrostyrene units results in surface-differentiated vesicles containing lipid oligomers in the inner bilayer leaflet and lipid monomers in the outer bilayer leaflet.

2.1 Surface differentiation in bilayer vesicles of *beta*-nitrostyrene lipids

All biological membranes are asymmetric. This observation can be rationalised by the fact that each side of the membrane faces a different environment. Almost all membrane-associated proteins and most lipid components are distributed with a high or even absolute transverse asymmetry.[1,2] A striking example is the membrane of the human erythrocyte (red blood cell) which contains at least four asymmetrically distributed lipids: 75 % of phosphatidylcholine and 85 % of sphingomyeline are located in the outer membrane leaflet, and 80 % of phosphatidylethanolamine and over 95 % of phosphatidylserine are located in the inner membrane leaflet.[3] The origin and maintenance of biological membrane asymmetry is a complex phenomenon that is far from understood. Artificial asymmetric bilayer membranes provide interesting test models, but apart from the pioneering work of Moss[4,5,6,7,8] and Ringsdorf[9,10] and coworkers, the properties of such membranes remain largely unexploited.

This chapter describes the synthesis of a novel class of synthetic phospholipids containing a bifunctional *beta*-nitrostyrene (BNS) unit, and the preparation of small unilamellar vesicles of these lipids. The BNS unit is covalently attached to the phosphate head group and resides at the vesicle surface, partitioned between the inner bilayer leaflet (*endo*-surface) and the outer bilayer leaflet (*exo*-surface). Surface differentiation of the vesicles was obtained by two simple reactions of the BNS units. On the one hand, *beta*-nitrostyrenes are polymerisable - there is literature precedent for dimerisation[11] as well as for polymerisation[12] of *beta*-nitrostyrene. On the other

[I] The research described in this chapter has been published in *Langmuir* 1996, 12, 5773-5780.

hand, *beta*-nitrostyrenes undergo rapid cleavage in alkaline aqueous solution.[13] The cleavage reaction involves rate-determining nucleophilic attack by hydroxide ion at the *alpha* position of the styrene, leading to an intermediate that rapidly splits into a benzaldehyde and the anion of nitromethane. The polymerisation and hydrolysis of (derivatives of) *beta*-nitrostyrene are depicted in Figure 2.1. Both the hydrolysis and the polymerisation reaction can be conveniently monitored using UV-VIS spectroscopy, indicating the disappearance of the absorption of *beta*-nitrostyrene at 335 nm. The molar extinction coefficient of *beta*-nitrostyrene is *ca.* 10^4 M^{-1} cm^{-1}.

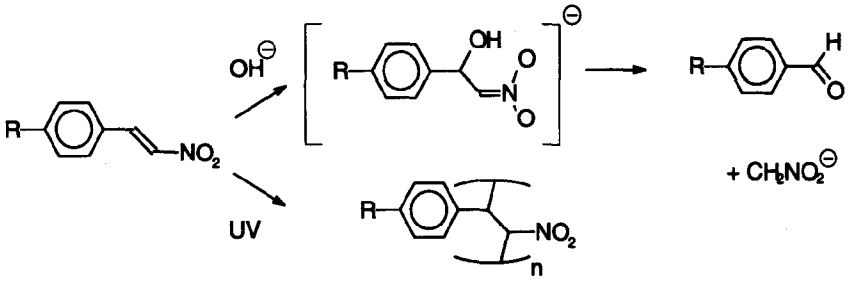

Figure 2.1 Alkaline hydrolysis and photopolymerisation of *beta*-nitrostyrenes. (Adapted from ref. 13.)

Surface-discrimination of reactions at a vesicle surface critically depends on (1) a negligible permeation of reactant(s) through the bilayer and (2) a slow rate of translocation of lipid molecules over the bilayer (*flip-flop*). These parameters are primarily governed by the thickness of the membrane and the thermotropic state of the membrane interior, which depend on the length of the hydrocarbon chains, and the temperature. In this study, lipids with *n*-dodecyl, *n*-tetradecyl, *n*-hexadecyl and *n*-octadecyl chains were examined (Figure 2.2). Since the cleavage reaction occurs in alkaline solution, non-hydrolysable *1,2*-di-*n*-alkoxypropanols rather than *1,2*-di-*n*-acyloxypropanols were used. The ether linkages make these lipids more robust against pH changes than the naturally abundant esters, without affecting other membrane properties.[14, 15] The product of hydrolytic cleavage of the BNS group in DHPBNS (*1,2*-di-*n*-hexadecyloxypropyl *p*-formylphenyl phosphate, DHPPFP) was synthesised independently. In the di-*n*-hexadecyl and di-*n*-octadecyl systems selective *exo*-vesicular cleavage of the BNS unit, followed by rapid UV-initiated polymerisation of the remaining *endo*-vesicular BNS units is possible. Thus, vesicles were obtained which contain a polymerised inner bilayer leaflet and a monomeric outer bilayer leaflet. To the best of our knowledge, these vesicles represent the first examples of surface-specifically polymerised bilayers. Only vesicles in which the counterions were polymerised in a surface-specific manner have been described previously.[9]

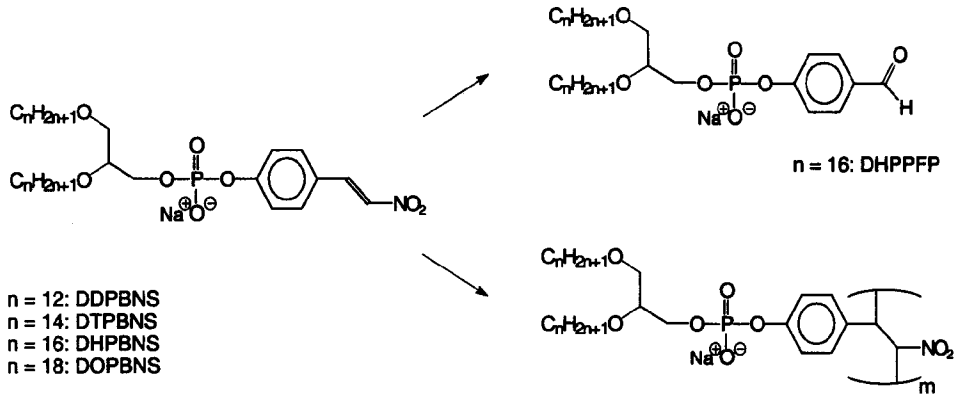

Figure 2.2 Molecular structures of the *beta*-nitrostyrene-containing lipids described in this thesis, and the products that result from alkaline hydrolysis and photopolymerisation, respectively.

2.2 Lipid synthesis

The synthetic procedures described in this section present a straightforward and efficient approach towards a new class of phospholipid derivatives, carrying a BNS unit. An outline of the synthesis is presented in Figure 2.3. The lipids were synthesised by stepwise arylation and alkylation of $POCl_3$ with 4-hydroxy-*beta*-nitrostyrene and the appropriate *1,2*-di-*n*-alkyloxypropanol. 4-Hydroxy-*beta*-nitrostyrene is most conveniently prepared by a Perkin condensation of 4-hydroxybenzaldehyde and nitromethane.[16] *1,2*-Di-*n*-alkoxypropanols were prepared by alkylation of *1*-benzyloxy-*2,3*-propanediol with *n*-alkyl triflates, followed by hydrogenation to remove the benzyl protecting group. These reactions are rapid and more efficient than other procedures previously reported.[17] All *1,2*-di-*n*-alkoxypropanols have been described,[17] and only the synthesis of *1,2*-di-*n*-dodecyloxypropanol is described in detail in the experimental section. Optimal purification of the *1,2*-di-*n*-alkoxypropanols is essential, since trace impurities such as mono-alkylated propanols, *n*-alcohols, or di-*n*-alkyl ethers may easily pass unnoticed in the final stages of the synthesis, but can be detrimental in the interpretation of bilayer studies.

Phosphorylation of 4-hydroxy-*beta*-nitrostyrene was carried out using an excess of $POCl_3$ to prevent formation of phosphodiesters and phosphotriesters. The monophenyl phosphorodichloridate thus obtained was not stable and was reacted as soon as possible with the *1,2*-di-*n*-alkyloxypropanols yielding the desired phosphodiesters. The phosphorylation reaction is applicable to the selective phosphorylation of any phenol and any primary alcohol. The final steps in the synthesis involve hydrolysis of the alkyl phenyl phosphorochloridate to the phosphoric acid, and the preparation of the sodium phosphate from the acid. These reactions may seem trivial, but the removal of chloride from the alkyl phenyl phosphorochloridate can be a surprisingly slow reaction at room temperature (see experimental), and completion is essential since remaining traces of monochloridate irreversibly react to triesters with *e.g.* alcohols.

Fortunately, the hydrolysis can be monitored easily by ^{31}P-NMR. Furthermore, addition of sodium ethanoate to the phosphoric acids should be carried out with utmost care (see experimental section) since the BNS group is extremely sensitive to alkaline media.

The results of the syntheses are summarised in Figure 2.2. Satisfying yields were obtained in most steps of the synthesis. The yields refer to the average of more than 4 experiments. No significant differences were found for yields of the syntheses of *n*-dodecyl, *n*-tetradecyl, *n*-hexadecyl, or *n*-octadecyl products. As a rule, the solubility of all intermediate compounds decreased as the hydrocarbon chain length increased.

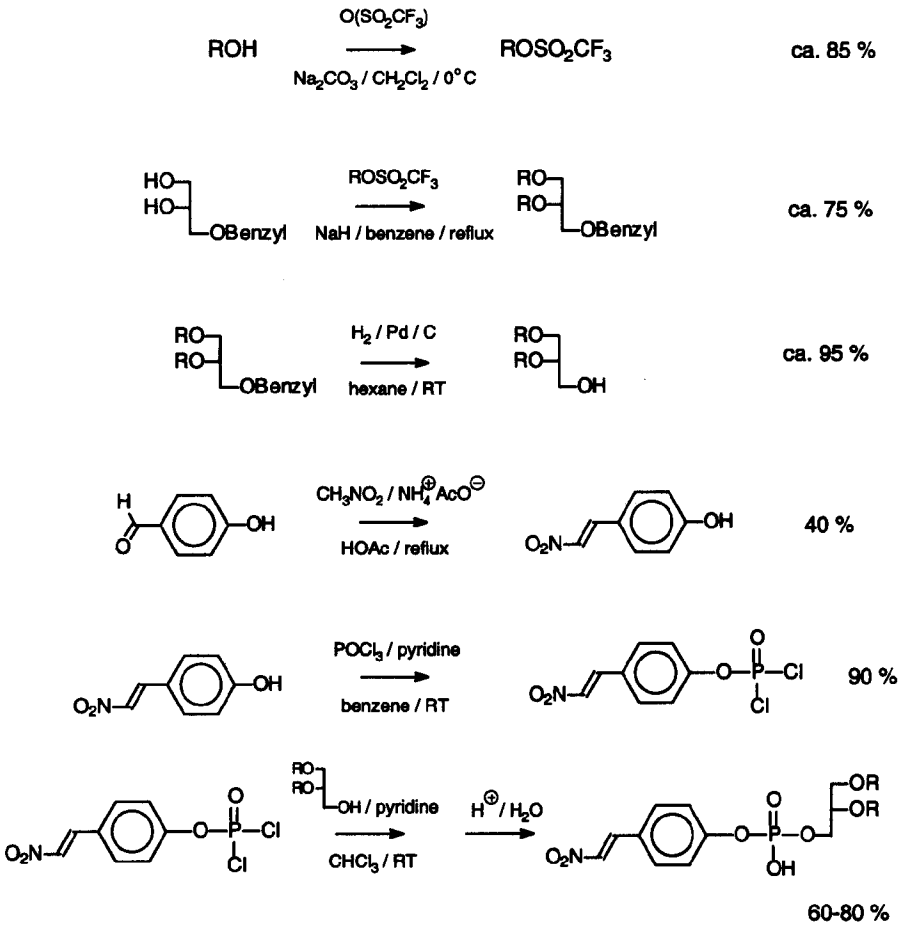

Figure 2.3 Outline of the synthesis of *1,2*-di-*n*-alkyloxypropyl-*4*-(*beta*-nitrostyryl) phosphoric acids.

2.3 Vesicle characterisation

Vesicle solutions were prepared by dispersion of the corresponding lipid films in water or 5 mM HEPES/NaAc buffer (pH 7.4) using a sonication immersion tip. Quasi-elastic light scattering revealed number-weighted averages of 50-100 nm for the diameter of vesicles of all lipids (Figure 2.4). These average diameters were confirmed using electron microscopy (Figure 2.9).

In water, all vesicle solutions are stable for at least one week. Vesicle solutions of DDPBNS and DTPBNS in buffer with physiological levels of NaCl (150 mM) are colloidally stable for many days, whereas solutions of DHPBNS and DOPBNS tend to flocculate after about 1 day at room temperature. This pattern is consistent with the general observation that vesicles are more stable at temperatures above their phase transition temperature (*vide infra*).

Differential scanning microcalorimetry revealed a clear-cut main phase transition temperature (T_m) for all lipids. The phase transitions were characterised by the temperature and enthalpy of transition, as well as the patch number n and the number of Van 't Hoff phase transitions (m) required to fit to the experimental data, which are a measure for the cooperativity of the phase transition.[18, 19] The results are summarized in Table 2.1.

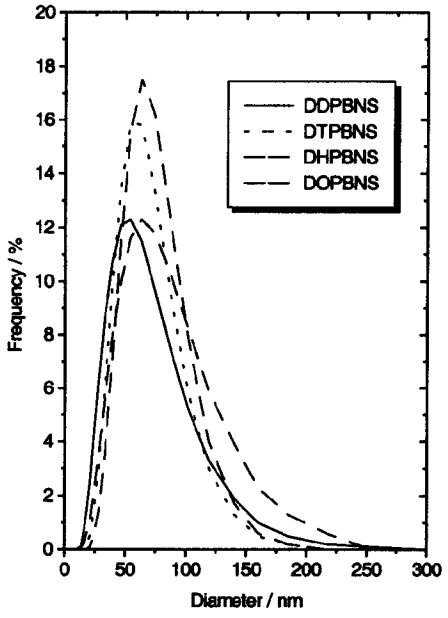

Figure 2.4 Number-weighted Gaussian size distribution of sonicated vesicles of DDPBNS, DTPBNS, DHPBNS and DOPBNS determined using quasi-elastic light scattering.

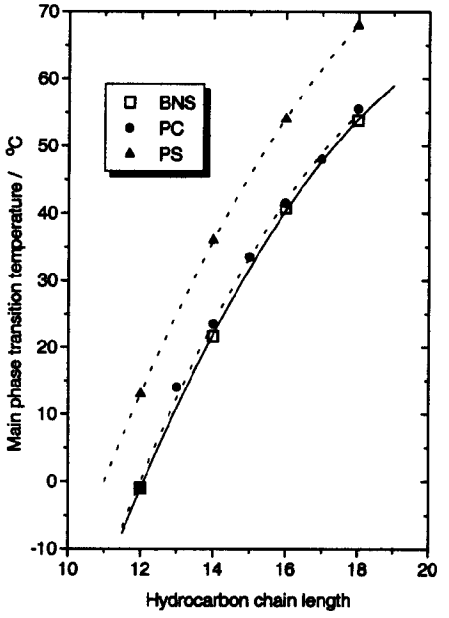

Figure 2.5 Hydrocarbon chain length dependence of the main phase transition temperature of lipids with *beta*-nitrostyryl phosphate (BNS), phosphatidylcholine (PC) and phosphatidylserine (PS) head groups.

Table 2.1 Differential scanning microcalorimetry of BNS lipid vesicles in water.

Compound	Small vesicles				Large vesicles			
	T_m (°C)	Enthalpy (kJ mol^{-1})	*n*	m	T_m (°C)	Enthalpy (kJ mol^{-1})	*n*	m
DDPBNS	n.d.	-	-	-	-1	25.0	n.d.	-
DTPBNS	n.d	-	-	-	21.6	28.5	143*	11*
DHPBNS	39.9	29.8	154	7	40.7	42.3	121	4
DOPBNS	52.0	21.6	200	6	53.8	37.8	201	5
DHPPFP	37.6	21.7	268	7	40.4	44.6	139	5

* Includes secondary transitions around 40 °C.

In accordance with the literature,[20] the phase transitions are more endothermic and more cooperative in large (possibly multilamellar) vesicles prepared by stirring (see experimental section) than in small unilammelar vesicles prepared by probe sonication. As indicated in Figure 2.5, the relation between T_m and the chain length compares well with the chain length dependence of T_m of phosphatidylcholines and phosphatidylserines reported in the literature.[21] The values of T_m for the BNS lipids are similar to those of phosphatidylcholine with identical chain length and *ca.* 13 °C lower than those reported for phosphatidylserine with identical chain length. The values of T_m for phosphatidylethanolamines are even higher than those for phosphatidylserines.[21] Apparently, the bilayer packing efficiency of the BNS lipid molecules is comparable to that of phosphatidylcholines with identical chain length. Usually, the higher T_m of phosphatidylserines and phosphatidyl-ethanolamines relative to phosphatidylcholines is attributed to more efficient head group packing due to increased head group attraction through hydrogen bonding, and concomitant reduction of head group hydration. But at pH 7.4 the phosphate head group of the BNS lipids is deprotonated, and extensive hydrogen bonding between head groups is not expected. Since there is no difference in the UV-VIS absorption spectrum of BNS lipid monomers (in water containing 25 mol% of ethanol) and BNS lipids aggregated in bilayer vesicles, specific aromatic stacking interactions of the BNS units can be excluded.

2.4 Specific *exo*-vesicular hydrolysis of *beta*-nitrostyrene in vesicle bilayers

Hydrolytic cleavage of the BNS units at the vesicle surface was initiated by dilution of an aliquot of a solution of vesicles prepared at neutral pH into an alkaline solution (pH 11.5). Alternatively, a small aliquot of NaOH solution of known concentration was added to a sample of vesicles, raising the external pH from 7.4 to 11.5. In either way, vesicles with neutral internal pH and high external pH were obtained. Surface differentiation now critically depends on the ratio between the rate of BNS hydrolysis and (1) the permeability of the bilayer to hydroxide ion (or protons) and (2) the rate of exchange of lipid molecules between the two bilayer leaflets (*flip-flop*).

Hydroxide ion/proton permeation through the bilayer (at room temperature) depends on the length of the hydrocarbon chains. The acid-base indicator Neutral Red was cosonicated

in water with DDPBNS and with DHPBNS. At 25 °C, in the case of DHPBNS, the decrease of absorbance of protonated indicator at 515 nm, representing the fraction of material included in the vesicles, amounted to less than 5 % over the time scale of the cleavage experiments. When CTAB was added to dissolve the vesicles, the absorbance at 515 nm rapidly disappeared. This observation implies that the pH gradient is maintained during the cleavage experiments in vesicles of DHPBNS, and that hydroxide ion (or proton) permeation is negligible. For DDPBNS, all protonated indicator was lost over the time scale of the cleavage experiments: therefore, at temperatures above T_m, hydroxide leakage is considerable. Similar observations were made for the bilayer permeation of carboxyfluorescein (Section 3.5).

Secondly, surface differentiation is favoured by an increase of the length of the alkyl chains and by low temperatures ($T < T_m$), because *flip-flop* is retarded by these factors.[22, 23] However, the rate of *flip-flop* also strongly depends on the nature of the hydrophilic head group.[22, 23] To date, no rationale for the head group dependence of *flip-flop* has been put forward.

In a first approximation, the cleavage process can be analysed in terms of a model in which it is assumed that the BNS units are partitioned between the *exo*-vesicular and *endo*-vesicular surface of the vesicles, and that the *exo*-vesicular part of the BNS groups is easily accessible to nucleophilic attack by hydroxide ion and will undergo a relatively rapid cleavage reaction. On the other hand, the *endo*-BNS groups are much less easily accessible (since prior to cleavage they will have to translocate over the membrane) and will undergo a much slower cleavage. The ratio of $[BNS]_{exo,0}$ and $[BNS]_{endo,0}$ depends on the vesicle diameter and the thickness of the bilayer, and may be estimated from the ratio of *endo*-surface and *exo*-surface. For spherical vesicles with a bilayer thickness of 5 nm, the *exo*-vesicular surface area as a fraction of the total surface area is 0.57 for a diameter of 80 nm, 0.55 for a diameter of 100 nm and 0.53 for a diameter of 200 nm. In kinetic equations:

$$d[BNS]_{exo}/dt = - k_{fast}[OH^-][BNS]_{exo} \quad \text{and} \quad d[BNS]_{endo}/dt = - k_{slow}[OH^-][BNS]_{endo}$$

UV-VIS spectroscopy does not discriminate between $[BNS]_{exo}$ and $[BNS]_{endo}$, and so the decrease of $[BNS]_{exo+endo}$ in time is monitored:

$$[BNS]_{exo+endo,t} = [BNS]_{exo,0} \exp(- k_{fast} [OH^-] t) + [BNS]_{endo,0} \exp(- k_{slow} [OH^-] t)$$

The latter equation may be simplified to a double pseudo-first-order rate equation:

$$[BNS]_{exo+endo,t} = [BNS]_{exo,0} \exp(- k'_{fast} t) + [BNS]_{endo,0} \exp(- k'_{slow} t)$$

In a system in which the *endo*-BNS groups are as easily accessible to hydroxide as the *exo*-BNS groups (k'_{fast} equals k'_{slow}), no surface differentiation is possible and the kinetics simplify to a pseudo-first-order rate equation:

$$[BNS]_{tot,t} = [BNS]_{tot,0} \exp(- k'' t)$$

Table 2.2 Rate constants of alkaline hydrolysis of BNS lipids.

Experiment*			k'_{fast}	k'_{slow}	k'_2	k_1	k'_2/k_1	BNS_{endo}/BNS_{tot}
1	*p*-OH-BNS		2.56					
2	DDPBNS	+ 25 % EtOH	12.8					
3		tip	10.2				1.0	
4		injection	9.89					
5		+ CTAB	142					
6	DTPBNS	tip	5.11	0.584	4.32	0.680	6.4	<0.20
7	DHPBNS	+ 25 % EtOH	13.3					
8		tip	5.49	0.316	5.13	0.343	15	0.43
9		tip, T = 46 °C	21.4					
10		injection	7.33	0.769	6.32	0.893	7.1	<0.30
11		+ CTAB	133					
12	DOPBNS	tip	6.24	0.095	6.15	0.100	62	0.47

* Vesicle solutions were prepared by sonication with an immersion tip (tip) or by the ethanol injection method (injection). T = 25 °C unless indicated otherwise. Rate constants are reported in units of 10^{-4} s^{-1}.

The results of several experiments are presented in Table 2.2. As expected, the cleavage of 4-hydroxy-*beta*-nitrostyrene (which is deprotonated, therefore anionic above pH 7.8) is slower than that of the BNS lipid monomers (run 1 *vs* 2, 7). Also, the cleavage in BNS lipid monomer solutions (aqueous solutions containing 25 mol% of ethanol) is more rapid than the cleavage of lipids aggregated in vesicles (run 2 *vs* 3, 4 and 7 *vs* 8, 10). Obviously, the negatively charged membrane retards the nucleophilic attack by hydroxide ion. Disruption of the bilayer structure by the detergent CTAB leads to a 15-25 fold increase of the rate of cleavage (runs 3, 4 *vs* 5 and 8,10 *vs* 11). In the presence of CTAB, the reaction is even accelerated ten-fold relative to the cleavage in a solution of lipid monomers (runs 2 *vs* 5 and 7 *vs* 11), which suggests cationic CTAB micelles have a catalytic effect.

Runs 1-5, 7 and 11 all follow smooth first-order kinetics, indicating equal accessibility of all BNS groups present to hydroxide nucleophilic attack. Apparently, in vesicles of DDPBNS, $k'_{slow} = k'_{fast}$ and surface differentiation is impossible at room temperature. However, cleavage of the BNS unit in vesicles formed from DTPBNS, DHPBNS and DOPBNS can be treated much more accurately in terms of a double exponential decay, reflecting fast cleavage of the *exo*-vesicular BNS and slow cleavage of the *endo*-vesicular BNS (runs 6, 8, 10, 12). In these cases, the analysis in terms of a fast and a slow process is satisfying, but perhaps oversimplified. Therefore the model was extended to include *flip-flop* of lipid molecules, as indicated in Figure 2.6. With lipid *flip-flop* characterised by k_1 and k_{-1} and *exo*-vesicular hydrolysis of BNS by $k'_2 = k_2[OH^-]$:

$$d[BNS]_{endo}/dt = - k_1[BNS]_{endo} + k_{-1}[BNS]_{exo}$$

$$d[BNS]_{exo}/dt = k_1[BNS]_{endo} - k_{-1}[BNS]_{exo} - k'_2[BNS]_{exo}$$

Leading to an equation of the form:

$$[BNS]_{endo+exo,t} = C_a\exp(-k'_{slow}t) + C_b\exp(-k'_{fast}t)$$

The solution for $[BNS]_{endo+exo,t}$ may be found using Laplace transforms, as described in the appendix of this chapter. C_a, C_b, k'_{slow} and k'_{fast} are combinations of $[BNS]_{exo,0}$, $[BNS]_{endo,0}$, k_1, k_{-1} and k'_2. Thus, assuming k_1 equals k_{-1} (lipid molecules *flip* and *flop* at equal rate), k_1 and k'_2 may be calculated from the experimentally determined values of k'_{slow} and k'_{fast}. The results are reported in Table 2.2.

The second model is superior to the first model. Whereas k'_2 values are quite similar for all BNS derivatives (the differences are attributed to small variations in external pH and perhaps vesicle composition), there is a clear trend in k_1. As can be seen from the value of k'_2/k_1 in Table 2.2, *endo*-vesicular cleavage is most significant in the vesicles of the lipid with the shortest alkyl chain (DTPBNS, run 6), in which most rapid *flip-flop* is anticipated.[22, 23] At 25 °C, surface differentiation in these vesicles is difficult to carry out experimentally, since k_1 is relatively large.

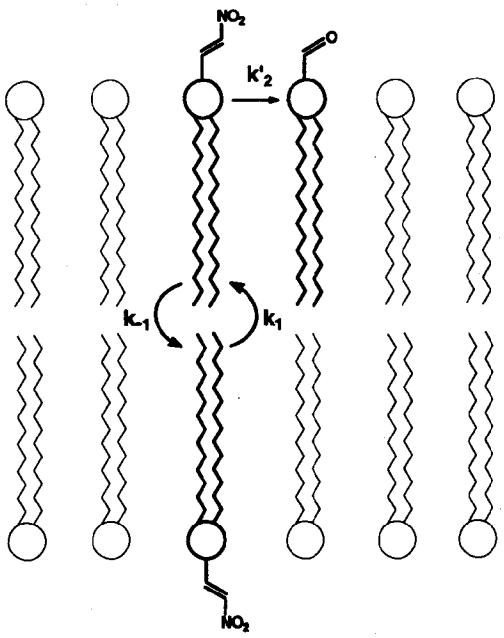

Figure 2.6 Kinetic model for the surface-specific hydrolysis of the BNS moiety and lipid *flip-flop* in bilayer vesicles. Top: *exo*-vesicular leaflet. Bottom: *endo*-vesicular leaflet. Lipid structures have been simplified for clarity.

On the other hand, in vesicles of DHPBNS and DOPBNS, k_1 is small relative to k'_2 (runs 8 and 12). Surface differentiation is easily achieved and can be maintained over periods of several hours (the half-life of *flip-flop* in vesicles of DHPBNS is more than 6 hrs). These rates of *flip-flop* are similar to those reported for comparable model systems.[7] The BNS persisting in the DHPBNS and DOPBNS vesicle systems after more than 4 half-lifes of the exo-vesicular cleavage reaction is unreacted *endo*-BNS. The relative amounts of *exo*-BNS and *endo*-BNS match expectations from theory.

At temperatures above T_m, k_1 approaches k'_2 and the cleavage reaction follows first-order kinetics (runs 3, 4, 9). Most likely, this result is due to much faster *flip-flop* above T_m. Also, above T_m considerable hydroxide leakage is expected. In either case, the T_m of DDPBNS is too low to allow specific *exo*-vesicular cleavage at room temperature. In vesicles of DHPBNS prepared by the ethanol injection method (run 10), a much higher k_1 was found. Possibly, the small amount of ethanol in the system induces faster *flip-flop* and concomitantly more hydroxide leakage. Even very small amounts of ethanol affect bilayer phase transitions and dynamics.[24,25] Therefore, it is unadvisable to use the ethanol injection method for preparation of surface differentiated vesicles.

Figure 2.7 presents the hydrolysis of the BNS moieties in DHPBNS vesicles under various experimental conditions, and illustrates the approach to surface-differentiated vesicles. At 25 °C, the *exo*-vesicular BNS groups are hydrolysed with a half-life of *ca.* 25 minutes ($k'_2 = 5.13\ 10^{-4}\ s^{-1}$), but the *endo*-vesicular BNS groups remain unaffected for several hours because only slow *flip-flop* occurs ($k_1 = 3.43\ 10^{-6}\ s^{-1}$) and the pH gradient is maintained. When CTAB is added, the vesicles are solubilised and the remaining BNS groups hydrolyse rapidly under CTAB micellar catalysis. If the reaction is carried out at 46 °C, both *flip-flop* and leakage are rapid, and all BNS groups react equally fast ($k'_2 = 2.14\ 10^{-3}\ s^{-1}$).

Figure 2.7 also presents data for the hydrolysis of the BNS moieties in DDPBNS vesicles at room temperature and at 5 °C. At room temperature and pH 11.5, hydroxide/proton leakage and lipid *flip-flop* are rapid, and *exo* and *endo*-vesicular BNS groups hydrolyse equally fast ($k' = 1\ 10^{-3}\ s^{-1}$, Table 2.2). However, when the hydrolysis is performed at 5 °C and pH 12 (the hydrolysis is too slow at pH 11.5), a reasonable degree of surface discrimination can be achieved because leakage and *flip-flop* are reduced. A double exponential fit to the decrease of $[BNS]_{endo+exo}$ in time yields the rate of *exo*-vesicular hydrolysis $k'_2 = 3.4\ 10^{-4}\ s^{-1}$ and the rate of *flip-flop* $k_1 = 9.0\ 10^{-5}\ s^{-1}$. The ratio of $k'_2/k_1 = 4$ and surface discrimination in DDPBNS vesicles is possible if the vesicles are kept at *low* temperature.

Quasi-elastic light scattering (Figure 2.10) and electron microscopy (data not shown) showed that sonicated vesicles of DHPPFP, the product of the hydrolysis of DHPBNS, have similar size as vesicles of DHPBNS. In the DSC enthalpogram of large vesicles of DHPPFP, a T_m of 40.4 °C was observed (Table 2.1). Using the technique of diphenylhexatriene fluorescence depolarisation, a T_m of 40 °C was determined. (This alternative method is not compatible with the BNS lipids, because the strong absorbance at 335 nm quenches DPH excitation.) According to DSC, the enthalpy of the main phase transition is 44.6 kJ mol^{-1}. For DHPBNS, T_m is 40.7 °C and the enthalpy of transition is 42.3 kJ mol^{-1} (Table 2.1). Evidently, the cleavage reaction neither influences the vesicle size nor the thermotropic behaviour of the bilayer.

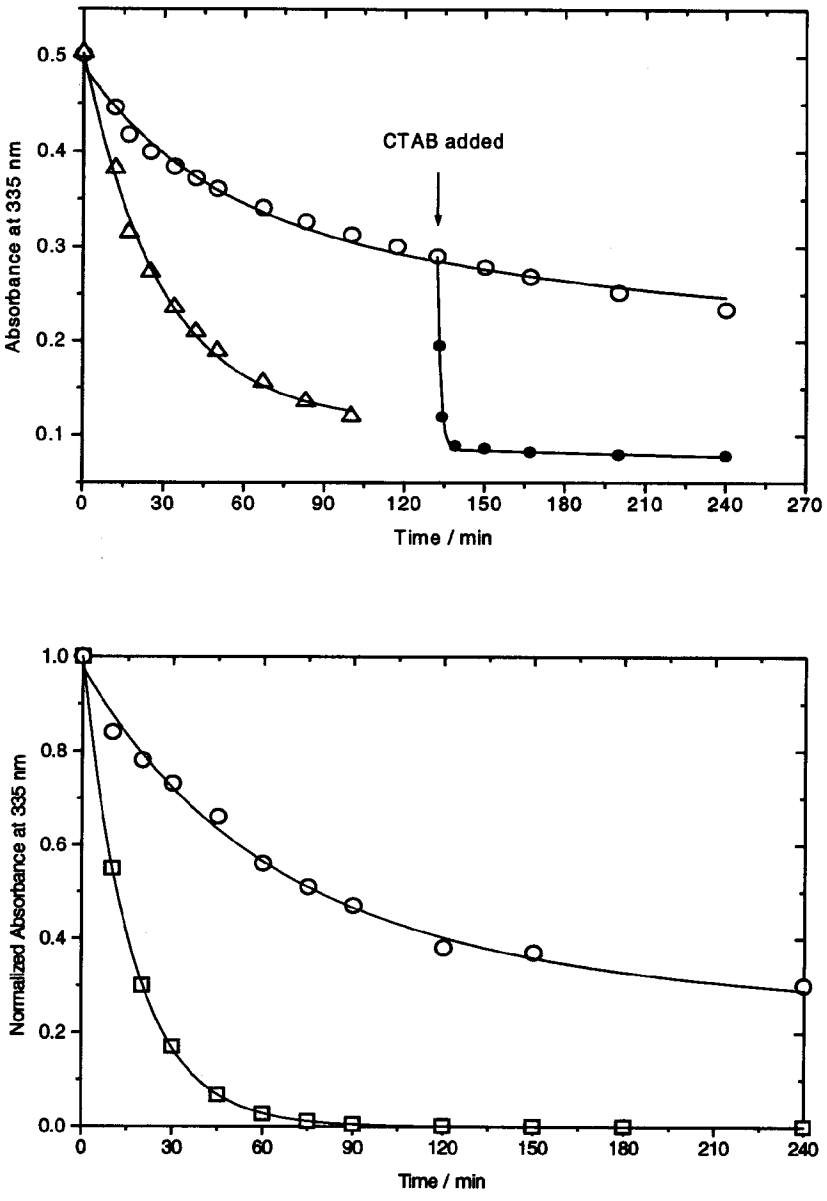

Figure 2.7 (Top) Decrease of BNS absorbance in time during hydrolysis of DHPBNS vesicles at pH 11.5. Circles: selective *exo*-vesicular hydrolysis at 25 °C. Triangles: aspecific hydrolysis at 46 °C. Closed circles: solubilisation of the vesicles by CTAB after two hours selective *exo*-vesicular hydrolysis at 25 °C, and fast hydrolysis of the remaining *endo*-vesicular BNS groups. (Bottom) Hydrolysis of the BNS groups of vesicles of DDPBNS. The absorbance has been normalised according to $A_{N,t} = (A_t - A_{inf})/(A_0 - A_{inf})$. Circles: selective *exo*-vesicular hydrolysis at 5 °C and pH 12. Squares: aspecific hydrolysis at 25 °C and pH 11.5.

2.5 Photopolymerisation of *beta*-nitrostyrene in vesicle bilayers

Rapid photopolymerisation of the BNS moiety was achieved by intense UV irradiation. No initiator was required. No monomer could be detected (^{1}H-NMR, UV-VIS) after irradiation for 10 minutes (Figure 2.8). Polymerisation of *beta*-nitrostyrene in organic solution is difficult,[11,12] but it is known that polymerisation reactions entropically benefit from the close proximity of the monomers in the bilayer.[26,27] In fact, it became apparent that polymerisation in vesicles also takes place under influence of sunlight and heating (as evidenced by a gradual loss of BNS absorbance at 335 nm), whereas the pure lipids or lipid stock solutions are stable. Therefore, vesicle solutions were always protected from sunlight and prolonged heating. Light scattering (Figure 2.9) and electron microscopy (Figure 2.10) showed that the average size, morphology and integrity of the vesicles were unaffected by the polymerisation.

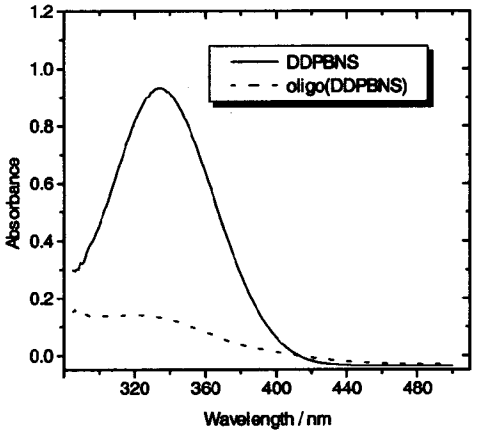

Figure 2.8 Disappearance of BNS absorbance after 10 minutes photopolymerisation of DDPBNS.

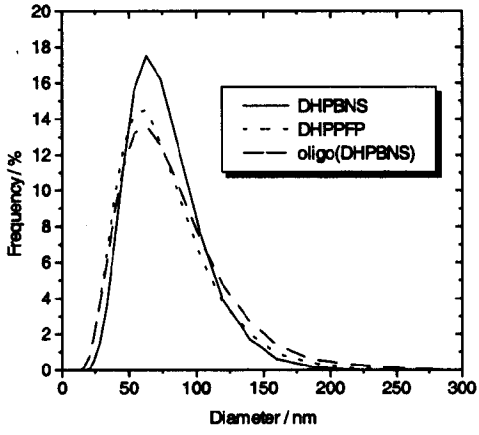

Figure 2.9 Number-weighted size distribution of sonicated vesicles of DHPBNS, DHPPFP ('hydrolysed DHPBNS') and polymerised DHPBNS, determined using light scattering.

Characterisation of a lipid polymer is difficult due to its amphiphilic nature and is usually accomplished after removal of the hydrophobic moiety by means of transesterification.[28,29,30,31] However, these compounds are alkyl ethers, and also the phosphodiester is surprisingly stable to hydrolytic conditions. Gel permeation chromatography (which has been applied succesfully to comparable materials)[27,32] of poly-(DHPBNS) was not successful. No cyclobutane-like dimers[11] could be detected in the electrospray mass spectrum of poly(DDPBNS). Vapour pressure osmometry yielded an average molecular weight (M_n) for poly(DDPBNS) of 2.47 10^3, corresponding to an average polymerisation degree of 3.8. Unfortunately, this technique is time-consuming and demands large amounts of material for each analysis. In addition, since osmometry is extremely sensitive to the presence of low-molecular weight impurities (such as water and salts) the molecular weight should be considered a low estimate.

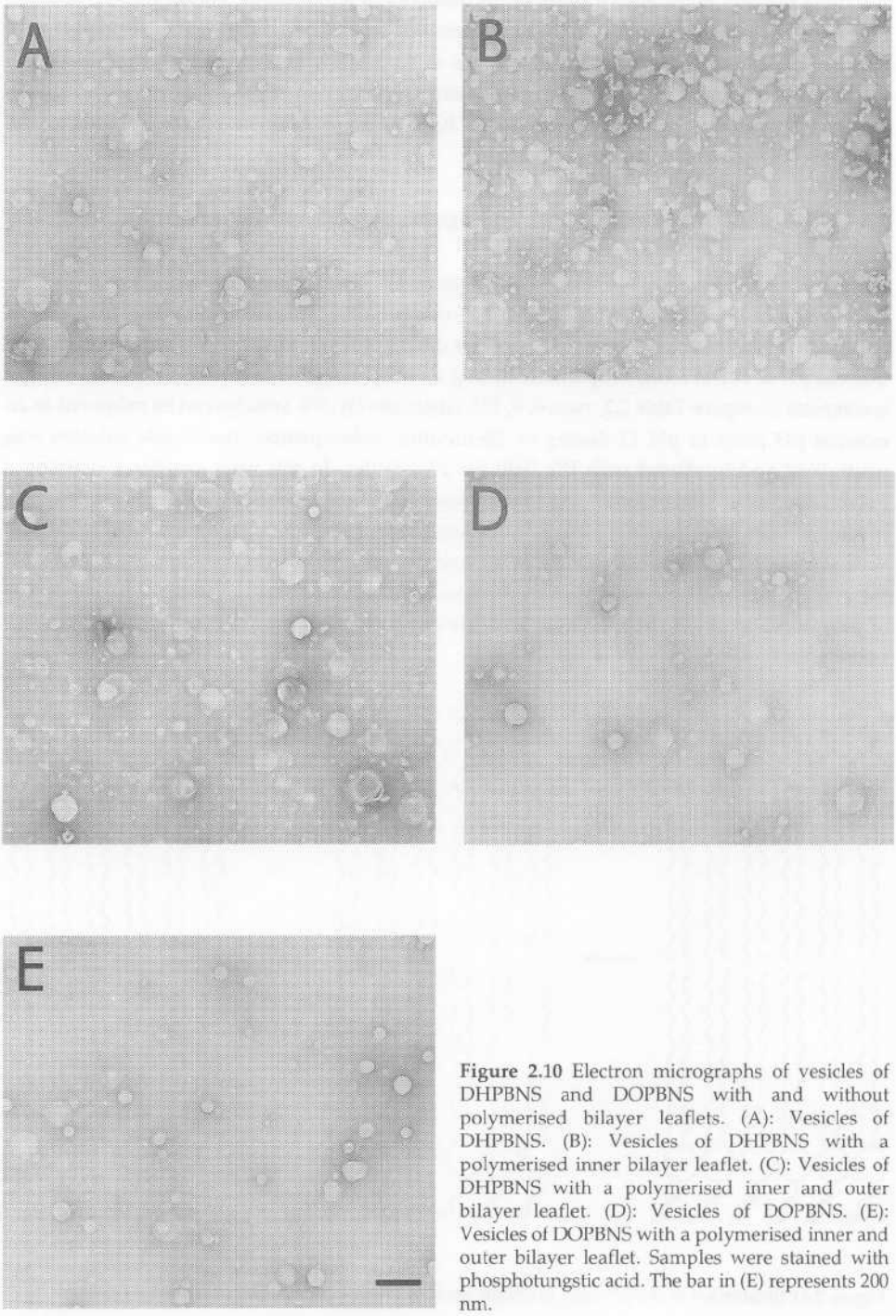

Figure 2.10 Electron micrographs of vesicles of DHPBNS and DOPBNS with and without polymerised bilayer leaflets. (A): Vesicles of DHPBNS. (B): Vesicles of DHPBNS with a polymerised inner bilayer leaflet. (C): Vesicles of DHPBNS with a polymerised inner and outer bilayer leaflet. (D): Vesicles of DOPBNS. (E): Vesicles of DOPBNS with a polymerised inner and outer bilayer leaflet. Samples were stained with phosphotungstic acid. The bar in (E) represents 200 nm.

For these reasons, no extensive study of the influence of temperature, concentration, addition of initiator, irradiation time, *etc.* on the polymerisation was carried out. It was concluded that 10 minutes of intense UV irradiation of vesicles of BNS lipids at room temperature results in formation of oligomers rather than long polymers. Optimisation of the polymerisation reaction awaits further study. The reader is refered to Chapter 3 for an extensive characterisation of the properties of vesicles of oligomerised lipids.

2.6 Preparation of vesicles with an oligomerised inner bilayer leaflet

Combination of selective *exo*-vesicular hydrolysis and *endo*-vesicular polymerisation of the BNS lipids presents a simple method for preparing vesicles having a highly asymmetric bilayer. The approach is illustrated in Figure 2.11. Vesicles of DHPBNS and DOPBNS were exposed to an external pH of 11.5 at room temperature during *ca.* 1.5 hours, after which *exo*-vesicular cleavage is complete (compare Table 2.2, runs 6, 8, 12). Alternatively, the vesicles can be subjected to an external pH jump to pH 12 during *ca.* 25 minutes. Subsequently, the vesicle solution was neutralised and irradiated with UV light for 10 minutes. In this way, vesicles containing a polymerised inner bilayer leaflet and a monomeric outer bilayer leaflet were obtained. Samples of these vesicles were examined using light scattering and electron microscopy. Neither the *exo*-vesicular hydrolytic cleavage, nor the *endo*-vesicular polymerisation had significantly affected the average size and morphology of the vesicles (Figure 2.9 and 2.10). Presumably, the degree of polymerisation of the inner bilayer leaflet is similar for vesicles in which both leaflets were polymerised.

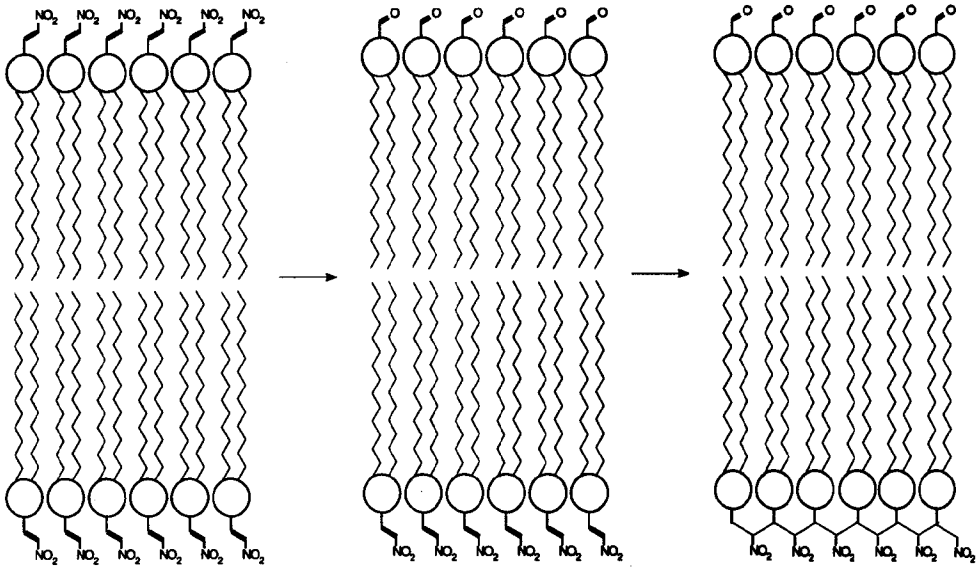

Figure 2.11 Illustration of the protocol to obtain vesicles with a polymerised inner bilayer leaflet.

2.7 Conclusions

This chapter presented a new class of bifunctional vesicle-forming amphiphiles containing BNS units linked to the phosphate headgroup. Under the appropriate experimental conditions, these units are amenable to specific *exo*-vesicular hydrolysis and can undergo rapid photopolymerisation in the bilayer. In addition, it is possible to generate vesicles containing a polymerised inner bilayer leaflet, and a monomeric outer bilayer leaflet. Such vesicles represent an extreme case of transverse bilayer membrane asymmetry. A general characterisation of the properties of vesicles with oligomerised lipid bilayers will be described in Chapter 3, and studies of the fusogenic behaviour of such bilayers are presented in Chapters 4 to 7.

2.8 Experimental section

Synthesis The phosphorylation reactions were carried out under nitrogen atmosphere. NMR spectra were recorded in deuterated chloroform solution using 200 or 300 MHz Varian machines, unless a different solvent is indicated. Elemental analyses were carried out in the analytical department of our laboratory by Jan Ebels, Jannes Hommes and Harm Draaijer. All solvents used were dried and purified by distillation.

***n*-Dodecyltriflate** A solution of *n*-dodecanol (9.3 g, 50 mmol, 1.0 eq.) in CH_2Cl_2 (25 mL) was added dropwise into a suspension of Na_2CO_3 (5.3 g, 50 mmol, 1.0 eq.) and trifluoromethanesulfonic acid anhydride (10 mL, 60 mmol, 1.2 eq.) in dry CH_2Cl_2 (50 mL) at 0 °C. The mixture was stirred at 0 °C for 2 hours. The solids were removed by column filtration (2.5 cm, 30 g silica). The column was rinsed with 200 mL of CH_2Cl_2. The solvent was evaporated and a colourless solid (12.7 g, 40 mmol, 80 %) was obtained. ^{1}H-NMR: 4.55 (t, 2H, OCH_2), 1.82 (m, 2H, $OCH_2\underline{CH_2}$), 1.27 (m, 18H, chain), 0.89 (t, 3H, CH_3) ppm.

***1*-Benzyloxy-2,3-di-*n*-dodecyloxypropane** A solution of *1*-benzyloxypropanol (2.80 g, 15.3 mmol, 1.0 eq.) in benzene (20 mL) was slowly added to a suspension of sodium hydride (1.3 g, 32 mmol, 2.1 eq., rinsed twice with 5 mL hexane) in benzene (50 mL). The mixture was refluxed for 1.5 hours. After cooling to room temperature, a solution of *n*-dodecyltriflate (10.0 g, 31 mmol, 2.0 eq.) in benzene (20 mL) was added to the reaction mixture. After 2 hours a small additional amount of NaH was added. The gel-like solution was refluxed for 8 hours. Complete conversion of the triflate was verified by ^{1}H-NMR. Subsequently the solution was diluted with ether (100 mL) and the precipitate was removed by filtration over celite. After evaporation of the solvent, the crude product was obtained as a viscous oil (7.0 g, 13.5 mmol, 88 %). ^{1}H-NMR: 7.33 (s, 5H, Ph), 4.55 (s, 2H, OCH_2Ph), 3.56 (m, 9H, $4CH_2O$+CHO), 1.59 (m, 4H, $2OCH_2\underline{CH_2}$), 1.25 (s, 36H, chains), 0.88 (t, 6H, $2CH_3$) ppm. ^{13}C-NMR: 128.29 (CH), 127.58 (CH), 127.48 (CH), 77.91 (CHO), 73.34 (CH_2O), 71.66 (CH_2O), 70.72 (CH_2O), 70.62 (CH_2O), 70.28 (CH_2O), 31.94 (CH_2), 30.12 (CH_2), 29.71 (CH_2), 29.66 (CH_2), 29.52 (CH_2), 29.37 (CH_2), 26.12 (CH_2), 22.70 (CH_2), 14.14 (CH_3) ppm.

***1,2*-Di-*n*-dodecyloxypropanol** A solution of *1*-benzyloxy-2,3-di-*n*-dodecyloxypropane (7.0 g, 13.5 mmol) in hexane (75 mL) containing palladium on carbon (0.3 g, 5 % Pd) was stirred under H_2

for 16 hours. The catalyst was removed by column filtration (1.5 cm, 5 g celite). The column was rinsed with $CHCl_3$ (100 mL). The solvent mixture was evaporated and a solid was obtained (5.4 g, 12.6 mmol, 93 %). The crude product was purified by chromatography over a column of 80 g silicagel using $CHCl_3$ (gradually enriched with diethyl ether) as eluent. R_f ($CHCl_3$/ether 3/1) = 0.5, R.t. (GC 200/150) = 6.8 minutes. The main impurity was identified as didodecyl ether (R_f 0.8, R.t. 2.3 minutes). M.p. of the product is 38-39 °C. ^{1}H-NMR: 3.52 (m, 9H, $4OCH_2$+OCH), 2.23 (br s, 1H, OH), 1.57 (m, 4H, $2OCH_2\underline{CH_2}$), 1.27 (s, 36H, chains), 0.89 (t, 6H, $2CH_3$) ppm. ^{13}C-NMR: 78.23 (CHO), 71.85 (CH_2O), 70.92 (CH_2O), 70.40 (CH_2O), 63.12 (CH_2OH), 31.93 (CH_2), 30.08 (CH_2), 29.71 (CH_2), 29.63 (CH_2), 29.48 (CH_2), 29.37 (CH_2), 26.10 (CH_2), 22.70 (CH_2), 14.12 (CH_3) ppm.

4-Hydroxy-*beta*-nitrostyrene The product was prepared in 40 % yield from 4-hydroxybenzaldehyde and nitromethane according to a literature procedure.[16] ^{1}H-NMR (D_6-DMSO): 8.04 (s, 2H), 7.70 (d, J_{ortho} = 8.5 Hz, 2H), 6.82 (d, J_{ortho} = 8.5Hz, 2H) ppm. ^{1}H-NMR (C_6D_6): 7.79 (d, J_{trans} = 13 Hz, 1H), 7.33 (d, J_{trans}, 1H), 7.15 (br s, 2H), 7.02 (br s, 2H) ppm. ^{13}C-NMR (D_6-DMSO): 161.52 (C_q), 139.86 (CH), 134.81 (CH), 132.28 (CH), 121.08 (C_q), 116.15 (CH) ppm.

4-(*beta*-Nitro)styrylphosphorodichloridate A solution of pyridine (0.50 mL, 6.2 mmol, 1.0 eq.) in benzene (5 mL) was slowly added to a mixture of 4-hydroxy-*beta*-nitrostyrene (1.00 g, 6.1 mmol, 1.0 eq.) and $POCl_3$ (10 mL, 110 mmol, 15.7 eq.) in benzene (20 mL). The mixture was stirred at room temperature for 1 hour. The reaction mixture coloured from orange to yellow-green. Pyridinium chloride precipitated, and was removed by filtration. Subsequently ether (20 mL) was added to the filtrate, and remaining pyridinium chloride precipitate was removed. The solvents and the surplus of $POCl_3$ were removed by evaporation and ether (20 mL) was added again. The yellow solution was kept at -20 °C and the product crystallised. The solvent was removed with a pipet (alternatively, if no crystallisation occurred, the product was isolated by evaporation) and the product was dried in vacuum (< 1 mm Hg). A bright yellow solid (1.46 g, 5.2 mmol, 86 %) was obtained, m.p. = 85-88 °C. It colours upon standing, and should be used within a few hours. ^{1}H-NMR: 8.00 (d, J_{trans} = 13.7 Hz, 1H), 7.62 (d, J_{ortho} = 9 Hz, 2H), 7.57 (d, J_{trans}, 1H), 7.40 (dd, J_{ortho}, J_{PH} = 2 Hz, 2H) ppm. ^{13}C-NMR: 151.90 (C_q), 137.95 (CH), 137.00 (CH), 131.08 (CH, d, J_{PC} = 2.4 Hz), 129.12 (C_q, d, J_{PC} = 2.4 Hz), 121.69 (CH, d, J_{PC} = 6.4 Hz) ppm.^{31}P-NMR: 3.45 ppm.

1,2-Di-*n*-dodecyloxypropyl-4-(*beta*-nitrostyryl) phosphoric acid (DDPBNS) A solution of pyridine (0.22 mL, 2.7 mmol) and 1,2-di-*n*-dodecyloxypropanol (0.64 g, 1.5 mmol) in CH_2Cl_2 (10 mL) was slowly added to 4-(*beta*-nitro)styrylphosphorodichloridate. (0.75 g, 2.7 mmol) in CH_2Cl_2 (12 mL). The mixture was stirred for 2 hours at room temperature. The reaction mixture was quenched by adding it to a mixture of 50 mL ether, 15 mL H_2O and 2.5 mL 1 M HCl. After 1 night stirring, it was verified that the phosphoromonochloridate had completely hydrolysed, and its characteristic signals at 4.4 ppm (^{1}H-NMR) and 1.5 ppm (^{31}P-NMR) had disappeared. The aqueous layer was removed. The ether solution was washed with water (pH 5) and brine, dried over Na_2SO_4, and the solvent was removed. The crude product (*ca.* 1 g) was crystallised from methanol at -20 °C and 0.74 mg (1.1 mmol, 75 %) of a yellow solid was obtained, m.p. 25 °C. ^{1}H-NMR: 7.93 (d, J_{trans} = 13.5 Hz, 1H), 7.55 (d, J_{ortho} = 10 Hz, 2H), 7.55 (d, J_{trans}, 1H), 7.29 (d, J_{ortho}, 2H),

4.20 (m, 2H), 3.47 (m, 7H, $3OCH_2$+OCH), 1.52 (m, 4H, $2OCH_2\underline{CH_2}$), 1.25 (s, 36H, chains), 0.88 (t, 6H, $2CH_3$) ppm. ^{31}P-NMR: -6.00 ppm. Analysis calculated for $C_{35}H_{62}NPO_8$: C 64.08 %, H 9.53 %, N 2.14 %, P 4.72 %. Found: C 64.30 %, H 9.75 %, N 2.09 %, P 4.70 %. HPLC on Chiralpak AD using hexane/2-propanol/TFA 75/25/0.1 as eluent: R.t. = 22 minutes.

1,2-Di-*n*-tetradecyloxypropyl-4-(*beta*-nitrostyryl) phosphoric acid (DTPBNS) The product was prepared from 4-(*beta*-nitro)styrylphosphorodichloridate (410 mg, 1.45 mmol) and 1,2-di-*n*-tetradecyloxypropanol (480 mg, 1.0 mmol) as described for DDPBNS. 700 mg (0.98 mmol, 98 %) of a yellow solid was obtained, m.p. = 43-45 °C. ^{1}H-NMR: 7.95 (d, J_{trans} = 14 Hz, 1H), 7.55 (d, J_{trans}, 1H), 7.55 (d, J_{ortho} = 9 Hz, 2H), 7.30 (d, J_{ortho}, 2H), 4.25 (m, 2H), 3.55 (m, 7H), 1.55 (m, 4H), 1.30 (s, 44H, chains), 0.90 (t, 6H, $2CH_3$) ppm. ^{31}P-NMR: -5.04 ppm. Analysis calculated for $C_{39}H_{70}NPO_8$: C 65.82 %, H 9.85 %, N 1.97 %, P 4.36 %. Found: C 65.64 %, H 9.74 %, N 1.91 %, P 4.15 %.

1,2-Di-*n*-hexadecyloxypropyl-4-(*beta*-nitrostyryl) phosphoric acid (DHPBNS) The product was prepared from 4-(*beta*-nitro)styrylphosphorodichloridate (410 mg, 1.45 mmol) and 1,2-di-*n*-hexadecyloxypropanol (540 mg, 1.0 mmol) as described for DDPBNS. The crude product was crystallised from methanol (0.90 g in 40 mL). 420 mg (0.55 mmol, 55 %) of product with m.p. = 49-52 °C was isolated. ^{1}H-NMR: 7.95 (d, J_{trans} = 13.5 Hz, 1H), 7.51 (d, J_{ortho} = 8.5 Hz, 2H), 7.51 (d, J_{trans}, 1H), 7.27 (d, J_{ortho}, 2H), 4.20 (m, 2H, CH_2OP), 3.48 (m, 7H, $3CH_2O$+CHO), 1.52 (m, 4H, $2OCH_2\underline{CH_2}$), 1.25 (s, 52H, chain), 0.90 (t, 6H, $2CH_3$) ppm. ^{13}C-NMR: 153.41 (C_q), 137.67 (CH), 136.81 (CH), 130.67 (CH, d, J_{PC} = 8.5 Hz), 126.77 (C_q), 121.06 (CH, d, J_{PC} = 4.9 Hz), 71.83 (CH_2O), 70.79 (CH_2O), 69.17 (CH_2O), 67.71 (CH_2OP, d, J_{PC} = 6.1 Hz), 31.82 (CH_2), 29.96 (CH_2), 29.84 (CH_2), 29.80 (CH_2), 29.73 (CH_2), 29.62 (CH_2), 29.57 (CH_2), 29.47 (CH_2), 29.39 (CH_2), 29.26 (CH_2), 25.96 (CH_2), 25.88 (CH_2), 22.60 (CH_2), 14.02 (CH_3) ppm (CHO under solvent signal). ^{31}P-NMR: -5.90 ppm. Analysis calculated for $C_{43}H_{78}NPO_8$: C 67.28 %, H 10.17 %, N 1.83 %, P 4.04 %. Found: C 67.88 %, H 10.52 %, N 1.59 %, P 3.82 %.

1,2-Di-*n*-octadecyloxypropyl-4-(*beta*-nitrostyryl) phosphoric acid (DOPBNS) The product was prepared from 4-(*beta*-nitro)styrylphosphorodichloridate (841 mg, 3.00 mmol) and 1,2-di-*n*-octadecyloxypropanol (1.40 g, 2.34 mmol) as described for DDPBNS. The crude product was crystallised from methanol (80 mL) and from a mixture of acetone (25 mL) and acetonitrile (5 mL). 1.17 mg (1.42 mmol, 61 %) of pure product with m.p. = 55-57 °C was isolated. ^{1}H-NMR: 7.96 (d, J_{trans} = 13.5 Hz,1H), 7.53 (d, J_{ortho} = 8.5 Hz, 2H), 7.53 (d, J_{trans}, 1H), 7.30 (d, J_{ortho}, 2H), 4.17 (m, 2H, CH_2OP), 3.49 (m, 7H, $3CH_2O$+CHO), 1.54 (m, 4H, $2OCH_2\underline{CH_2}$), 1.26 (s, 60H, chains), 0.89 (t, 6H, $2CH_3$) ppm. ^{13}C-NMR: 153.43 (C_q), 137.65 (CH), 136.87 (CH), 130.61 (CH), 126.84 (C_q), 121.10 (CH, d, J_{PC} = 6.1 Hz), 77.00 (CHO), 71.84 (CH_2O), 70.83 (CH_2O), 69.24 (CH_2O), 67.77 (CH_2OP, d, J_{PC} = 6.1 Hz), 31.84 (CH_2), 29.81 (CH_2), 29.80 (CH_2), 29.64 (CH_2), 29.57 (CH_2), 29.49 (CH_2), 29.41 (CH_2), 29.28 (CH_2), 25.98 (CH_2), 25.91 (CH_2), 22.60 (CH_2), 14.02 (CH_3) ppm. ^{31}P-NMR: -5.35 ppm. Analysis calculated for $C_{47}H_{86}NPO_8$: C 68.49 %, H 10.52 %, N 1.70 %, P 3.76 %. Found: C 67.82 %, H 10.59 %, N 1.44 %, P 3.43 %.

4-Formylphenylphosphorodichloridate The product was prepared from 4-hydroxy benzaldehyde (366 mg, 3.0 mmol) and $POCl_3$ (4.0 mL, 42 mmol) as described for the synthesis

of 4-(*beta*-nitro)styrylphosphorodichloridate from 4-hydroxy-*beta*-nitrostyrene and $POCl_3$. A greenish oil (410 mg, 1.7 mmol, 57 %) was obtained. ^{1}H-NMR: = 10.03 (s, 1H), 7.98 (d, J_{ortho} = 9 Hz, 2H), 7.49 (d, J_{ortho} = 9 Hz, 2H) ppm. ^{13}C-NMR: 190.31 (CH), 153.60 (C_q, d, J_{PC} = 11 Hz), 134.86 (C_q, d, J_{PC} = 3.2 Hz), 131.92 (CH), 127.35 (C_q), 121.32 (CH, d, J_{PC} = 6.4 Hz) ppm.^{31}P-NMR: 3.10 ppm.

1,2-Di-*n*-hexadecyloxypropyl-4-formylphenyl phosphoric acid (DHPPFP) The product was prepared from 4-(formyl)phenylphosphorodichloridate (353 mg, 1.48 mmol) and 1,2-di-*n*-hexadecyloxypropanol (540 mg, 1.0 mmol) as described for the synthesis of DDPBNS. The crude product was crystallised from methanol (0.70 g in 20 mL). 450 mg (0.62 mmol, 62 %) of pure product with m.p. = 41-42 °C was isolated. ^{1}H-NMR: 9.94 (s, 1H), 7.85 (d, J_{ortho} = 8 Hz, 2H), 7.35 (d, J_{ortho}, 2H), 6.85 (br s, 1H, POH) 4.20 (m, 2H, CH_2OP), 3.48 (m, 7H, $3CH_2O$+CHO), 1.51 (m, 4H, $2OCH_2\underline{CH_2}$), 1.24 (s, 52H, chains), 0.87 (t, 6H, $2CH_3$) ppm. ^{13}C-NMR: 190.61 (CH), 155.29 (C_q, d, J_{PC} = 6.1 Hz), 133.29 (C_q), 131.55 (CH), 120.69 (CH, d, J_{PC} = 6.1 Hz), 77.11 (CHO), 71.88 (CH_2O), 70.87 (CH_2O), 69.33 (CH_2O), 67.79 (CH_2OP, d, J_{PC} = 7.1 Hz), 31.93 (CH_2), 29.90 (CH_2), 29.71 (CH_2), 29.66 (CH_2), 29.56 (CH_2), 29.50 (CH_2), 29.37 (CH_2), 26.05 (CH_2), 25.98 (CH_2), 22.70 (CH_2), 14.12 (CH_3) ppm. ^{31}P-NMR: -5.99 ppm. Analysis calculated for $C_{42}H_{77}PO_7$: C 69.58 %, H 10.70 %, P 4.27 %. Found: C 68.97 %, H 10.49 %, P 4.13 %.

Sodium salts of the phosphoric acids All sodium phosphate salts were prepared by slow and careful addition of 1.0 equivalent of a 0.149 mmol/g NaOEt solution in ethanol (three to five-fold diluted with ethanol or $CHCl_3$) to a 0.1 M solution of the phosphoric acid in dry $CHCl_3$. The sodium salts of the lipids were stored as stock solutions in $CHCl_3$ (usually 10 or 20 mM, with trace amounts of ethanol) in a cold and dark place. Characteristic shifts were observed in the ^{1}H and ^{31}P-NMR spectra of the sodium salts relative to the acids. For the sodium salt of DDPBNS: ^{1}H-NMR (CD_3OD): 8.03 (d, J_{trans}, 1H), 7.84 (d, J_{trans}, 1H), 7.65 (d, J_{ortho}, 2H), 7.33 (d, J_{ortho}, 2H), 3.95 (m, 2H), 3.40 (m, 7H), 1.48 (m, 4H), 1.27 (s, 36H), 0.89 (t, 6H) ppm. ^{31}P-NMR (CD_3OD): -5.57 ppm.

Vesicle preparation Vesicle solutions were prepared from stock solutions of the sodium salts of the lipids in chloroform. Aliquots of these solutions were rotary-evaporated in pyrex tubes to yield thin lipid films, which were dried in vacuum for 30 minutes. Subsequently, 0.5 to 5.0 mM vesicle solutions were prepared by dispersion of the lipid films in bidistilled water or 5.0 mM HEPES/NaAc buffer (pH 7.4) at temperatures *ca.* 10 °C above T_m by means of a Branson B15 sonication immersion tip (30-40 % power output in 30-40 % cycles, *ca.* 2 min/mL), or by the ethanol injection method (2.0 µmol lipid in 100 µL ethanol injected into 2.0 mL water or buffer). For DSC, large (multilamellar) vesicles were prepared by rapid stirring of the lipid suspension at temperatures *ca.* 20 °C above T_m.

Quasi-elastic Light Scattering Vesicle solutions were analysed using a Nicomp Submicron Particle Sizer Model 370. The lipid concentration was between 0.1 and 1.0 mM. Diameters reported are mean diameters derived from number-weighted Gaussian analysis of the scattering data at 23 °C. The volume-weighted analysis yields significantly higher diameters, indicating the presence of a small number of large vesicles.

Electron Microscopy Samples of vesicle solutions were brought on formvar/carbon coated 400 mesh grids made hydrophilic by glow discharge in air directly before sample preparation. After *ca.* 30 seconds, the sample solution was removed by gentle blotting with filter paper, and the sample was stained with uranyl acetate or phosphotungstic acid (1 % w/v). A drop of staining agent was applied for 3-5 seconds and removed by blotting. The samples were air dried for *ca.* 15 minutes, and examined in a Philips EM 300 electron microscope operated at 80 kV, or a Jeol JEM EX1200 electron microscope operated at 100 kV.

Differential Scanning Calorimetry Most DSC enthalpograms were recorded on a MC-2 differential scanning microcalorimeter (MicroCal Ltd., USA) at the University of Leicester, UK. Small vesicles were prepared by probe sonication and large vesicles were prepared by rapid stirring of the lipid suspension. The lipid concentration was 2.0 mM and all samples were prepared in bidistilled water. The samples were degassed prior to injection into the sample cell of the microcalorimeter. Heating scans from *ca.* 20 °C to 60-85 °C (depending on the lipid) were reproduced three or four times immediately after cooling to low temperature, and once after 8 hours equilibration at low temperature. The analysis of the transitions in terms of enthalpies, patch numbers and Van 't Hoff enthalpies were performed by Dr. Barbara Briggs (University of Leicester), using Origin software. The phase transition of DDPBNS was measured on a Perkin-Elmer DSC-7 using a concentration of 40 mM.

Kinetics Cleavage of the BNS unit was quantified by monitoring the decrease of its intense characteristic absorption at 335 nm (molar extinction coefficient *ca.* 10^4 M^{-1} cm^{-1}) using a Perkin-Elmer Lambda 5 spectrophotometer equipped with a cell compartment thermostated at 25 °C (46 °C in some experiments). Vesicle solutions were prepared by sonication with an immersion tip or by the ethanol injection method in 5 mM HEPES/NaAc buffer of pH 7.4. To initiate the hydrolysis, the external pH was quickly raised to 11.5. Usually, 100 µL aliquots of a 1.0 mM vesicle solution prepared at neutral pH were added rapidly to 1.9 mL of buffer with the pH adjusted to 11.5 by the addition of a NaOH solution. Alternatively, small aliquots of 1 M NaOH were added to the appropriate vesicle solution at neutral pH, leading to a pH jump to 11.5. The initial concentration of BNS lipid was 50 µM. In some experiments, 1.0 mM CTAB was added to solubilise the vesicles. Control experiments of the hydrolysis of *p*-hydroxy-*beta*-nitrostyrene were carried out at 31 µM concentration. The hydrolysis of DDPBNS at low temperature was performed in a solution with [DDBNS] = 2 mM and pH 12 incubated at 5 °C. Samples of this solution were taken at distinct time intervals, quenched with a small aliquot of Hcl solution, and [BNS] was measured using UV-VIS absorbance.The pH was measured with an Orion SA 720 pH electrode. Kinetic data were analysed in terms of pseudo-first-order rate constants, or in terms of a double exponential decay. Reported rate constants are averages of at least four reproducible runs.

Preparation of vesicles with oligomerised lipids by photopolymerisation Polymerisation of *beta*-nitrostyrene in the bilayer was achieved by irradiation of 0.5-2.0 mL samples of 0.5-2.0 mM solutions at room temperature in quartz cuvets or pyrex NMR tubes for 10 minutes with a Hanau SN81 medium pressure mercury lamp. Samples were placed at a distance of 1 cm from

the lamp. The extent of polymerisation was determined by the disappearance of the characteristic UV-VIS absorption and the ^{1}H-NMR signal of the vinyl protons of the monomer. A sample of polymerised material was freeze-dried. It dissolves readily in chloroform and THF. The sample was analysed by electrospray mass spectrometry (in CH_2Cl_2) in the Laboratory of Mass Spectrometry of the Department of Pharmacy of this University, and vapour pressure osmometry (in THF) by the analytical department of this laboratory.

Appendix

Kinetic data for the specific *exo*-vesicular cleavage of *beta*-nitrostyrene (BNS) groups were analysed in terms of a model assuming (1) partitioning of the BNS groups over the inner and outer bilayer leaflets, defining BNS_{endo} and BNS_{exo}, respectively, (2) pseudo-first-order cleavage of BNS_{exo} at the outer bilayer leaflet, characterised by k'_2, (3) translocation of lipid molecules over the bilayer (*flip-flop*), resulting in exchange between BNS_{endo} and BNS_{exo}, characterised by k_1 and k_{-1} and (4) negligible permeation of hydroxide ion over the bilayer within the time scale of the cleavage experiment (Figure 2.5). The following kinetic equations result:

$$d[BNS_{exo}]/dt = k_1[BNS_{endo}] - k_{-1}[BNS_{exo}] - k'_2[BNS_{exo}] \quad (1)$$

$$d[BNS_{endo}]/dt = -k_1[BNS_{endo}] + k_{-1}[BNS_{exo}] \quad (2)$$

Thus:

$$x' = k_1y - (k'_2 + k_{-1})x \quad (3)$$

$$y' = k_{-1}x - k_1y \quad (4)$$

with $x = [BNS_{exo}]$ and $y = [BNS_{endo}]$ and x' and y' representing their functions of time. Applying Laplace transformation,[33] the following subsidiary equation is obtained:

$$sX - x_0 = k_1Y - (k'_2 + k_{-1})X \quad (5)$$

$$sY - y_0 = k_{-1}X - k_1Y \quad (6)$$

in which X and Y are Laplace transforms of x and y. Expressing Y through X:

$$Y = 1/k_1(sX - x_0 + (k'_2 + k_{-1})X) \quad (7)$$

Now substitution and solution for X yields:

$$x_0k_1 - sk_1X - k'_2k_1X = s^2X - sx_0 - y_0k_1 + s(k'_2 + k_{-1})X \quad (8)$$

so:

$$X = x_0(s + k_1 + k_1y_0/x_0)/(s^2 + s(k'_2 + k_1 + k_{-1}) + k'_2k_1) = x_0(s + k_1 + k_1y_0/x_0)/((s + k_4)(s + k_5)) \quad (9)$$

in which $k_3 = 1/2(k' + k_1 + k_{-1})$, $k_4 = k_3 + (k_3^2 - k'_2k_1)^{1/2}$ and $k_5 = k_3 - (k_3^2 - k'_2k_1)^{1/2}$.

Now we can separate:

$$X = A_1^x/(s + k_4) + A_2^x/(s + k_5) \quad (10)$$

in which $A_1^x = (k_1(x_0 + y_0) - k_4x_0)/2(k_3 - k_4)$ and $A_2^x = (k_1(x_0 + y_0) - k_5x_0)/2(k_3 - k_5)$. Using reverse Laplace transformation, we obtain the classic solution:

$$x = A_1^x\exp(-k_4t) + A_2^x\exp(-k_5t) \quad (11)$$

A similar solution can be obtained for y, with $A_1^y = (k_{-1}(x_0 + y_0) - k'_2y_0 - k_4x_0)/2(k_3 - k_4)$, and with $A_2^y = (k_{-1}(x_0 + y_0) - k'_2y_0 - k_5x_0)/2(k_3 - k_5)$. These results imply that $[BNS_{endo} + BNS_{exo}]$ as a function of time (which is monitored experimentally) can be expressed as:

$$x + y = (A_1^x + A_1^y)\exp(-k_4t) + (A_2^x + A_2^y)\exp(-k_5t) \quad (12)$$

In case of similar k_1, k_{-1} and k'_2 it is necessary to use the full equation, but if $k_1 = k_{-1} << k'_2$ it is possible to use a simplified form. In this case we can define:

$$B = k_4 + k_5 = 2k_3 = k'_2 + k_1 + k_{-1} = k'_2 + 2k_1 \quad (13)$$

$$C = 1/4((k_4 + k_5)^2 - (k_4 - k_5)^2) = k_1k'_2 = k_1(B - 2k_1) \quad (14)$$

so $k_1^2 - B/2(k_1) + C/2 = 0$ and therefore:

$$k_1 = 1/4(B - (B^2 - 8C)^{1/2}) \text{ and } k'_2 = 1/2(B + (B^2 - 8C)^{1/2}) \quad (15)$$

Since k_4 and k_5 can be determined accurately from a double exponential fit to the experimental data (in the text, they are reported as k'_{fast} and k'_{slow}), k_1 (the rate constant for *flip-flop*) and k'_2 (the rate constant for cleavage of the BNS group in the outer bilayer leaflet) can be calculated. The results of the calculation are summarised in Table 2.3 (all values in units of 10^4 s^{-1}):

Table 2.3 Correction of hydrolysis rate constants to include lipid *flip-flop*.

lipid	k_4 (k'_{fast})	k_5 (k'_{slow})	B	C	k_1	k'_2
DOPBNS	6.25	0.095	6.35	0.610	0.100	6.15
DHPBNS	5.49	0.316	5.81	1.75	0.343	5.13
DHPBNS*	7.33	0.769	8.10	5.64	0.893	6.32
DTPBNS	5.11	0.584	5.69	2.97	0.680	4.32

* Vesicles prepared by the ethanol injection method.

Acknowledgments

Konrad Siegel (ERASMUS exchange student from the University of Göttingen, Germany) synthesised DTPBNS and Prof. Michael Blandamer and Dr. Barbara Briggs (University of Leicester, UK) performed and analysed most DSC measurements. Dr. Konstantin Surkov (University of St. Petersburg, Russia) is acknowledged for his help in the analysis of the kinetic data. Anno Wagenaar is gratefully acknowledged for helpful advice on synthetic procedures and Erik van Echten is acknowledged for HPLC analysis of DDPBNS at Syncom BV.

2.9 References

(1) Rothman, J.E.; Lenard, J. Membrane asymmetry. *Science* 1977, 195, 743-755.

(2) Op den Kamp, J.A.F. Lipid asymmetry in membranes. *Ann. Rev. Biochem.* 1979, 48, 47-71.

(3) Gennis, R.B. Biomembranes: molecular structure and function. Springer Verlag, New York, 1989, pp 138-165.

(4) Moss, R.A.; Swarup, S. Surface-specific phosphate cleavage of a substrate-functionalized vesicular surfactant. *J. Am. Chem. Soc.* 1986, 108, 5341-5342.

(5) Moss, R.A.; Bhattacharya, S.; Scrimin, P.; Swarup, S. Surface-specific cleavage of a cationic carbonate-functionalized vesicular surfactant. *J. Am. Chem. Soc.* 1987, 109, 5740-5744.

(6) Moss, R.A.; Bhattacharya, S.; Chatterjee, S. Chemical differentiation of bilayer surfaces in functional dialkylammonium ion vesicles: observation of surfactant flip-flop. *J. Am. Chem. Soc.* 1989, 111, 3680-3687.

(7) Moss, R.A.; Bhattacharya, S. Transverse membrane asymmetry in model phospholipid bilayers: NBD-phosphatidylethanolamine and the separation of flip from flop. *J. Am. Chem. Soc.* 1995, 117, 8688-8689.

(8) Moss, R.A.; Park, B.D.; Scrimin, P.; Ghirlanda, G. Lanthanide cleavage of phosphodiester liposomes. *J. Chem. Soc., Chem. Commun.* 1995, 1627-1628.

(9) Ringsdorf, H.; Schlarb, B. Preparation and characterization of unsymmetrical 'liposomes in a net'. *Makromol. Chem.* 1988, 189, 299-315.

(10) Ringsdorf, H.; Schlarb, B.; Venzmer, J. Molecular architecture and function of polymeric oriented systems: models for the study of organization, surface recognition, and dynamics of biomembranes. *Angew. Chem,. Int. Ed. Engl.* 1988, 27, 113-158.

(11) Miller, D.B. Structure and chemistry of photodimers of trans-*beta*-nitrostyrene. Ph.D. Thesis, Ohio State University, 1957 (*Dissertation Abstr.* 1958, 18, 1981).

(12) Topchiev, A.V.; Alaniya, V.P. Synthesis of nitroolefins and an investigation of their ability to polymerize. *J. Polym. Sci. A* 1963, 1, 599-604.

(13) Stewart, R. A kinetic study of the alkaline scission of 4-hydroxy-3-methoxy-*beta*-nitrostyrene. *J. Am. Chem. Soc.* 1952, 74, 4531-4533.

(14) Paltauf, F.; Hauser, H.; Phillips, M.C. Monolayer characteristics of some 1,2-diacyl, 1-alkyl-2-acyl and 1,2-dialkyl phospholipids at the air-water interface. *Biochim. Biophys. Acta* 1971, 249, 539-547.

(15) Bittman, R.; Clejan, S.; Lund-Katz, S.; Phillips, M.C. Influence of cholesterol on bilayers of ester- and ether-linked phospholipids. *Biochim. Biophys. Acta* 1984, 772, 117-126.

(16) Gairaud, C.B.; Lappin, G.R. The synthesis of *omega*-nitrostyrenes. *J. Org. Chem.* 1953, 18, 1-3.

(17) (a) *1,2*-Di-*n*-dodecyloxypropanol and *1,2*-di-*n*-hexadecyloxypropanol: Paltauf, F.; Spener, F. An improved synthesis of 1,2-dialkyl glycerol ethers and the synthesis of ^{14}C-labeled-trialkyl glyceryl ethers. *Chem. Phys. Lipids* 1968, 2, 168-172 (b) *1,2*-di-*n*-tetradecyloxypropanol: Chen, J.S.; Barton, P.G. Studies of dialkyl ether phospholipids. II. *Can. J. Biochemistry* 1971, 49, 1362-1375 (c) *1,2*-di-*n*-tetradecyloxypropanol, *1,2*-di-*n*-hexadecyloxypropanol and *1,2*-di-*n*-octadecyloxypropanol: Six, L.; Ruess, K.P.; Liefländer, M. Influence of carbohydrate moieties on monolayer properties of dialkyl glyceryl ether glucosides. *J. Colloid Interface Sci.* 1983, 93, 109-114.

(18) Blandamer, M.J.; Briggs, B.; Cullis, P.M.; Green, J.A.; Waters, M.; Soldi, G.; Engberts, J.B.F.N.; Hoekstra, D. Differential scanning microcalorometric study of vesicles in aqueous solutions formed by dimethyldioctadecylammonium bromide. *J. Chem. Soc. Faraday Trans.* 1992, 88, 3431-3434.

(19) Blandamer, M.J.; Briggs, B.; Cullis, P.M.; Engberts, J.B.F.N.; Hoekstra, D. Differential scanning microcalorimetric study of sodium di-*n*-dodecylphosphate vesicles in aqueous solution. *J. Chem. Soc. Faraday Trans.* 1994, 90, 1905-1907.

(20) Grünewald, B.; Stankowski, S.; Blume, A. Curvature influence on the cooperativity and the phase transition enthalpy of lecithin vesicles. *FEBS Letters* 1979, 102, 227-229.

(21) Cevc, G. (Ed.) Phospholipids Handbook. Marcel Dekker, New York, 1993.

(22) Homan, R.; Powell, H.J. Transbilayer diffusion of phospholipids: dependence on head group structure and acyl chain length. *Biochim. Biophys. Acta* 1988, 938, 155-166.

(23) Moss, R.A. Dynamics of lipids in synthetic membranes. *Pure Appl. Chem.* 1994, 66, 851-858, and references therein.

(24) Blandamer, M.J.; Briggs, B.; Cullis, P.M.; Engberts, J.B.F.N. Gel to liquid crystal transitions in synthetic amphiphile vesicles. *Chem. Soc. Rev.* 1995, 24, 251-257.

(25) Blandamer, M.J.; Briggs, B.; Butt, M.D.; Waters, M.; Cullis, P.M.; Engberts, J.B.F.N.; Hoekstra, D.; Mohanty, R.K. Sodium di-n-dodecylphosphate vesicles in aqueous solution: effects of ethanol, propanol, and tetrahydrofuran on the gel to liquid phase transition. *Langmuir* 1994, 10, 3488-3492.

(26) Reed, W.; Guterman, L.; Tundo, P.; Fendler, J.H. Polymerized surfactant vesicles: kinetics and mechanism of photopolymerization. *J. Am. Chem. Soc.* 1984, 106, 1897-1907.

(27) Meier, H.; Sprenger, I.; Bärmann, M.; Sackmann, E. Radical polymerization of amphiphiles in a two-dimensional solution (mixed vesicles). *Macromolecules* 1994, 27, 7581-7588.

(28) Matsushita, Y.; Hasegawa, E.; Eshima, K.; Ohno, H.; Tsuchida, E. Synthesis and properties of polymerizable phospholipids, 5. Molecular weights of polymeric liposomes. *Makromol. Chem., Rapid Commun.* 1987, 8, 1-6.

(29) Singh, A.; Schnur, J.M. Polymerizable phospholipids. In: Phospholipids Handbook (Cevc, G., Ed.). Marcel Dekker, New York, 1993, pp 233-291.

(30) Sells, T.D.; O'Brien, D.F. Two-dimensional polymerization of lipid bilayers: degree of polymerization of acryloyl lipids. *Macromolecules* 1994, 27, 226-233.

(31) Lamparski, H.; O'Brien, D.F. Two-dimensional polymerization of lipid bilayers: degree of polymerization of sorbyl lipids. *Macromolecules* 1995, 28, 1786-1794.

(32) Ohkatsu, Y.; Yokota, M.; Kusano, T. Synthesis and polymerization of a macromonomer derived from phosphatidylcholine. *Makromol. Chem.* 1988, 189, 755-760.

(33) Kreyszig, E. Advanced Engineering Mathematics. Wiley, New York, 1988, pp 249-252.

Chapter 3

Characterisation of vesicles of oligomerised lipids[I]

The effect of lipid oligomerisation on the bilayer properties of small unilamellar vesicles of lipids that contain a beta-nitrostyrene unit has been examined. Differential scanning microcalorimetry, ^{31}P-NMR spectroscopy, monolayer compression experiments, contents leakage assays and vesicle solubilisation studies provides insight into the thermotropic phase behaviour, the molecular mobility and the permeability of the lipid bilayer prior to and after oligomerisation of the lipid head groups. Oligomerisation leads to denser lipid head group packing without affecting the flexibility of the hydrocarbon chains. As a result, the lateral diffusion of the lipids and the permeability of the membrane are strongly reduced.

3.1 Introduction

Since the early 1980's, a large variety of lipids which can be polymerised in the bilayer has been synthesised.[1, 2, 3, 4] Polymerisable groups have been introduced at either end and in the middle of the hydrophobic chains of lipids, as well as in the hydrophilic head groups, and even in the counterions of ionic lipids.[5, 6, 7] Photopolymerisations are known as well as chemically-initiated polymerisations. The kinetics and degree of polymerisation has been examined in detail for several polymerisable lipids.[8, 9, 10] Depending on the structure of the polymerisable lipid, and particularly the position of the polymerisable unit, the effect of polymerisation on the bilayer can be very different. Roughly speaking, polymerisable lipids can be divided into two classes: (1) a large class of lipids that stabilise the bilayer upon polymerisation, and (2) a small group of lipids that destabilise the bilayer upon polymerisation. Polymerisable lipids of the first kind are of interest for therapeutic applications because covalent linking of the lipid molecules yields liposomes with a higher colloidal, physical and chemical stability. Furthermore, liposomes of polymerised lipids retain their aqueous contents much longer than their monomer lipid counterparts.[4] Polymerisable lipids of the second kind are often unstable because the polymerised lipid tends to adopt a non-bilayer structure which leads to leakage of the liposome contents and (in some cases) liposome aggregation and fusion.[11, 12] This destabilisation opens challenging possibilities for photo-induced liposomal contents release and/or fusion.

This chapter reports a study of the influence of lipid oligomerisation on the properties of small unilamellar vesicles of lipids that carry a *beta*-nitrostyrene (BNS) unit. As described in Chapter 2, the BNS group is a bifunctional reactive group that can be either hydrolysed or polymerised. Brief UV irradiation of a solution of BNS lipid vesicles leads to formation of oligomers of at least 4-5 lipid molecules in both bilayer leaflets. Alternatively, the BNS units in

[I] Parts of the research described in this chapter have been accepted for publication in *Biophys. J.*

the outer leaflet of bilayer vesicles can be cleaved efficiently during an *exo*-vesicular pH jump, after which the remaining BNS groups in the inner leaflet can be oligomerised by UV irradiation. In this way, vesicles can be obtained which contain lipid oligomers exclusively in the inner leaflet.

Vesicles of oligomerised lipids were characterised using differential scanning microcalorimetry (DSC), monitoring the thermotropic behaviour of the lipid oligomers, and using ^{31}P-NMR, reporting changes in lipid phosphate head group mobility upon oligomerisation. Furthermore, the photopolymerisation was studied in a monolayer of lipids on the air-water interface. This technique provides information on the molecular surface area of lipid molecules. Finally, the effect of lipid oligomerisation on permeability and detergent resistance of unilamellar vesicles were analysed.

3.2 Differential scanning microcalorimetry

Thermotropic phase transitions in bilayers of polymerisable lipids have been reviewed by Blume,[13] and it is evident that the changes in thermotropic behaviour of bilayers upon lipid polymerisation are highly dependent of the molecular structure of the lipid and the location of the polymerisable unit. Polymerisation of hydrocarbon chains generally leads to a loss of a well-defined main phase transition, whereas polymerisation of head groups leads to an increased head group packing without significantly affecting hydrocarbon chain flexibility. Polymerisation of counterions influences the packing efficiency by its drastic effect on the hydration of head groups.

As described in Section 2.3, bilayers of the BNS lipids studied in this thesis have main phase transition temperatures (T_m) similar to those of phosphatidylcholines, but much lower than for phosphatidylserines or phosphatidylethanolamines with identical chain length. Upon oligomerisation of the lipids, a different thermotropic behaviour is found. Figure 3.1 shows the enthalpograms for small vesicles of DHPBNS (1) prior to oligomerisation, (2) after oligomerisation of the inner bilayer leaflet and (3) after oligomerisation of both bilayer leaflets. Although only a marginal shift of T_m was observed upon oligomerisation, a pronounced 'shoulder' (extending over 10-15 °C) develops at the high temperature side of the main peak in the enthalpogram. The overall enthalpy of the phase transition(s) is unaffected, but the number of Van't Hoff phase transitions (m) required to fit to the experimental data increases and the patch number *n* decreases upon oligomerisation. If only the inner bilayer leaflet is oligomerised, the results are similar but the 'shoulder' is less pronounced. As reported in Chapter 2, hydrolysis of the BNS group has no detectable influence on the thermotropic behaviour of the lipid bilayer. DOPBNS and DHPBNS show comparable thermotropic behaviour upon oligomerisation, as illustrated in Figure 3.1.

Oligomerisation of the BNS groups has two distinguished effects on the bilayer melting behaviour. In the first place, a modest but significant part of the lipid melts at higher temperature. This indicates a portion of the lipid material in which the lipid molecules are packed more efficiently after oligomerisation than before. Since the oligomerisation occurs in the lipid head group, rather than in the hydrocarbon chains themselves, this increased lipid packing is not a result of a reduced mobility of the hydrocarbon chains. Most likely, the lipid packing

efficiency increases because the head group packing becomes more efficient upon oligomerisation, both as a direct consequence of the covalent linking of the BNS groups, and indirectly because oligomerisation of the head groups could entail a loss of some hydration water (see Section 6.3). With reference to the comparison made above (and in Section 2.3), it is tentatively suggested that oligomers of BNS lipids have a lipid packing efficiency (and T_m) more similar to that of phosphatidylserines and of phosphatidylethanolamines rather than that of phosphatidylcholines because the lipid head group interaction is more favourable in bilayers of the oligomers than in bilayers of the monomers. However, most of the lipid still undergoes the main phase transition at the same temperature. Perhaps the shoulder only reflects the packing in the largest oligomers, and not in the short ones.

Secondly, the cooperativity of melting goes down, as anticipated on going from a homogeneous bilayer of identical lipids to disperse mixtures of oligomers (with various conformations), and a completely asymmetric membrane in case only the inner bilayer leaflet is oligomerised. This decrease in cooperativity has been reported for comparable lipid head group polymerisations.[14, 15] The constant enthalpy of transition reflects the fact that in all cases an identical number of identical hydrocarbon chains undergo the same phase transition.

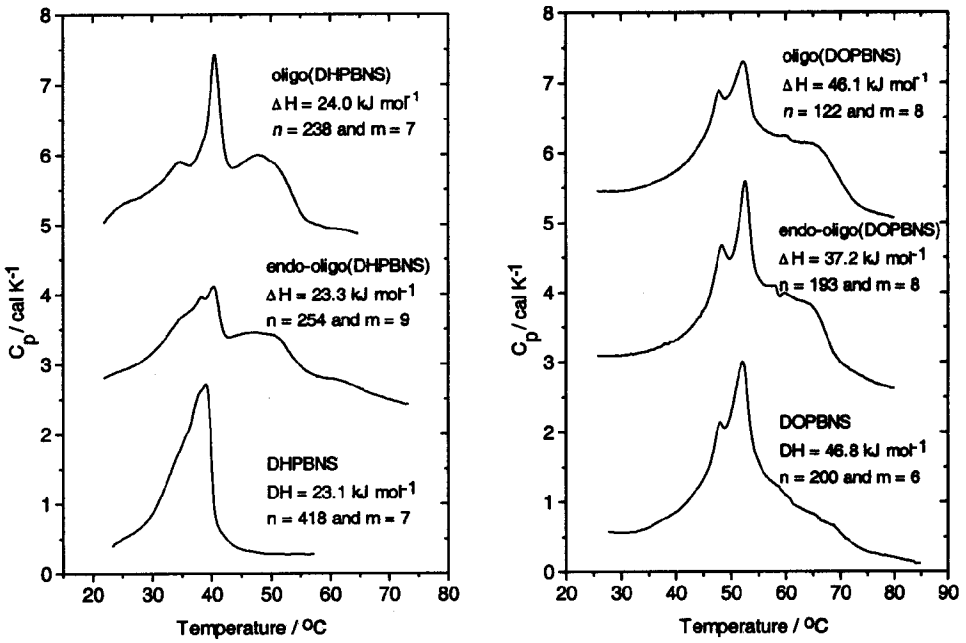

Figure 3.1 DSC enthalpograms of vesicles of DHPBNS (left) and DOPBNS (right) before oligomerisation, after oligomerisation of the inner bilayer leaflet ('endo-oligo(lipid)'), and after oligomerisation of both bilayer leaflets ('oligo(lipid)'). The curves have been shifted on the C_p axis for a clear presentation.

3.3 Monolayer experiments

Studies of lipid monolayers on the air-water interface provide valuable insight into minimal molecular surface area, the thermotropic behaviour and the miscibility of lipids in bilayer membranes.[16,17] Polymerisation of lipid molecules may affect all these properties.[3,18] Preliminary experiments were carried out with DHPBNS at room temperature (Figure 3.2). This lipid spreads readily on the air-water interface, and the area-pressure curve at 20 °C shows a minimal molecular surface area of 65 $Å^2$ and a collapse pressure of about 60 mN m^{-1}. The bump in the curve at 35 mN m^{-1} represents a transition from a liquid phase to a liquid-crystalline phase. The molecular surface area is rather high for a monolayer of lipids with two saturated hydrocarbon chains (it is *ca.* 45 $Å^2$ for phosphatidylcholines),[17] which indicates an irregular packing of DHPBNS in the monolayer, even though the temperature is well below the T_m of the corresponding bilayer vesicles (40 °C). Perhaps the bulky and hydrophobic BNS head groups obstruct a regular monolayer packing.

Upon UV-irradiation of the monolayer *at moderate compression* (30 mN m^{-1}) and constant area, a gradual decrease in the pressure-time diagram is observed. This decrease in pressure probably reflects partial collapse of the monolayer as a result of increasing packing stress in the course of the polymerisation reaction. The surface pressure is relieved because the monolayer (partially) becomes a bi- or multilayer. One might argue that the packing of the lipid oligomers that are formed is more compact than the loose assembly of monomers at 30 mN m^{-1} compression, and that contraction of the lipid head groups due to oligomerisation leads to

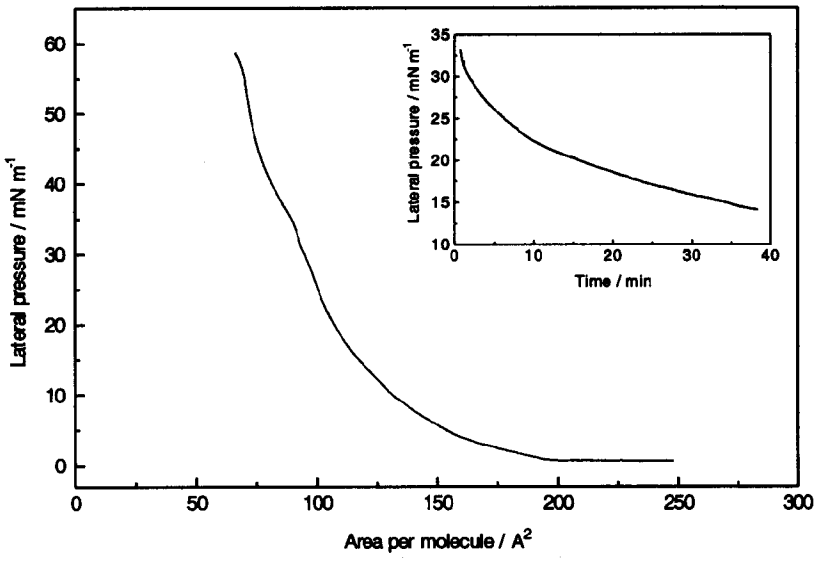

Figure 3.2 Lateral pressure *vs* molecular area curve for compression of a monolayer of DHPBNS on the air-water interface. Insert: Decrease of lateral pressure with time during UV irradiation of a monolayer of DHPBNS at moderate compression.

curvature stress in the monolayer.[19] The pressure-time curve of the monolayer under UV-irradiation (Figure 3.2, insert) was used to estimate the kinetics of the photopolymerisation. Photopolymerisation of the monolayer at ambient temperature proceeds with a half-life of about 10 minutes. It should be noted that the intensity of the UV source used in the monolayer experiment is much lower than that routinely used for photopolymerisation of bilayer vesicles. The kinetics of oligomerisation need not be the same in both systems.

According to the pressure-time diagram, once the oligomerisation reaction is complete, the oligomerised monolayer can be compressed to a limited extent. Since the monolayer has most probably collapsed at least partially during the polymerisation reaction, a reliable estimate of the molecular surface area of the oligomerised lipid cannot be made. Upon compression, the oligomerised monolayer collapses into multilayers in a stepwise manner, much like icefloes which glide over each other. After each collapse, the surface pressure returns to its original value of low compression. The collapse pressure of the oligomerised monolayer is much lower than 60 mN m^{-1}, indicating a destabilisation of the monolayer upon lipid oligomerisation. The collapse of oligomerised monolayers under lateral compression is unlikely to occur in bilayer vesicles, in which there is a constant lateral pressure, but no restricted area per molecule, so that local density fluctuations may readily relieve packing stress resulting from oligomer formation.

3.4 ^{31}P-NMR and lipid head group mobility

^{31}P-NMR spectra of small unilamellar vesicles of DDPBNS yield insight into the effect of oligomerisation on the head group mobility of the lipids in the bilayer. Prior to oligomerisation, the spectrum shows one isotropic signal with a line width of *ca.* 30 Hz and a relaxation time T_1 of 0.5 s (Figure 3.3). This result is indicative of small vesicles that tumble fast and have rapid lipid lateral diffusion.[20,21] After oligomerisation, a line width of *ca.* 230 Hz, and an unchanged T_1 of 0.5 s were determined (Figure 3.3). Since slower tumbling of oligomerised lipid vesicles relative to monomer lipid vesicles can be excluded because no significant change of vesicle diameter was observed upon oligomerisation (see Chapter 2), the increased line width indicates slower lateral diffusion of the lipid oligomers in the bilayer. A contributing line-broadening effect due to chemical shift differences between the various oligomers cannot be ruled out. Although the relaxation time T_1 is indifferent to lipid oligomerisation, a change in lipid head group mobility cannot be excluded solely on this ground. Interpretation of T_1 values in bilayer systems is often ambiguous.[22]

At 202 MHz, an eight-fold increase of the ^{31}P line width was observed upon oligomerisation. For comparison, a five-fold *decrease* in ^{31}P line width (at 129 MHz) was reported for small unilamellar vesicles of dipalmitoyl phosphatidylcholine upon an increase in temperature from 30 °C to 50 °C, *i.e.* from below to above the main phase transition temperature.[23] By means of a viscosity dependence study of the line width, this decrease in line width was correlated with a twenty-fold increase of the lateral diffusion coefficient of the lipid molecules.[19] These NMR data show that oligomerisation results in a drastic decrease of lateral diffusion.

Furthermore, these findings are corroborated with results from computer simulations of bilayers of lipids with polymerisable head groups,[24] which indicate that even when present in

small amounts (less than 10 mol%) short, linear lipid polymers (20 monomers per polymer) have a lateral diffusion coefficient which is at least two orders of magnitude smaller than that of the monomers. Using the technique of fluorescence recovery after photobleaching, Sackmann[25] measured a 70 % decrease of the *overall* lateral diffusion coefficient in bilayers of a lipid with polymerised head groups. In this case, the degree of polymerisation was estimated to be *ca.*100, and the polymer concentration was only 0.5 mol% (50 mol% monomer and complete polymerisation). In the case of the BNS lipids used in this study, although the degree of polymerisation is lower, the concentration of oligomer is much higher (*ca.* 100 mol%), and a drastic decrease of the lateral diffusion coefficient is indeed anticipated.

For most lipids in a liquid-crystalline bilayer, the lateral diffusion coefficient (D_{lat}) is about 1 $\mu m^2 s^{-1}$.[26] The mean square lateral displacement of a lipid molecule in time t is given by $4D_{lat}t$. On the basis of the discussion above, the reduction of the diffusion coefficient upon oligomerisation of DDPBNS is estimated to be at least twenty-fold, which means that whereas the lipid monomer would take almost 25 ms to travel around a vesicle with a diameter of 100 nm, the lipid oligomers would need more than 500 ms.

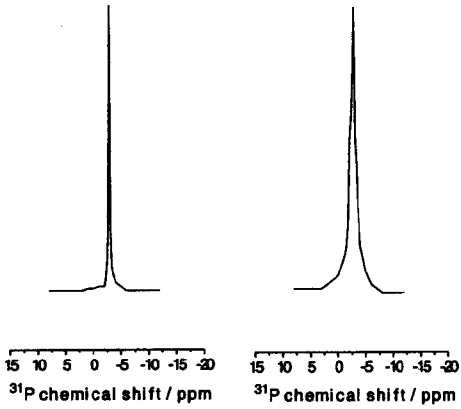

Figure 3.3 ^{31}P-NMR spectra of small DDPBNS vesicles before and after oligomerisation of the lipid head groups.

3.5 Contents leakage

A straightforward method for measuring the permeability of bilayer membranes involves encapsulation of a fluorescent solute at self-quenching concentration in the aqueous interior of unilamellar vesicles. After removal of non-encapsulated solute by column filtration, the release of the entrapped fluorescent solute results in high dilution, with concomitant relief of self-quenching and increase of fluorescence intensity. In this study, contents leakage of small vesicles of DDPBNS and DHPBNS was monitored by measuring the release of entrapped carboxyfluorescein (CF). The encapsulation efficiency for both types of lipid vesicles measured using UV-VIS spectroscopy is 8-12 nmol CF per µmol of lipid. This efficiency is normal for small unilamellar vesicles.[27] Release of entrapped CF is strongly dependent on the lipid, lipid oligomerisation, and temperature. Results are presented in Figure 3.4.

For DDPBNS, the vesicles are rather leaky at room temperature. The half-life of contents release is only 10 minutes. Upon oligomerisation of DDPBNS in both bilayer leaflets of the vesicles, the vesicles retain their contents much longer - for oligomerised DDPBNS, the half-life of release is 60 minutes. Carboxyfluorescein acts as a strong UV filter and oligomerisation is much less efficient in its presence. Up to 30 % of the lipid remains in its monomeric form. Addition of 25 mol% of cholesterol to the monomer lipid vesicles leads to an increased half-life of release of 50 minutes. This effect is well-known: above T_m, cholesterol condenses the hydrophobic interior and reduces the permeability of the bilayer.[28] Apparently, oligomerisation has a comparable effect on contents release.

Compared to DDPBNS, vesicles of DHPBNS are not leaky (Figure 3.4). At room temperature, less than 3 % of entrapped CF is lost from the vesicles after two days, irrespective of whether the lipids have been oligomerised or not. At 50 °C however, well above their T_m, vesicles of DHPBNS are permeable for CF. Prior to oligomerisation, most of the entrapped CF is released within 15 minutes. If both bilayer leaflets are oligomerised, the bilayer is much less permeable. The half-life of contents release increases to more than 2 hours. If only the inner bilayer leaflet is oligomerised, the vesicles are only slightly more permeable. Hence, the inner bilayer leaflet poses the primary barrier for outward permeation.

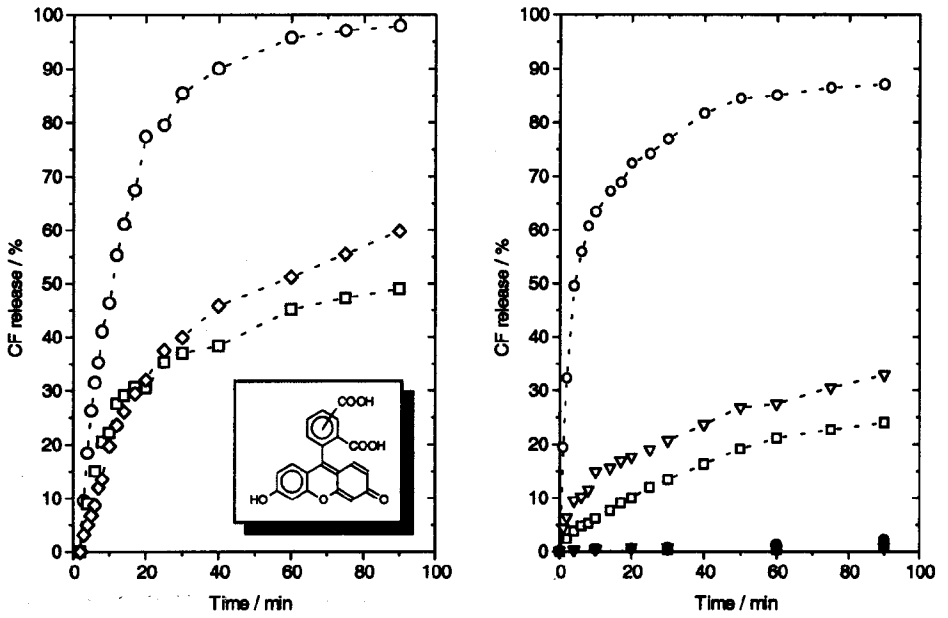

Figure 3.4 (Left): Release of encapsulated CF (insert) from vesicles of DDPBNS at 25 °C. Circles: DDPBNS, diamonds: DDPBNS with 25 mol% cholesterol, squares: oligo(DDPBNS). (Right): Release of CF from vesicles of DHPBNS at 25 °C (closed symbols) and at 50 °C (open symbols). Circles: DHPBNS, down triangles: DHPBNS with oligomerised inner leaflet, squares: DHPBNS with both leaflets oligomerised.

3.6 Vesicle solubilisation by Triton X-100

The initial rate of solubilisation of small unilamellar vesicles by the nonionic detergent Triton X-100 was measured as the initial rate of relief of self-quenching of *n*-octadecyl rhodamine (R18) upon addition of 0.5 % (w/v) of the detergent to the vesicle solution. R18 fluorescence is low when the fluorophore is present in self-quenching concentrations in the bilayer (2-4 mol%). Solubilisation by Triton X-100 results in a strong increase in fluorescence due to the formation of mixed micelles of Triton X-100 and lipid, in which R18 is diluted to such an extent that self-quenching is completely relieved. The rate at which self-quenching of R18 is relieved is a measure for the rate at which the vesicles are solubilised.

For DHPBNS a rate of 34 ± 4 % s^{-1} was measured. For vesicles with an oligomerised inner leaflet, the rate decreased to 17 ± 3 % s^{-1}, and for vesicles with both leaflets oligomerised a rate of 17 ± 2 % s^{-1} was found. Thus, solubilisation is slower by a factor of two for the oligomerised bilayer relative to the monomer lipid bilayer, irrespective of whether only the inner or both bilayer leaflets are oligomerised. Possibly, the process of bilayer swelling due to uptake of detergent, which is considered to be the first step in solubilisation by nonionic detergents,[29] proceeds less readily in oligomerised bilayers than in monomeric bilayers, irrespective of whether the oligomers are present in both bilayer leaflets, or only in the inner one.

3.7 Conclusions

A consistent picture of the properties of vesicles of oligomerised lipids emerges. Compared to their monomer lipid counterparts, the oligomerised lipid vesicles are less permeable and more resistant toward detergent solubilisation. Oligomerisation can be considered a mild form of polymerisation, for which similar observations are reported: generally, vesicles of polymerised lipids retain their contents longer and have a higher stability towards solubilisation by detergents and alcohols.[4] Permeability and detergent solubilisation are affected to an equally large extent when either both or only the inner bilayer leaflet is oligomerised. Apparently, penetration into the bilayer of large molecules such as carboxyfluorescein and Triton X-100 is considerably retarded upon covalent linking of the lipid head groups.

Slower penetration into the bilayer suggests a denser packing of lipid in the bilayer upon oligomerisation. Comparison of ^{31}P-NMR and DSC data indicates that the oligomerisation reaction results in a more rigid packing of the head groups of the lipid molecules in the bilayer, without drastically affecting the flexibility of the hydrocarbon chains in the bilayer interior.Thus, the main effect of oligomerisation is a reduced mobility of the head groups in a fluid bilayer. This restrained head group mobility implies a reduction of the lateral diffusion of the lipid molecules. These conclusions correspond nicely to the results of a study of the influence of head group polymerisation on the molecular mobility of synthetic cationic lipids.[30]

3.8 Experimental section

Materials The synthesis of DDPBNS, DHPBNS and DOPBNS was described in Chapter 2. Cholesterol was obtained from Sigma. Carboxyfluorescein (a mixture of 5- and 6-

carboxyfluorescein, Eastman Kodak Co.) and R18 (*n*-octadecyl rhodamine B chloride, Molecular Probes Inc.) were generously provided by the Laboratory of Physiological Chemistry.

Preparation of small unilamellar vesicles Small vesicles were prepared by probe sonication in the appropriate buffer solution as described in Section 2.8. The procedure for the preparation of vesicles with oligomerised lipids was described in Section 2.8.

Differential scanning microcalorimetry DSC was carried out as described in Section 2.8. It is important to note that for these experiments, small unilamellar vesicles (lipid concentration of 2.0 mM) prepared in 5 mM HEPES/NaAc buffer were used. Small differences between the DSC results of vesicles in water (Section 2.3) and in buffer were observed. These differences are not easily accounted for, but have been reported before.[31]

Monolayer studies Monolayer compression experiments were carried out with a filmbalance of the Wilhelmy type. The measurement equipment and the motor for the barrier are from Riegeler & Kirchstein. The trough contained bidistilled water. DHPBNS (20 µL of a 1.0 mM $CHCl_3$ solution) was spread at 20 °C. The lateral surface pressure was monitored continuously while the area of the air-water interface was reduced. Photopolymerisation was carried out by irradiation of the monolayer with a mercury lamp placed at 10 cm from the monolayer surface. During irradiation, the lateral pressure was monitored while the area was held constant.

^{31}P-NMR Line widths and relaxation times were measured at 30 °C for small unilamellar vesicles of 20 mM DDPBNS in 5 mM HEPES/NaAc buffer (pH 7.4) containing 10 % of D_2O. T_1 was determined using the inversion-recovery method. Spectra were recorded on a Varian VXR500 500 MHz machine (with ^{31}P resonance at 202 MHz).

Carboxyfluorescein leakage assays Leakage assays were performed according to literature procedures.[32] Briefly, small unilamellar vesicles were prepared by sonication of 5 mM of the appropriate lipid(s) in a solution of 20 mM carboxyfluorescein (CF) in 5 mM HEPES/NaAc buffer (pH 7.4, 120 mM NaCl). Non-encapsulated CF was removed by rapid filtration over Sephadex G75 at room temperature, using 5 mM HEPES/NaAc buffer (pH 7.4, 140 mM NaCl) as eluent. Oligomerisation of the lipids in the vesicles was carried out *immediately after* this separation. Leakage at time t was expressed in percentage relative to the initial fluorescence F_0 and the maximum fluorescence F_{TX} obtained after solubilisation of the vesicles by 0.5 % w/v of Triton X-100 according to: $(F_t - F_0)/(F_{TX}-F_0) \times 100$ %. Fluorescence was recorded on a SLM-Aminco SPF-500C spectrofluorometer. An excitation wavelength of 490 nm and an emission wavelength of 520 nm were used.

Vesicle solubilisation Vesicle solubilisation by Triton X-100 was measured as the initial rate of relief of self-quenching of R18 upon disruption of the vesicles by the detergent. Small vesicles containing 2 mol% of R18 were prepared by sonication and solubilised by the addition of 0.5 % w/v of Tritin X-100. The initial rate of solubilisation was taken from the tangent of the increase of fluorescence versus time, and expressed in percentage of the maximum fluorescence per

second. Fluorescence was recorded on a SLM-Aminco SPF-500C spectrofluorometer. An excitation wavelength of 560 nm and an emission wavelength of 590 nm were used.

Acknowledgments

DSC was carried out during a visit to the University of Leicester, UK. Prof. Michael Blandamer and Dr. Barbara Briggs are acknowledged for their expert help in performing the experiments and analysing the results. Dr. Volker Oberle carried out the monolayer studies at the University of Halle, Germany. Wim Kruizinga and Jan Herrema are gratefully acknowledged for measuring the ^{31}P relaxation times.

3.8 References

(1) Regen, S.L.; Czech, B.; Singh, A. Polymerized vesicles. *J. Am. Chem. Soc.* 1980, 102, 6638-6639.

(2) Hub, H.; Hupfer, B.; Koch, H.; Ringsdorf, H. Polymerizable phospholipis analogues - new stable biomembrane and cell models. *Angew. Chem., Int. Ed. Engl.* 1980, 19, 938-940.

(3) Ringsdorf, H.; Schlarb, B.; Venzmer, J. Molecular architecture and function of polymeric oriented systems: models for the study of organization, surface recognition, and dynamics of biomembranes. *Angew. Chem., Int. Ed. Engl.* 1988, 27, 113-158.

(4) Singh, A.; Schnur, J.M. Polymerizable phospholipids. In: Phospholipids Handbook (Cevc, G., Ed.). Marcel Dekker, New York, 1993, pp 233-291.

(5) Regen, S.L.; Shin, J.; Yamaguchi, K. Polymer-encased vesicles. *J. Am. Chem. Soc.* 1984, 106, 2446-2447.

(6) Ringsdorf, H.; Schlarb, B.; Tyminski, P.N.; O'Brien, D.F. Permeability characteristics of liposomes in a net - membranes of dihexadecyl phosphate with polymerizable gegenions. *Macromolecules* 1988, 21, 671-677.

(7) Ringsdorf, H.; Schlarb, B. Preparation and characterization of unsymmetrical 'liposomes in a net'. *Makromol. Chem.* 1988, 189, 299-315.

(8) Reed, W.; Guterman, L.; Tundo, P.; Fendler, J.H. Polymerized surfactant vesicles: kinetics and mechanism of photopolymerization. *J. Am. Chem. Soc.* 1984, 106, 1897-1907

(9) Sells, T.D.; O'Brien, D.F. Two-dimensional polymerization of lipid bilayers: degree of polymerization of acryloyl lipids. *Macromolecules* 1994, 27, 226-233.

(10) Lei, J.; O'Brien, D.F. Two-dimensional polymerization of lipid bilayers: rate of polymerization of acryloyl and methacryloyl lipids. *Macromolecules* 1994, 27, 1381-1388.

(11) Bennett, D.E.; O'Brien, D.F. Photoinduced fusion of liposomes. *J. Am. Chem. Soc.* 1994, 116, 7933-7934.

(12) Bennett, D.E.; O'Brien, D.F. Photoactivated enhancement of liposome fusion. *Biochemistry* 1995, 34, 3102-3113.

(13) Blume, A. Phase transitions of polymerizable phospholipids. *Chem. Phys. Lipids* 1991, 57, 253-273.

(14) Hirano, K.; Fukuda, H.; Regen, S.L. Polymerizable ion-paired amphiphiles. *Langmuir* 1991, 7, 1045-1047.

(15) Kusumi, A.; Singh, M.; Tirrell, D.A.; Oehme, G.; Singh, A.; Samuel, N.K.P.; Hyde, J.S.; Regen, S.L. Dynamic and structural properties of polymerized phosphatidylcholine vesicle membranes. *J. Am. Chem. Soc.* 1983, 105, 2975-2980.

(16) MacDonald, R.C.; Simon, S.A. Lipid monolayer states and their relationships to bilayers. *Proc. Natl. Acad. Sci. USA* 1987, 84, 4089-4093.

(17) Möhwald, H. Phospholipid monolayers. In: Phospholipid Handbook (Cevc, G., Ed.). Marcel Dekker, New York, 1993, pp 579-602.

(18) Ringsdorf, H.; Schmidt, G.; Schneider, J. Oriented ultrathin membranes from monomeric and polymeric amphiphiles: monolayers, liposomes and multilayers. *Thin Solid Films* 1987, 152,207-222.

(19) Meier, H.; Sprenger, I.; Bärmann, M.; Sackmann, E. Radical polymerization of amphiphiles in a two-dimensional solution (mixed vesicles). *Macromolecules* 1994, 27, 7581-7588.

(20) Cullis, P.R. Lateral diffusion rates of phosphatidylcholine in vesicle membranes: effects of cholesterol and hydrocarbon phase transitions. *FEBS Letters* 1976, 70, 223-228.

(21) Burnell, E.E.; Cullis, P.R.; De Kruiff, B. Effects of tumbling and lateral diffusion on phosphatidylcholine model membrane ^{31}P NMR line shapes. *Biochim. Biophys. Acta* 1980, 603, 63-69.

(22) Smith, I.C.P.; Ekiel, I.H. Phosphorus-31 NMR of phospholipids in membranes. In: Phosphorus-31 NMR, Principles and Applications (Gorenstein, D.G., Ed.). Academic Press, Orlando, 1984, pp 447-475.

(23) McLaughlin, A.C.; Cullis, P.R.; Berden, J.A.; Richards, R.E. ^{31}P NMR of phospholipid membranes: effects of chemical shift anisotropy at high magnetic field strengths. *J. Magn. Resonance* 1975, 20, 146-165.

(24) Pink, D.A.; Merkel, R.; Quinn, B.; Sackmann, E.; Pencer, J. Intersecting polymers in lipid bilayers: cliques, static order parameters and lateral diffusion. *Biochim. Biophys. Acta* 1993, 1150, 189-198.

(25) Sackmann, E.; Eggl, P.; Fahn, C.; Bader, H.; Ringsdorf, H.; Schollmeier, M. Compound membranes of linearly polymerized and cross-linked macrolipids: preparation, microstructure and applications. *Ber. Bunsenges. Phys. Chem.* 1985, 89, 1198-1208.

(26) Gennis, R.B. Biomembranes: molecular structure and function. Springer Verlag, New York 1989, pp 182-187.

(27) Szoka, F.; Papahadjopoulos, D. Procedure for preparation of liposomes with large internal aqueous space and high capture by reverse-phase evaporation. *Proc. Natl. Acad. Sci. USA* 1978, 75, 4194-4198.

(28) Yeagle, P.L. Cholesterol and the cell membrane. *Biochim. Biophys. Acta* 1985, 822, 267-287.

(29) Kragh-Hansen, U.; Le Maire, M.; Noël, J.P.; Gulik-Krzywicki, T.; Møller, J.V. Transitional steps in the solubilization of protein-containing membranes and liposomes by nonionic detergent. *Biochemistry* 1993, 32, 1648-1656.

(30) Ebelhäuser, R.; Spiess, H.W. Deuteron NMR study of molecular mobility in a polymer model membrane. *Ber. Bunsenges. Phys. Chem.* 1985, 89, 1208-1214.

(31) Blandamer, M.J.; Briggs, B.; Butt, M.D.; Cullis, P.M.; Waters, M.; Engberts, J.B.F.N.; Hoekstra, D. Enthalpies of interaction between dimethyldioctadecylammonium bromide vesicles in aqueous solution and either dipicolinate or sulfate anions. *J. Chem. Soc. Faraday Trans.* 1994, 90, 727-732.

(32) Weinstein, J.N.; Yoshikami, S.; Henkart, P.; Blumenthal, R.; Hagins, W.A. Liposome - cell interaction: transfer and intracellular release of a trapped fluorescent marker. *Science* 1977, 195, 489-492.

Chapter 4

Calcium-induced fusion of vesicles of oligomerisable lipids[1]

Membrane fusion has been examined in a model system of small unilamellar vesicles of negatively charged lipids which can be oligomerised through the lipid head groups. Oligomerisation can be induced either in both bilayer leaflets or in the inner leaflet exclusively. As shown by lipid mixing assays, electron microscopy and light scattering, calcium-induced fusion of bilayer vesicles is strongly retarded and inhibited by the oligomerisation. Remarkably, oligomerisation of only the inner leaflet of the bilayer is already sufficient to affect fusion. Calcium-induced aggregation of the vesicles is not affected. The efficiency of inhibition and retardation of fusion critically depends on the relative amount of oligomeric lipid present, on the concentration of Ca^{2+} ions, and on temperature. Implications for the mechanism of bilayer membrane fusion are discussed in terms of lipid lateral diffusion and membrane curvature effects.

4.1 Introduction

Calcium-induced fusion of liposomes was the first model system for biological membrane fusion that was studied in detail, particularly in the pioneering work of Papahadjopoulos *c.s.*[1, 2, 3] Divalent calcium ions bind strongly to the negatively charged phosphate in the lipid head groups,[4] reducing electrostatic repulsion, and removing large amounts of hydration water. In this way, Ca^{2+} induces formation of local hydrophobic domains at the bilayer surface[5, 6] which mutually attract each other. This results in aggregation of adjacent bilayers. At low concentration of Ca^{2+} ion, 'cis' (intravesicular) binding prevails, but at sufficiently high concentrations of Ca^{2+}, 'trans' (intervesicular) Ca^{2+} binding occurs, which leads to an additional bridging interaction between membranes, bringing them into molecular contact. Presumably, membrane merging is triggered by local packing defects in the bilayer due to phase separation and domain formation[6, 7, 8] that accompany the onset of calcium-induced phase transitions of certain lipids from the lamellar liquid-crystalline to either the lamellar gel-like or inverted hexagonal state.[2, 9, 10, 11]

It has always been tacitly assumed that a decreased fusogenicity of polymerised bilayers in part explains their increased colloidal stability,[12] but there are no systematic experimental studies of the fusion of vesicles of polymerised lipids. In Chapter 3 it has been shown that oligomerisation of the head groups of *beta*-nitrostyrene lipids leads to slower lateral diffusion of the lipids and denser packing of the lipid head groups. The work described in this chapter is based on the hypothesis that when lipid mobility in the bilayer is retarded and the curvature of

[1] The research reported in this chapter has been accepted for publication in *Biophys. J.*

the inner bilayer leaflet is reduced by means of covalent oligomerisation of the lipids, calcium-induced bilayer fusion proceeds slower and less efficiently. Calcium-induced vesicle aggregation of vesicles should not be affected by lipid oligomerisation. This chapter presents an investigation into calcium-induced fusion of small unilamellar vesicles (50-100 nm) containing lipid oligomers in either both leaflets or exclusively in the inner bilayer leaflet. These vesicles were prepared according to the procedures described in Chapter 2. By means of a combination of lipid mixing and contents leakage assays, electron microscopy (EM) and quasi-elastic light scattering (QELS), this study presents evidence that it is possible to develop a dilute system of vesicles in which 'slow motion fusion' occurs. It should be emphasised that the strict transmembrane asymmetry makes these vesicles fundamentally different from mixed liposomes of fusogenic and non-fusogenic lipids (such as phosphatidylserine and phosphatidylcholine[13,14,15] or phosphatidic acid and phosphatidyl-choline[16]), which are known to fuse progressively slower as the phosphatidylcholine content is increased. Also, these vesicles are different from liposomes composed of membrane-spanning, 'bolaform' lipids, which are known to exhibit very slow fusion due to the fact that the membrane leaflets cannot diffuse independently.[17,18]

4.2 Calcium-induced fusion of *beta*-nitrostyrene lipid vesicles

The extent and the rate of lipid mixing during vesicle fusion was measured by the *n*-octadecyl rhodamine (R18) assay.[19] Under certain circumstances the R18 assay disagrees with other fusion assays.[20,21] The resonance energy transfer (RET) assay employing rhodamine and NBD-labeled phosphatidylethanolamine[22] or assays employing pyrene-labeled lipids[23] provide no suitable alternative since the BNS moiety inhibits efficient NBD or pyrene excitation, either through quenching or absorbance in the excitation wavelength range. However, the R18 and the RET assay yield identical results for calcium-induced fusion of small vesicles of DHPPFP (which does not interfere with NBD excitation), and therefore the R18 assay was employed with confidence. Moreover, in all experiments it was carefully verified that no probe exchange occurred spontaneously, and probe dilution was not observed in the absence of unlabeled vesicles.

An overview of the extent of fusion of small vesicles (50-100 nm) of BNS lipids as recorded by the R18 assay is presented in Figure 4.1. The assay was carried out at 50 °C, except for the experiment with DOPBNS vesicles, where the assay was performed at 60 °C. All lipid vesicles fuse quite efficiently and rapidly. A constant fluorescence signal (indicating completion of the fusion process) was reached within 5 minutes. The threshold Ca^{2+} concentration for fusion is 0.5 mM. The highest extent of fusion was obtained at *ca.* 5 mM of Ca^{2+} ion. At higher Ca^{2+} concentrations, flocculation of fusion products becomes a dominant process. Small vesicles of lipids with short alkyl chains fuse more efficiently than small vesicles of lipids with longer alkyl chains (DDPBNS >DTPBNS > DHPBNS > DOPBNS). Cleavage of the BNS moiety has a marginal effect on the extent of fusion of small vesicles (compare DHPBNS and DHPPFP). No significant fusion occurs below the main phase transition temperature of the bilayers.

Vesicle fusion was examined in more detail for small vesicles of DHPBNS at 50 °C (Tables 4.1 and 4.2). The extent of fusion was dependent on the Ca^{2+} concentration: fusion is negligible below 0.5 mM of Ca^{2+}, increases with Ca^{2+} concentration up to 5 mM, and levels off at higher Ca^{2+} concentrations. Fusion is strongly inhibited by oligomerisation of the lipids in the vesicles.

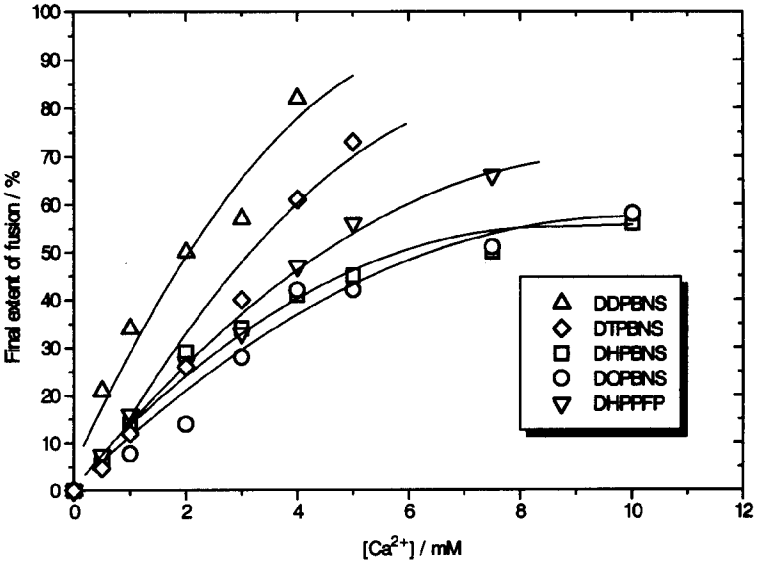

Figure 4.1 Ca^{2+} concentration dependence of the extent of symmetric fusion of small vesicles of DDPBNS, DTPBNS, DHPBNS, DOPBNS and DHPPFP. Extents of fusion were recorded by the R18 assay for lipid mixing at 50 °C (60 °C for DOPBNS).

No significant fusion occurs below 3 mM of Ca^{2+}. Interestingly, inhibition is comparable for vesicles in which both bilayer leaflets are oligomerised and vesicles in which only the inner (*endo*) bilayer leaflet is oligomerised. The relative efficiency of inhibition is dependent on the Ca^{2+} concentration: it is optimal (> 90 %) up to 3 mM, and decreases to 50 % at higher Ca^{2+} concentrations. Similar observations were made for the rate of fusion. Representative values of the rate of lipid mixing upon addition of Ca^{2+} are reported in Table 4.2. Fusion is fastest at the highest Ca^{2+} concentrations, and is strongly retarded by oligomerisation of the bilayer. A constant level of fluorescence is reached after 20 minutes, indicating completion of the fusion process. Retardation of fusion is more than 95 % at low Ca^{2+} concentration, and only slightly less at higher Ca^{2+} concentrations. Furthermore, fusion proceeds slower in vesicles in which both bilayer leaflets are oligomerised than in vesicles in which only the inner bilayer is oligomerised. Comparable results were obtained for vesicles of DDPBNS (see Section 6.2).

Because small and large vesicles can show different fusion behaviour,[24] fusion of large unilamellar vesicles of 200 nm diameter was tested in a control experiment. Compared to small vesicles, the extent of fusion of large vesicles was slightly higher (max. 20 % higher at 10 mM of Ca^{2+}), but the rate of fusion much lower (max. 80 %). However, upon oligomerisation of both bilayer leaflets, inhibition and retardation of fusion were quantitatively similar to the effect observed in fusion of small vesicles. Apparently, small and large unilamellar vesicles respond identically to lipid oligomerisation.

Table 4.1 Extent of fusion of small unilamellar vesicles of DHPBNS and DOPBNS.*

[Ca^{2+}] (mM)	*mono*-BNS extent (%)	*endo-oligo*-BNS extent (%)	inhibition (%)	*oligo*-BNS extent (%)	inhibition (%)
4:1 DHPBNS symmetric fusion					
1.0	14	0	100	0	100
3.0	35	3.7	89	2.8	92
5.0	45	23	49	21	53
10	56	32	57	28	50
4:1 DHPBNS-DOPBNS (R18) asymmetric fusion					
1.0	3.7	0	100	0	100
3.0	24	7.7	68	5.5	77
5.0	37	22	41	13	65
10	42	45	-7	33	21
4:1 DOPBNS-DHPBNS (R18) asymmetric fusion					
1.0	1.3	0	100	0	100
3.0	30	20	33	21	30
5.0	48	42	13	40	17
10	55	55	0	45	18
4:1 DOPBNS symmetric fusion					
1.0	7.7				
3.0	28				
5.0	42				
10	58				

Table 4.2 Initial rate of fusion of small unilamellar vesicles of DHPBNS and DOPBNS.*

[Ca^{2+}](mM)	*mono*-BNS rate (% s^{-1})	*endo-oligo*-BNS rate (% s^{-1})	retardation (%)	*oligo*-BNS rate (% s^{-1})	retardation (%)
4:1 DHPBNS symmetric fusion					
3.0	3.0	<<0.1	>95	<<0.1	>95
5.0	7.0	0.54	93	0.19	97
10	17	2.5	85	1.4	92
4:1 DHPBNS-DOPBNS (R18) asymmetric fusion					
3.0	0.45	0.17	62	<0.1	>78
5.0	2.0	0.87	56	0.22	89
10	2.7	2.7	0	0.83	69
4:1 DOPBNS-DHPBNS (R18) asymmetric fusion					
3.0	2.9	< 0.1	>95	< 0.1	>95
5.0	7.0	0.53	92	0.37	95
10	15	4.6	69	4.6	69
4:1 DOPBNS symmetric fusion					
3.0	1.0				
5.0	3.9				
10	9.4				

* Results of the R18 assay at 50 °C (60 °C for symmetric DOPBNS vesicle fusion).

The results from the lipid mixing assays were confirmed by EM of negatively-stained specimens of vesicles prior to and after fusion. The representative collection of micrographs in Figure 4.2 shows the disappearance of most small vesicles and the large overall increase in vesicle diameter that occurs upon induction of fusion of DHPBNS vesicles. In contrast, extensive aggregation, but relatively little fusion is found for DHPBNS vesicles in which both bilayer leaflets have been oligomerised. Similar results are obtained for vesicles of DDPBNS (see Section 6.2).

QELS provided the average changes in vesicle diameter during the fusion process. Figure 4.3 shows data obtained from scattering experiments. All vesicle solutions are rather polydisperse, particularly after fusion. These findings correspond well with the results obtained from EM. For a sample of vesicles of DDPBNS, the mean diameter prior to fusion was 90 nm. Upon addition of 5 mM of Ca^{2+} at room temperature, the mean diameter increased more than four-fold within 5 minutes, indicating extensive aggregation and fusion of vesicles. A stable, reproducible value was not reached. Instead, fusion was quenched by addition of EDTA (4 equivalents). The mean diameter after fusion is 300 nm, a three-fold increase, which means that on average about ten small vesicles fused into one large vesicle. Similarly, for a sample of vesicles of oligomerised DDPBNS with a mean diameter prior to fusion of 90 nm, a large increase in average particles size was found upon addition of Ca^{2+}, indicating extensive aggregation of vesicles. However, upon quenching with EDTA a mean diameter of

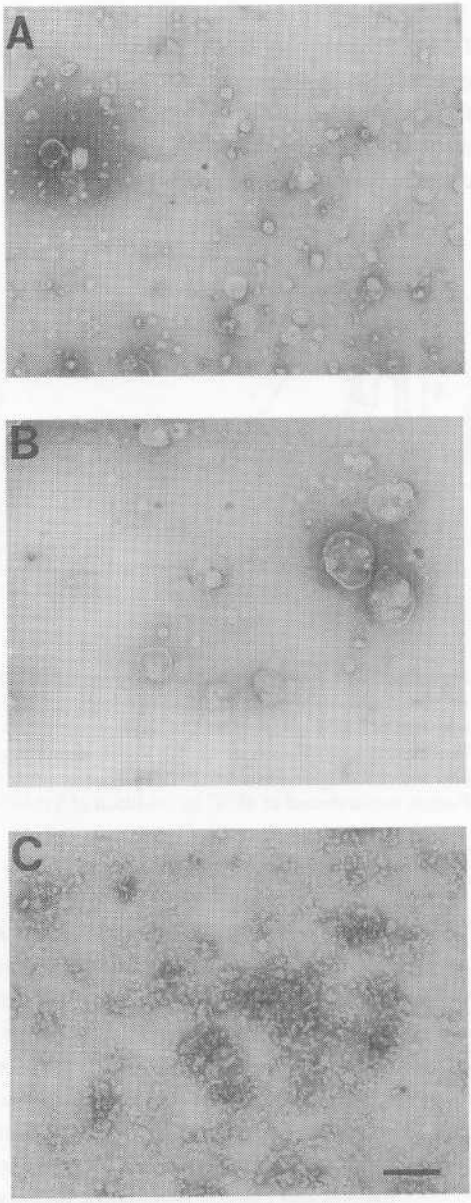

Figure 4.2 Electron micrographs of DHPBNS vesicles stained with PTA. (A): Small vesicles of DHPBNS. (B): Large vesicles of DHPBNS that result from fusion of the vesicles in (A) after addition of 5 mM of $CaCl_2$, 2 minutes incubation at 50 °C, and quenching with EDTA. (C): Persistence of small vesicles of oligomerised DHPBNS after addition of 5 mM of $CaCl_2$ at 50°C. The bar in (C) represents 500 nm.

110 nm was found, an increase of only 20 %, which means that the vesicles of oligomerised DDPBNS hardly fuse at all. The same experiment at 45 °C gave identical results. For a sample of DHPBNS, the number-weighted diameter was 70 nm prior to fusion and *ca.* 600 nm after fusion (experiments at 45 °C). After oligomerisation of the lipids, induction of fusion only resulted in an increase of the average diameter to 150 nm, indicative of strongly inhibited fusion compared to the monomer lipid vesicles.

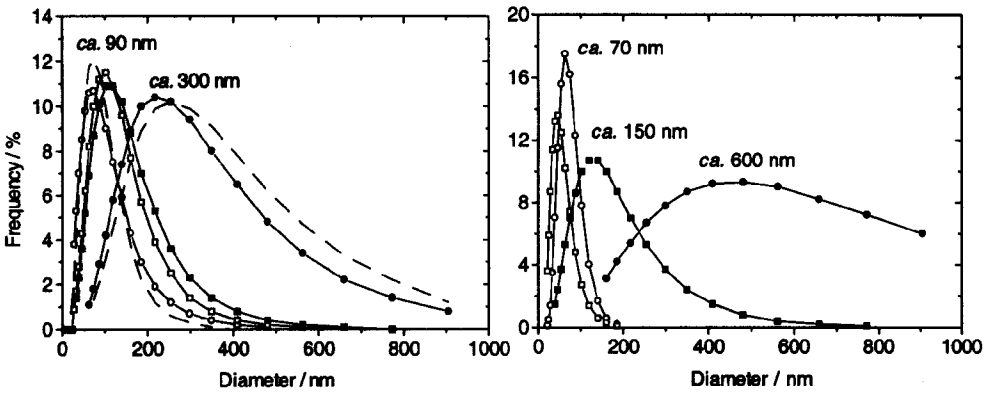

Figure 4.3 Left: number-weighted size distribution of vesicles of DDPBNS (circles) and oligomerised DDPBNS (squares) prior to (open symbols) and after fusion (closed symbols). Fusion was induced by addition of 5 mM of $CaCl_2$ at 25 °C and quenched by EDTA. The dashed lines show the size distributions that result from fusion at 45 °C. Right: number-weighted size distribution of vesicles of DHPBNS (circles) and oligomerised DHPBNS (squares) prior to (open symbols) and after fusion (closed symbols). Fusion was induced at 45 °C by addition of 5 mM of $CaCl_2$ and quenched by EDTA.

4.3 Asymmetric vesicle fusion

In addition to the symmetric vesicle fusion experiments described in Section 4.2, several asymmetric fusion experiments were monitored using the R18 assay. In these experiments, small vesicles of DHPBNS (with hexadecyl chains and T_m = 40 °C) were targeted at small vesicles of DOPBNS (with octadecyl chains and T_m = 54 °C), and *vice versa*. Since the experiments were carried out at 50 °C, vesicles of DOPBNS have a gel-like bilayer ($T < T_m$) and no symmetric fusion can take place. Vesicles of DHPBNS have a liquid-crystalline bilayer ($T > T_m$) and fusion occurs readily - both symmetrically and asymmetrically - but symmetric fusion is not reported by the assay, since it does not result in R18 dilution.

Extents and rates of asymmetric fusion are presented in Tables 4.1 and 4.2. Results are described for fusion of small vesicles of DOPBNS, labeled with R18, with 4 equivalents of small vesicles of DHPBNS (so that the assay reports dilution of R18 in target DOPBNS vesicles due to fusion with DHPBNS vesicles) and for fusion of small vesicles of DHPBNS, labeled with R18, with 4 equivalents of small vesicles of DOPBNS (so that the assay reports dilution of R18 in target DHPBNS vesicles due to fusion with DOPBNS vesicles). In either case it was observed that the extent and rate of fusion increase with increase in Ca^{2+} concentration. Below 1.0 mM no fusion is observed, and whereas the maximum extent of fusion is reached at 5 mM of Ca^{2+}

(and levels off at higher concentrations), the rate of fusion is highest at the highest Ca^{2+} concentration. The final extents of fusion are comparable to those observed in the symmetric fusion experiments. The observed rates of fusion are very different for the two asymmetric experiments. For DHPBNS targeted at DOPBNS, slow fusion is observed, with rates even smaller than those found for symmetric fusion of DOPBNS vesicles, perhaps due to competition of symmetric fusion of DHPBNS vesicles. For DOPBNS targeted at DHPBNS much faster fusion is observed, comparable to symmetric fusion of DHPBNS vesicles. Thus, in either case the target membrane composition is rate-determining.

Upon oligomerisation of the lipids in the DHPBNS vesicles (and *not* in the DOPBNS vesicles), lipid mixing is inhibited and retarded, and the fusion threshold concentration of Ca^{2+} increases to *ca.* 2 mM. If both bilayer leaflets of the DHPBNS vesicles are oligomerised, considerable inhibition (up to 75 %) and retardation (70-90 %) are observed when DHPBNS is targeted at DOPBNS, and modest inhibition (max. 30 %), but strong retardation (75-95 %) when DOPBNS is targeted at DHPBNS. If only the inner bilayer leaflet of the DHPBNS vesicles are oligomerised, considerable inhibition (max. 70 %) is observed when DHPBNS is targeted at DOPBNS, but only modest inhibition (max. 30 %) when DOPBNS is targeted at DHPBNS. Concerning the rates of fusion, modest retardation (max. 60 %) is observed when DHPBNS is targeted at DOPBNS but strong retardation (70-95 %) is found when DOPBNS is targeted at DHPBNS. In all fusion experiments, the inhibitory and retarding effects of oligomerisation decrease with increasing Ca^{2+} concentration. Both inhibition and retardation are more pronounced when DHPBNS is targeted at DOPBNS than *vice versa*, and both are clearly less pronounced in the asymmetric experiments compared to the symmetric fusion experiments.

The temperature dependence of the rate of fusion of DHPBNS vesicles targeted at DOPBNS vesicles labeled with R18 is illustrated in Figure 4.4. As anticipated, the rate of fusion for the monomer DHPBNS vesicles follows a sigma profile with a sharp increase around 40 °C, which corresponds to the T_m of DHPBNS. Below 40 °C, fusion activity is very low, and slightly above T_m the maximum rate of fusion is reached. No additional increase is found above 54 °C, which is the T_m of DOPBNS. Upon oligomerisation of both bilayers in DHPBNS vesicles, fusion is considerably retarded. Around T_m of DHPBNS, a gradual increase of the extent of fusion sets in, but only once the temperature approaches T_m of DOPBNS a significant increase of fusion rate is observed.

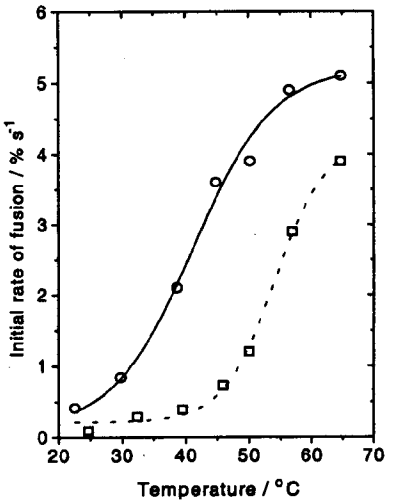

Figure 4.4 Temperature dependence of the rate of asymmetric fusion of vesicles of DHPBNS before (circles) and after (squares) oligomerisation, targeted at vesicles of DOPBNS. Rates of fusion were recorded by the R18 assay for lipid mixing.

At high temperature, monomer and oligomerised DHPBNS vesicles fuse nearly equally fast with DOPBNS vesicles. This implies that the optimal temperature window for inhibition of fusion is between the T_m's of DHPBNS and DOPBNS, *i.e.* between 40 °C and 54 °C.

In a second set of asymmetric fusion experiments, vesicles of DDPBNS (with dodecyl chains and T_m = -1 °C) were targeted at vesicles of DHPBNS (with hexadecyl chains and T_m = 40 °C). In order to monitor both lipid mixing and contents leakage in the course of fusion, vesicles of DHPBNS were either labeled with R18 or loaded with carboxyfluorescein (CF). The experiments were carried out at 25 °C, *i.e.* above T_m of DDPBNS, but below T_m of DHPBNS. Therefore, DDPBNS vesicles can fuse both symmetrically and asymetrically, but vesicles of DHPBNs can only fuse asymmetrically. It was carefully verified that under these conditions, no spontaneous lipid mixing or CF leakage did occur. Therefore, any R18 or CF dilution must result from asymmetric fusion. The results are presented in Figure 4.5.

According to the R18 assay, vesicles of DDPBNS targeted at vesicles of DHPBNS fuse efficiently. *No* significant leakage of CF is observed upon addition of Ca^{2+}, indicating an essentially non-leaky fusion process. The 1 to 5 dilution of contents that results from complete fusion does not lead to measurable relief of CF self-quenching.[25] However, CF is rapidly released *after addition of EDTA*, that is after quenching of the fusion process and after break-up of the aggregated clusters of fused vesicles. Hence, leakage during fusion is limited, but leakage is significant from the large, mixed DDPBNS/DHPBNS vesicles that result from fusion. This conclusion is consistent with (a) the finding that DHPBNS vesicles are impermeable to CF, whereas DDPBNS vesicles are very leaky (Section 3.5), and (b) literature data indicating that calcium-induced liposome fusion can occur with retention of aqueous contents.[26, 27] Also, CF leakage is secondary to lipid and contents mixing in calcium-induced fusion of phosphatidylserine liposomes.[28]

When vesicles of oligomerised DDPBNS were targeted at vesicles of oligomerised DHPBNS, only low extents of lipid mixing and contents release were observed. As expected, the target vesicles retain their contents in the absence of fusion. Again, in all experiments the extent of lipid mixing and contents release increases with Ca^{2+} concentration, but the inhibition due to oligomerisation decreases.

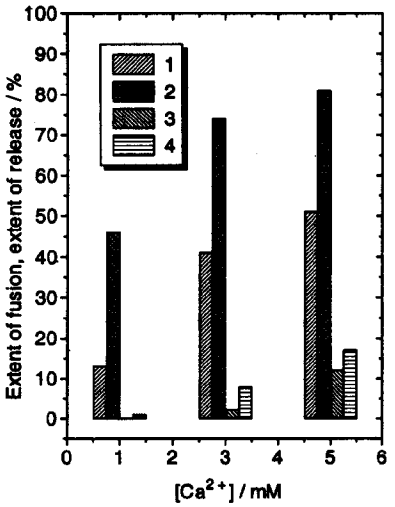

Figure 4.5 Comparison of the extent of lipid mixing and release of encapsulated CF as a result of calcium-induced fusion between vesicles of DDPBNS targeted at vesicles of DHPBNS at 25 °C. $[Ca^{2+}]$ = 1.0, 3.0 and 5.0 mM. Extents of lipid mixing prior to and after lipid oligomerisation are given in lanes 1 and 3, respectively. Extents of contents release are given in lanes 2 and 4, respectively.

4.4 Effects of EDTA addition

In all experiments using the R18 assay for lipid mixing, the observed extent of fusion reported in Table 4.1 and Figures 4.1, 4.4 and 4.5 was determined when the fluorescence had reached its maximum, and calcium ion had been removed by addition of 4 equivalents of EDTA. In the experiments with monomer lipid vesicles, addition of EDTA resulted in an instantaneous decrease of fluorescence. This decrease can be attributed to a break-up of vesicle aggregation, and to a decrease in turbidity and scattering in the sample, with concomitant decrease in the recorded fluorescence. In line with this explanation, the effect was most significant (up to 30 %) at the highest Ca^{2+} concentrations, but small at low Ca^{2+} concentrations. In contrast, in the experiments with vesicles of oligomerised lipids (either in both leaflets or only in the inner leaflet) addition of EDTA resulted in an *increase* of fluorescence. This suggests further lipid mixing upon removal of Ca^{2+}. The increase amounted to up to 25 % and increased with Ca^{2+} concentration, but decreased with temperature.

Furthermore, Ca^{2+} binding causes domain formation in bilayer membranes of anionic lipids, which is relieved upon removal of Ca^{2+} by EDTA.[6,7,8] Possibly, the same process occurs in bilayers of lipids with *beta*-nitrostyrene head groups. This conclusion is supported by the observation that at sub-fusion threshold concentrations of Ca^{2+}, and even in the absence of unlabeled vesicles (so that no R18 dilution can occur), Ca^{2+} induces a minor decrease of fluorescence (domain formation, clustering of R18, increased self-quenching), which is relieved by addition of EDTA (removal of Ca^{2+}, homogenisation of the bilayer, relief of self-quenching).

4.5 Fusion of oligomerised bilayer vesicles

Oligomerisation of lipid molecules does not influence calcium-induced vesicle aggregation, but strongly affects bilayer fusion of vesicles of *beta*-nitrostyrene lipids. Fusion is inhibited up to ten-fold in its extent, and fusion proceeds more than ten times slower. Lipid mixing and contents release assays, electron microscopy and quasi-elastic light scattering yield consistent results. In all of the experiments described above, the inhibitions are less pronounced than the retardations. Lipid oligomerisation has an influence on the kinetics rather than on the extent of bilayer fusion. In absolute terms, lipid mixing during calcium-induced fusion of vesicles of BNS lipids occurs within 1-5 minutes, depending on temperature and Ca^{2+} concentration. These rates are normal for calcium-induced vesicle fusion[13,14,15,16,24,28] and comparable to the rates recently reported for poly(ethylene glycol)-induced fusion, and biological membrane fusion.[29] However, upon oligomerisation of the lipids, fusion proceeds much slower and takes up to 20 minutes to arrive at much lower final extents. Oligomerised lipid membranes 'fuse in slow motion'. Inhibition (as well as retardation) of fusion is similar for vesicles in which both the outer and the inner bilayer leaflets, or only the inner bilayer leaflet is oligomerised. The additional inhibiting and/or retarding effect of oligomerisation of the lipids in the outer bilayer leaflet is almost negligible. In accordance with previous observations, the composition of the inner rather than the outer bilayer leaflet controls completion of bilayer fusion.[30,31,32]

It is important to note that the inhibitions that are reported by the R18 assay are undoubtedly inhibitions of lipid mixing as a result of fusion, and not inhibitions of the *assay*

as a result of slower lateral diffusion of the probe in the oligomerised membrane. As reported in Section 3.4, scrambling of lipid oligomers over the vesicle occurs on a time scale of seconds, whereas slow fusion requires up to 15 minutes.

The effect of lipid oligomerisation is dependent on three parameters. Firstly, the effect is more pronounced when more of the membranes participating are oligomerised, *e.g.* compare symmetric experiments (in which two oligomerised membranes fuse) and asymmetric experiments (in which only one of two fusing membranes is oligomerised). Alternatively, one could state that the effect of lipid oligomerisation is stronger at a higher relative oligomer content of the membranes participating in fusion, irrespective of the location of the oligomerised lipids. This observation matches the results from studies using mixed liposomes composed of fusogenic phosphatidylserine or phosphatidic acid and non-fusogenic phosphatidylcholine, in which fusion is progressively slower if the phosphatidylcholine content is increased.[13, 14, 15, 16] Secondly, the effect of oligomerisation decreases at higher Ca^{2+} concentration. Presumably, more fusion contact sites can be established when more Ca^{2+} is present, resulting in more rapid fusion. This is consistent with the notion that calcium-induced liposome fusion is normally aggregation rate-limited, but becomes fusion rate-limited at high Ca^{2+} concentration and reduced fusion rate.[28, 33] Finally, the effect of lipid oligomerisation decreases with temperature. As will be discussed below, this is consistent with the concept of oligomerised lipids posing a kinetic barrier for fusion.

Membrane fusion is a localised event in which two adjacent membranes approach, establish a microscopic region of 'molecular contact', bend into sharply curved transient structures, and eventually merge into one continuous membrane. This process demands flexibility of the membrane, which is largely governed by the thermotropic state of the hydrocarbon interior, the lateral diffusion coefficient of the lipid molecules, and the spontaneous curvature of the membrane leaflets.

As to the hydrocarbon interior, fusion activity is low if not absent below the main phase transition temperature of the membrane.[34] In the gel-like lamellar state, the hydrocarbon interior has a rigid packing, lipids diffuse only slowly across and over the bilayer, and the membrane is stiff compared to the fluid state above T_m. However, according to the DSC data (Section 3.2), the influence of lipid oligomerisation on the thermotropic phase behaviour of the hydrocarbon interior is modest, and cannot be invoked to explain the strong inhibition and retardation of fusion observed upon oligomerisation.

A high lateral diffusion coefficient of the lipid molecules in the membrane is a prerequisite for efficient membrane fusion. The molecular rearrangement of the lipid bilayers required in the course of fusion will only take place at an appreciable rate if the lipid molecules have sufficient degrees of freedom. As noted in Section 3.4, oligomerisation of the *beta*-nitrostyrene lipid head groups results in a large reduction of the lipid lateral diffusion. If both the inner and the outer bilayer leaflets are oligomerised, fusion is probably inhibited because the membrane will resist formation of membrane defects that would otherwise result in stalk-like fusion intermediates (*vide infra*). If only the inner bilayer leaflet is oligomerised, stalks may be formed but fusion pore formation is expected to be very slow. These considerations explain the strong inhibition and retardation of membrane fusion, even if the oligomerisation is induced in the inner bilayer leaflet only. The observation that inhibition and retardation of

fusion increase with a higher oligomer content of the membranes undergoing fusion, irrespective of the location of the oligomers, is entirely consistent with the fact that the lateral diffusion coefficient decreases with an increasing oligomer content.[35, 36] Furthermore, the observation that inhibition and retardation of fusion decrease with temperature is consistent with the notion of a decreased lateral diffusion of the oligomerised lipids: at higher temperatures, lateral diffusion is faster, and the effects of lipid oligomerisation diminish.

Concerning the spontaneous curvature of the bilayer, hemifusion is inhibited by lipids with a positive curvature (that tend to form micelles) in the *outer* membrane leaflet, because they disfavour formation of stalk-like fusion sites with negative curvature.[30, 31] In some cases, lipids with negative curvature (that tend to form inverted phases) have a modest promoting effect.[30, 31] In contrast, fusion pore formation and full fusion benefit from the presence of lipids with a positive curvature in the *inner* bilayer leaflet, whereas lipids with a negative curvature have a strongly inhibiting effect.[30, 31, 32] The data in Chapter 3 demonstrate that the head groups of BNS lipids pack closer upon oligomerisation, which would promote increased negative curvature of the oligomerised bilayer leaflet.[36, 37] Thus, pore formation and full fusion would be inhibited if the inner bilayer leaflet is oligomerised. This conclusion implies that hemifusion can occur, but full fusion is inhibited. In terms of bilayer spontaneous curvature, oligomerisation of the outer membrane leaflet may have only a small effect on the membrane fusion process.[30, 31]

The role of Ca^{2+} in the stages of the fusion process is not clear beyond the establishment of a region of molecular membrane contact. It is assumed that calcium-induced bilayer fusion is triggered by changes in lateral compressibility and structural defects that result from binding of Ca^{2+} to negatively charged lipid head groups.[3] Complexation of Ca^{2+} yields an essentially anhydrous Ca^{2+}-lipid complex, but electrostatic interactions and (de)hydration effects are not taken into account in the stalk-pore hypothesis of membrane fusion.[38, 39] Nevertheless, analogous models have been proposed for non-leaky calcium-induced membrane fusion.[3] One could speculate that structural defects as well as phase transitions are kinetically suppressed in bilayers of oligomerised lipids, and that this suppression poses an additional barrier to calcium-induced fusion. Similarly, it is anticipated that structural defects and phase transitions occur more readily in bilayers of lipids with short hydrophobic chains than in bilayers of lipids with long hydrophobic chains, which may explain why the former fuse more readily.

In addition, the observation of further lipid mixing upon removal of Ca^{2+} from the oligomerised vesicles could be an indication for a collapse of hemifused structures into full fusion. It is known that Ca^{2+} binding to anionic lipid head groups leads to denser head group packing as a result of a reduction of electrostatic and hydration repulsions and potential inter-lipid binding.[5] Denser head group packing leads to increased negative curvature, resulting in calcium-induced lamellar to inverted hexagonal phase transitions in bilayers containing phosphatidic acid or cardiolipin.[9, 10, 11] However, this phenomenon is not general since Ca^{2+} does not generate inverted hexagonal phases with phosphatidylserine despite strong promotion of fusion.[1] Possibly, the presence of Ca^{2+} is a prerequisite not only for stalk formation, but also for persistence of negatively curved hemifusion intermediates, which either relapse into unfused vesicles or collapse into full fusion upon removal of Ca^{2+} by EDTA.

In summary, a 'slow motion fusion' system has been devised that may allow fusion intermediate structures to be studied by ultrastructural techniques. Lipid oligomerisation leads to a reduced rate and extent of calcium-induced vesicle fusion. In the case of vesicles with an oligomerised inner bilayer leaflet only, it is anticipated that highly curved stalk and hemifusion intermediates may form readily, but completion of fusion is strongly inhibited. This concept is elaborated in Chapter 5.

4.6 Experimental section

Materials DDPBNS, DTPBNS, DHPBNS, DHPPFP and DOPBNS were synthesised as described in Chapter 2. Lipids were stored as 10-20 mM stock solutions in chloroform. Carboxyfluorescein (mixture of 5 and 6-carboxyfluorescein, Eastman Kodak Co.) and R18 (*n*-octadecyl rhodamine B chloride, Molecular Probes Inc.) were generously provided by the Laboratory of Physiological Chemistry of this University.

Preparation of unilamellar vesicles Small unilamellar vesicles were prepared by sonication as described in Section 2.8. Large unilamellar vesicles were prepared by hydration of a thin lipid film obtained by rotary-evaporation of a chloroform solution of the appropriate lipid (mixture) in the desired buffer solution at temperatures well above the lipid's T_m. The turbid lipid dispersion was freeze-thawed at least five times, and large unilamellar vesicles were obtained by repeated extrusion (at least ten times) through a 200 nm polycarbonate membrane in a LiposoFast Basic extruder (Avestin Inc.). Extrusion was performed at temperatures well above T_m, and the extruder was heated in a hot water bath if necessary. The procedure for the preparation of vesicles with oligomerised lipids has been described in Section 2.8. For oligomerisation of only the inner bilayer leaflet, the vesicles were subjected to an external pH jump (25 minutes at pH 12) that results in hydrolysis of the oligomerisable BNS groups at the outer bilayer leaflet exclusively, prior to photopolymerisation.

***n*-Octadecyl rhodamine fusion assay** Vesicle fusion was monitored using the *n*-octadecyl rhodamine (R18) assay for lipid mixing.[19] Lipid mixing is recorded as a relief of self-quenching of rhodamine as it is diluted upon fusion of labeled and unlabeled vesicles. 5 μM of vesicles with 2 mol% R18 and 20 μM of vesicles without fluorescent label were mixed in 2 mL of 5 mM HEPES/NaAc buffer (pH 7.4, 140 mM NaCl) at the appropriate temperature. Fusion was initiated by the addition of 0.5-10 mM of $CaCl_2$. Once the fluorescence increase had stopped, 4 equivalents of EDTA were added. Fluorescence prior to addition of $CaCl_2$ was taken as 0 % fusion (F_0), and the extent of mixing (F_{obs}) was determined after addition of EDTA. The value for complete fusion (F_{100}, complete mixing, i.e. 1 to 5 dilution of R18) was calculated from the fluorescence at infinite dilution (F_{inf}) upon addition of 0.5 % w/v of Triton X-100. F_{obs} and F_{inf} were corrected for volume changes. The extent of fusion for each experiment was calculated as: extent (%) = $(F_{obs}-F_0)/0.8(F_{inf}-F_0) \times 100$ %. The initial rate of fusion was calculated from the tangent of the increase of fluorescence versus time, and was expressed in percentage of fusion per second. In all experiments it was carefully verified that no lipid mixing occurred spontaneously, and no dilution was measured in the absence of unlabeled vesicles. Inhibition

of fusion (a decreased extent of fusion) was expressed in percentage relative to a reference experiment according to: (1 - $extent_{obs}/extent_{ref}$) x 100 %, and retardation of fusion (a decreased initial rate of fusion) was expressed according to: (1 - $rate_{obs}/rate_{ref}$) x 100 %. The results reported in Tables 4.1 and 4.2 and Figures 4.1, 4.4 and 4.5 are the averages of 3 to 5 independent experiments. Standard deviations do not exceed 20 %, but it was observed that the R18 assay is sensitive to small variations in vesicle sonication time and temperature, sample temperature, and concentration. Fluorescence was recorded using a SLM-Aminco SPF-500C spectrofluorometer using a thermostated cuvet holder. The sample was stirred continuously. An excitation wavelength of 560 nm and an emission wavelength of 590 nm were used.

Carboxyfluorescein leakage during vesicle fusion Carboxyfluorescein (CF) was entrapped in vesicles of DHPBNS as described in Section 3.8. 5 μM of DHPBNS vesicles containing 20 mM of CF and 20 μM of DDPBNS vesicles were mixed in 2 mL of 5 mM HEPES/NaAc buffer (pH 7.4, 140 mM NaCl added), and fusion was induced by the addition of 1-5 mM of $CaCl_2$. The sample was stirred continuously. After 5-10 minutes, fusion was quenched by the addition of 4 equivalents of EDTA. Finally, the vesicles were solubilised with 0.5 % (w/v) of Triton X-100. The extent of leakage as a result of fusion was calculated from F_0, the fluorescence prior to fusion, F_{obs}, the fluorescence observed after addition of $CaCl_2$ *and* EDTA, and F_{TX}, the fluorescence recorded after detergent solubilisation of the vesicles, as described in Section 3.8.

Electron microscopy Experiments were performed as described in Section 2.8.

Quasi-elastic light scattering Measurements were performed at 23 °C and at 46 °C as described in Section 2.8.

Acknowledgments

Nadia Bordin (ERASMUS exchange student from the University of Padova, Italy) performed some preliminary lipid mixing assays. Prof. Alain Brisson and Jan van Breemen are acknowledged for hospitality in the Electron Microscopy Department, and Prof. Dick Hoekstra for discussion of the results and for hospitality in the Laboratory of Physiological Chemistry.

4.7 References

(1) Papahadjopoulos, D.; Vail, W.J.; Jacobson, K.; Poste, G. Cochleate lipid cylinders: formation by fusion of unilamellar lipid vesicles. *Biochim. Biophys. Acta* 1975, 394, 483-491.

(2) Papahadjopoulos, D. Calcium-induced phase changes and fusion in natural and model membranes. *Cell Surf. Rev.* 1978, 5, 765-790.

(3) Papahadjopoulos, D.; Nir, S.; Düzgünez, N. Molecular mechanisms of calcium-induced membrane fusion. *J. Bioenerg. Biomembr.* 1990, 22, 157-179.

(4) The literature treasures a wealth of contradictory values of the binding constants of calcium to lipid head groups. For a review, see: Tatulian, S.A. Ionisation and ion binding. In: Phospholipids Handbook (Cevc, G., Ed.). Marcel Dekker, New York, 1993, pp 511-552.

(5) Ohki, S. A mechanism of divalent ion-induced phosphatidylserine membrane fusion. *Biochim. Biophys. Acta* 1982, 689, 1-11.

(6) Leckband, D.E.; Helm, C.A.; Israelachvili, J. Role of calcium in the adhesion and fusion of bilayers. *Biochemistry* 1993, 32, 1127-1140.

(7) Hoekstra, D. Fluorescence method for measuring the kinetics of Ca^{2+}-induced phase separations in phosphatidylserine-containing lipid vesicles. *Biochemistry* 1982, 21, 1055-1061.

(8) Haverstick, D.M.; Glaser, M. Visualisation of Ca^{2+}-induced phospholipid domains. *Proc. Natl. Acad. Sci. USA* 1987, 84, 4475-4479.

(9) Cullis, P.R.; De Kruijff, B. Lipid polymorphism and the functional roles of lipids in biological membranes. *Biochim. Biophys. Acta* 1979, 559, 399-420.

(10) Verkleij, A.J.; De Maagd, R.; Leunissen-Bijvelt, J.; De Kruiff, B. Divalent cations and chlorpromazine can induce non-bilayer structures in phosphatidic acid-containing model membranes. *Biochim. Biophys. Acta* 1982, 684, 255-262.

(11) Hong, K.; Baldwin, P.A.; Allen, T.M.; Papahadjopoulos, D. Fluorometric detection of the bilayer-to-hexagonal phase transition in liposomes. *Biochemistry* 1988, 27, 3947-3955.

(12) Fendler, J.H. Polymerized surfactant vesicles: novel membrane mimetic agents. *Science* 1984, 223, 890-894.

(13) Düzgünez, N.; Wilschut, J.; Fraley, R.; Papahadjopoulos, D. Studies on the mechanism of membrane fusion. Role of head group composition in calcium and magnesium-induced fusion of mixed phospholipid vesicles. *Biochim. Biophys. Acta* 1981, 642, 182-195.

(14) Düzgünez, N.; Nir, S.; Wilschut, J.; Bentz, J.; Newton, C.; Portis, A.; Papahadjopoulos, D. Calcium and magnesium-induced fusion of mixed phosphatidylserine/phosphatidylcholine vesicles: effect of ion binding. *J. Membr. Biol.* 1981, 59, 115-125.

(15) Silvius, J.R.; Gagné, J. Calcium-induced fusion and lateral phase separations in phosphatidylcholine/phosphatidylserine vesicles. Correlation by calorimetric and fusion measurements. *Biochemistry* 1984, 23, 3241-3247.

(16) Leventis, R.; Gagné, J.; Fuller, N.; Rand, R.P.; Silvius, J.R. Divalent cation induced fusion and lipid lateral segregation in phosphatidylcholine-phosphatidic acid vesicles. *Biochemistry* 1986, 25, 6978-6987.

(17) Relini, A.; Cassinadri, D.; Fan, Q.; Gulik, A.; Mirghani, Z.; De Rosa, M.; Gliozzi, A. Effect of physical constraints on the mechanisms of membrane fusion: bolaform lipid vesicles as model systems *Biophys. J.* 1996, 71, 1789-1795.

(18) Elferink, M.G.L.; van Breemen, J.F.L.; Konings, W.N.; Driessen, A.J.M.; Wilschut, J. Slow fusion of liposomes composed of membrane-spanning lipids. *Chem. Phys. Lipids* 1997, 88, 37-43.

(19) Hoekstra, D.; De Boer, T.; Klappe, K.; Wilschut, J. Fluorescence method for measuring the kinetics of fusion between biological membranes. *Biochemistry* 1984, 23, 5675-5681.

(20) Stegmann, T.; Schoen, P.; Bron, R.; Wey, J.; Bartoldus, I.; Ortiz, A.; Nieva, J.L.; Wilschut, J. Evaluation of viral membrane fusion assays. Comparison of the octadecyl rhodamine assay with the pyrene eximer assay. *Biochemistry* 1993, 32, 11330-11337.

(21) Stegmann, T.; Orsel, J.G.; Jamieson, J.D.; Padfield, P.J. Limitations of the octadecyl rhodamine dequenching assay for membrane fusion. *Biochem. J.* 1995, 307, 875-876.

(22) Struck, D.K.; Hoekstra, D.; Pagano, R.E. Use of resonance energy transfer to monitor membrane fusion. *Biochemistry* 1981, 20, 4093-4099.

(23) Pal, Y.; Barenholz, Y.; Wagner, R.R. Pyrene phospholipid as a biological fluorescent probe for studying the fusion of virus membrane with liposomes. *Biochemistry* 1988, 27, 30-36.

(24) Nir, S.; Wilschut, J.; Bentz, J. The rate of fusion of phospholipid vesicles and the role of bilayer curvature. *Biochim. Biophys. Acta* 1982, 688, 275-278.

(25) Chen, R.F.; Knutson, J.R. Mechanism of fluorescence concentration quenching of carboxyfluorescein in liposomes: energy transfer to nonfluorescent dimers. *Anal. Biochem.* 1988, 172, 61-77.

(26) Wilschut, J.; Düzgünez, N.; Hong, K.; Hoekstra, D.; Papahadjopoulos, D. Retention of aqueous contents during divalent cation-induced fusion of phospholipid vesicles. *Biophys. Biochim. Acta* 1983, 734, 309-318.

(27) Hui, S.W.; Nir, S.; Stewart, T.P.; Boni, L.T.; Huang, S.K. Kinetic measurements of fusion of phosphatidylserine containing vesicles by electron microscopy and fluorometry. *Biochim. Biophys. Acta* 1988, 941, 130-140.

(28) Wilschut, J.; Düzgünez, N.; Fraley, R.; Papahadjopoulos, D. Studies on the mechanism of membrane fusion: kinetics of calcium ion induced fusion of phosphatidylserine vesicles followed by a new assay for mixing of aqueous vesicle contents. *Biochemistry* 1980, 19, 6011-6021.

(29) Lee, J.; Lentz, B.R. Evolution of lipidic structures during model membrane fusion and the relation of this process to cell membrane fusion. *Biochemistry* 1997, 36, 6251-6259.

(30) Chernomordik, L.V.; Chanturiya, A.; Green, J.; Zimmerberg, J. The hemifusion intermediate and its conversion to complete fusion: regulation by membrane composition. *Biophys. J.* 1995, 69, 922-929.

(31) Chernomordik, L.V.; Kozlov, M.M.; Zimmerberg, J. Lipids in biological membrane fusion. *J. Membrane Biol.* 1995, 146, 1-14.

(32) Melikyan, G.B.; Brener, S.A.; Ok, D.C.; Cohen, F.S. Inner but not outer membrane leaflets control the transition from glycosylphosphatidylinositol-anchored influenza haemagglutinin-induced hemifusion to full fusion. *J. Cell Biol.* 1997, 136, 995-1005.

(33) Nir, S.; Bentz, J.; Wilschut, J. Mass action kinetics of phosphatidylserine vesicle fusion as monitored by coalescence of internal vesicle volumes. *Biochemistry* 1980, 19, 6030-6036.

(34) Wilschut, J.; Düzgünez, N.; Hoekstra, D.; Papahadjopoulos, D. Modulation of membrane fusion by membrane fluidity: temperature dependence of divalent cation induced fusion of phosphatidylserine vesicles. *Biochemistry* 1985, 24, 8-14.

(35) Pink, D.A.; Merkel, R.; Quinn, B.; Sackmann, E.; Pencer, J. Intersecting polymers in lipid bilayers: cliques, static order parameters and lateral diffusion. *Biochim. Biophys. Acta* 1993, 1150, 189-198.

(36) Sackmann, E.; Duwe, H.P.; Engelhardt, H. Membrane binding elasticity and its role for shape fluctuations and shape transformations of cells and vesicles. *Faraday Discuss. Chem. Soc.* 1986, 81, 281-290.

(37) Meier, H.; Sprenger, I.; Bärmann, M.; Sackmann, E. Radical polymerization of amphiphiles in a two-dimensional solution (mixed vesicles). *Macromolecules* 1994, 27, 7581-7588.

(38) Siegel, D.P. Energetics of intermediates in membrane fusion: comparison of stalk and inverted micellar intermediate mechanisms. *Biophys. J.* 1993, 65, 2124-2140.

(39) Chernomordik, L.V.; Zimmerberg, J. Bending membranes to the task: structural intermediates in bilayer fusion. *Curr. Opin. Struct. Biol.* 1995, 5, 541-547.

Chapter 5

Electron microscopic investigations of calcium-induced fusion of vesicles with an oligomerised inner bilayer leaflet

The morphology and calcium-induced fusion of vesicles of the lipids DHPBNS and DDPBNS were investigated using cryo-electron microscopy. DHPBNS vesicles are not spherical but flattened, ellipsoidal structures. Although indications were obtained for hemifusion of DHPBNS vesicles with an oligomerised inner bilayer leaflet, it is difficult to provide unambiguous electron microscopic proof due to the irregular morphology of the fusing vesicles. DDPBNS vesicles show the expected spherical morphology. Upon addition of excess $CaCl_2$, DDPBNS vesicles fuse into dense aggregates that show a regular spacing corresponding to the bilayer width. Upon addition of EDTA, the aggregates readily disperse into large unilamellar vesicles. At low concentration of calcium, DDPBNS vesicles with an oligomerised inner bilayer leaflet form small multilamellar aggregates, in which a spacing corresponding to the bilayer width appears. Addition of excess EDTA results in slow redispersal of the calcium-lipid aggregates into a heterogeneous mixture of mostly bilamellar, spherical vesicles and networks of thread-like vesicles.

5.1 Introduction

Structural characterisation of membrane fusion intermediates is a long-standing challenge to electron microscopists. The main obstacle is the inherent transient and local nature of the fusion event. In addition, microscopic studies are frustrated by potential artifacts during sample preparation. Staining, dehydration, vitrification, fracturing, and shear during blotting and film formation all pose risks to the fragile lipid structures that may occur during membrane fusion.[1] Therefore, compelling results obtained by skillful microscopists deserve admiration.

The very first indications of hemifused membranes were observed in freeze-fracture and thin-section electron microscopy (EM) of zoospores.[2] In fact, this early report is the first to mention the hemifusion diaphragm as a potential fusion intermediate. Chandler and Heuser[3] observed fusion pores in freeze-fracture EM of granules in mast cells. Also calcium-induced fusion of phosphatidylserine vesicles was studied by freeze-fracture EM.[4,5] 'Point defects' and 'lipidic intramembranous particles'(IMPs), indicative of primary contact sites of adjacent bilayers that may be on the verge of fusion, were observed in freeze-fracture EM studies of concentrated lipid suspensions containing substantial amounts of phosphatidylethanolamines.[6,7] Generally, these 'particles' were viewed as so-called 'inverted micellar intermediates' (IMIs) that were believed to consitute the onset of lamellar-to-inverted-hexagonal phase transitions. Based on theoretical considerations,[8] the search for inverted micellar intermediates was abandoned in

favour of a quest for stalk-like structures and early fusion pores or 'interlamellar attachments' (ILAs). Again, formation of stalks and ILAs was associated with lamellar to inverted hexagonal phase transitions which were characterised in cryo-EM studies of more dilute liposome solutions by Siegel *c.s.*[9, 10, 11] and by Frederik *c.s.*[12, 13] Recently, membrane microprotrusions as well as the initial fusion pores of Influenza virus-liposome fusion were revealed in freeze-fracture EM of pelleted virus/liposome mixtures.[14] Most of the studies mentioned above suffered from the inherent transient nature of the fusion event: all intermediate stages of membrane fusion have limited life-times, they are localized events that occur infrequently, and observations are essentially a matter of lucky shots. In many systems this problem has been circumvented by a drastic increase in concentration.

In this respect, the synthetic lipid vesicles described in Chapters 2, 3 and 4 present a promising avenue towards structural characterisation of intermediate structures of membrane fusion. Bilayer vesicles of *beta*-nitrostyrene lipids can be oligomerised exclusively in their inner bilayer leaflet, resulting in membranes with an extreme transverse asymmetry: while the outer leaflet is fusogenic, the inner leaflet is not. The stalk-pore model of membrane fusion predicts that extensive hemifusion occurs between such bilayers, whereas full fusion will be strongly inhibited. This hypothesis was experimentally verified using EM.

Unfortunately, the experimental work described in the following sections required a compromise between optimal conditions for cryo-EM and limitations to the model system of calcium-induced vesicle fusion. Cryo-EM would benefit from high lipid concentrations (> 5 mM), large vesicle diameters (*ca.* 200 nm), and spherical symmetry, since in transmission view of a thin film this would result in a neat coplanar arrangement of spheres in which interactions of adjacent bilayer membranes can be optimally resolved. On the other hand, selective *exo*-vesicular hydrolysis limits the lipid concentration (< 2 mM). Moreover, not all lipids yield perfectly spherical vesicles under all conditions, and binding of Ca^{2+} leads to formation of very dense aggregates which are not easily resolved.

5.2 Morphology and calcium-induced fusion of DHPBNS vesicles

Negatively-stained samples of sonicated vesicles of DHPBNS show 50-100 nm vesicles of spherical symmetry. Either uranyl acetate or phosphotungstic acid were used as staining agent. The morphology and integrity of the vesicles is not affected by oligomerisation of either both or exclusively the inner bilayer leaflet (Sections 2.5 and 2.6). Upon addition of calcium chloride (2.5 mM) to vesicles with an oligomerised inner bilayer leaflet, incubated above T_m, aggregates are formed consisting of 3 to 20 small vesicles (Figure 5.1). The aggregates become larger if either the calcium concentration or the incubation time is increased. It is difficult to establish whether these aggregates are either aggregates of intact vesicles with intact bilayers, or aggregates of vesicles that are hemifused and share a common bilayer diaphragm (Figure 5.2), as would be expected according to the stalk-pore model. Although some micrographs suggest the latter interpretation, they do not provide unambiguous evidence as a result of the poor resolution of the bilayer.

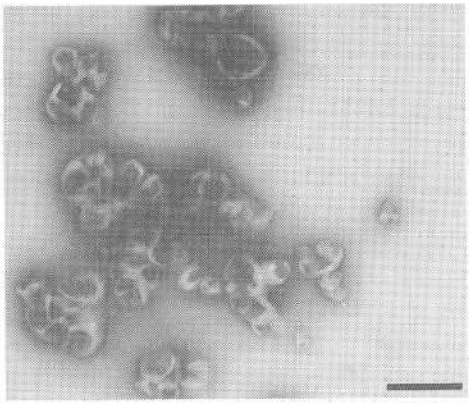

Figure 5.1 Micrograph of sonicated vesicles of DHPBNS (0.25 mM) with an oligomerised inner bilayer leaflet, incubated for 4 minutes with $CaCl_2$ (5.0 mM) at 50 °C. Negative staining with UAc. Bar represents 500 nm.

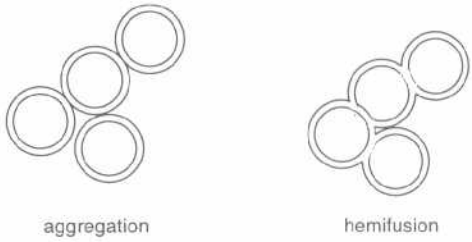

Figure 5.2 Hypothetical transmission view of aggregated unilamellar vesicles and hemifused unilamellar vesicles. Resolution of the bilayer is a must for unambiguous discrimination.

Cryo-EM is able to resolve the bilayer structure of liposomes, and some initial experiments were carried out using formvar/carbon coated grids as support for the vitrified sample solution. Again, addition of calcium chloride (2.5 mM) to sonicated vesicles with an oligomerised inner bilayer leaflet, incubated above T_m, resulted in the formation of small aggregates of vesicles (Figure 5.3). The individual bilayer leaflets of the vesicles can clearly be discriminated. Many of the aggregated vesicles share a common bilayer diaphragm, which is direct evidence for *hemifusion* of these vesicles. In several cases, the diaphragm extends over more than 20 nm. The diaphragms which extend furthest frequently show signs of rupture.

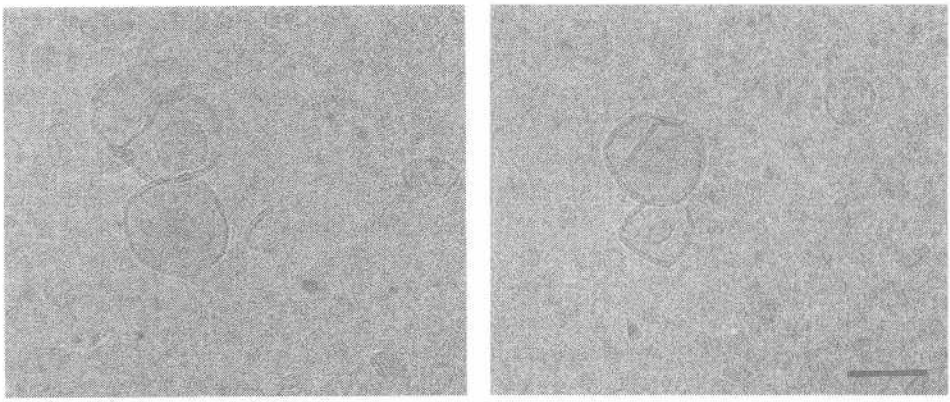

Figure 5.3 Micrograph collection of hemifused, sonicated vesicles of DHPBNS with an oligomerised inner bilayer leaflet incubated for 4 minutes with $CaCl_2$ (2.5 mM) at 50 °C. Cryo-EM on formvar/carbon support. Bar represents 100 nm.

Consequently, the samples were examined using vitrified aqueous films on holey carbon coated copper grids in order to exclude the influence of surface adsorption of the aggregated vesicles. Surprisingly, control experiments showed that vesicles of DHPBNS are flattened, ellipsoidal structures rather than perfect spheres (Figure 5.4). The flattened morphology was not affected by the method of preparation of the vesicles (sonication, extrusion, dialysis). In addition, the same flattened morphology was observed irrespective of whether vesicles were vitrified from a temperature above or below their main phase transition temperature (40 °C, see Chapter 2), whether or not the inner bilayer leaflet was oligomerised, and whether the vesicles were prepared either in buffer (with or without 140 mM NaCl) or in water. Apparently, the morphology is inherent to the molecular structure of DHPBNS. This has been observed for several other synthetic lipid vesicles.[15, 16, 17] Addition of 20 mol% of cholesterol to the vesicles seemed to improve the tendency of DHPBNS to form spherical vesicles, but such an amount of cholesterol makes the bilayers very stiff and most probably reduces their fusogenicity.[18] The atypical morphology can easily remain unnoticed in samples on a formvar/carbon support, since most vesicles absorb with their flattened side to the supporting film and appear spherical in projection. However, the unsupported film yields a view of more random orientations of the vesicles, and indeed many vesicles are observed edge-on, or partially edge-on (Figure 5.4). Clearly, many vesicles are bent, and even twisted.

Unfortunately, the irregular features of the flattened vesicles leads to an extremely complicated projection view. Aggregation and (hemi)fusion of such vesicles further increase the complexity, and it becomes very difficult to discriminate bilayer aggregation and (hemi)fusion, and to check bilayer integrity. Therefore, the investigations were continued using DDPBNS, which has shorter hydrocarbon chains than DHPBNS (dodecyl instead of hexadecyl), and should yield more flexible, spherical bilayer vesicles. An option for future studies could be to mix DHPBNS with a phospholipid, or with DDPBNS, in order to provide neatly spherical vesicles of which aggregation and fusion phenomena can be visualised with much less ambiguity.

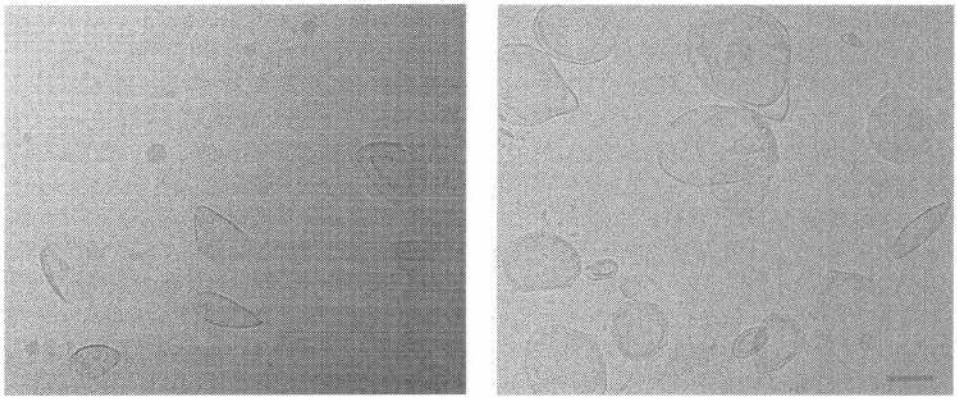

Figure 5.4 Flattened and ellipsoidal vesicles of DHPBNS obtained after extrusion through 200 nm polycarbonate membranes. Cryo-EM on holey carbon films. Bar represents 200 nm.

5.3 Calcium-induced fusion of DDPBNS vesicles

Vesicles of DDPBNS display the anticipated smooth and spherical morphology when they are examined by cryo-EM of a holey carbon-supported vitrified film (Figure 5.5). The vesicles have spherical morphology irrespective of their size and method of preparation, and the salt concentration of the aqueous medium. Occasionally, larger, multilamellar vesicles persist after sonication or extrusion. If vesicles are extruded through a 200 nm polycarbonate membrane, so-called 'vase-like' vesicles with large invaginations are frequently encountered.[19] In addition, the extruded vesicle solution contains relatively high numbers of small vesicles, which could reflect the relative ease of dispersion of DDPBNS in aqueous solution due to its short hydrophobic chains and relatively high water solubility.

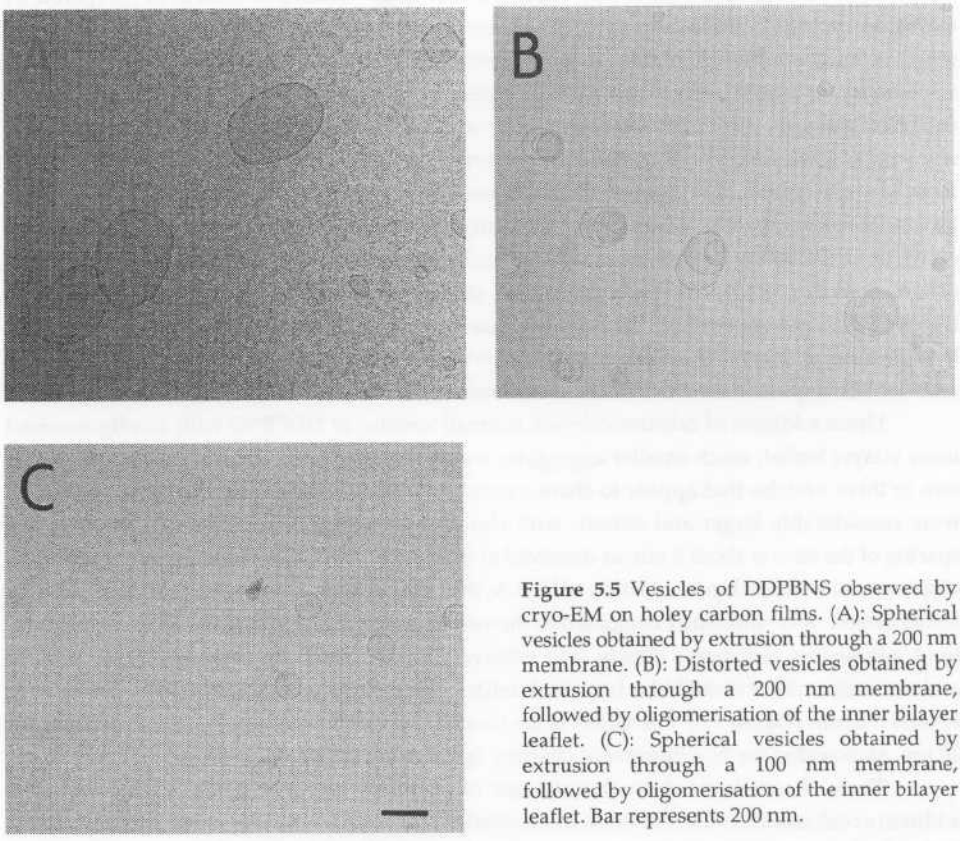

Figure 5.5 Vesicles of DDPBNS observed by cryo-EM on holey carbon films. (A): Spherical vesicles obtained by extrusion through a 200 nm membrane. (B): Distorted vesicles obtained by extrusion through a 200 nm membrane, followed by oligomerisation of the inner bilayer leaflet. (C): Spherical vesicles obtained by extrusion through a 100 nm membrane, followed by oligomerisation of the inner bilayer leaflet. Bar represents 200 nm.

Upon addition of calcium chloride to small or large vesicles of DDPBNS (prior to lipid oligomerisation) aggregates with diameters up to 300 nm are observed (EM data not shown). No unilamellar vesicles can be detected. These aggregates have high density and occasionally a regular spacing of *ca.* 3 nm can be observed in the lipid packing. The dimensions of this spacing correspond to the width of a dodecyl lipid bilayer, but they are much too small for a stacking of hydrated lipid bilayers at equilibrium distance, as in multilamellar vesicles. Possibly, the

extremely dense packing indicates almost completely dehydrated calcium-DDPBNS aggregates, as observed for phosphatidylserine.[4] However, freeze-fracture EM or X-ray diffraction rather than cryo-EM should be used to determine the structure of these dense aggregates. In addition, these observations contradict the retention of contents that was observed during fusion of DDPBNS with DHPBNS vesicles (see Section 4.3). Upon addition of a four-fold excess of EDTA (relative to calcium) to the calcium-DDPBNS aggregates, they redisperse within a few seconds and a solution of large unilamellar vesicles results (EM data not shown).

Preparation of vesicles of DDPBNS with an oligomerised inner bilayer leaflet is feasible at 5 °C, provided the selective hydrolysis of the *exo*-vesicular *beta*-nitrostyrene groups of DDPBNS vesicles (illustrated in Figure 2.6) is rapidly followed by photopolymerisation of the remaining *endo*-vesicular *beta*-nitrostyrene groups, and the vesicle solution is kept at low temperature. Using cryo-EM, it was observed that large vesicles of DDPBNS (prepared by extrusion through a 200 nm polycarbonate membrane) show a morphological response to selective oligomerisation of the inner bilayer leaflet: they loose their smooth spherical appearance and show invaginations and protrusions (Figure 5.5). Small vesicles (prepared by extrusion through a 100 nm membrane, or by sonication) do not show such a morphological response (Figure 5.5). Possibly, the invaginations and protrusions are a consequence of an increasingly negative curvature of the inner leaflet as a result of oligomerisation of the head groups of the lipids in the inner leaflet. This curvature effect was suggested in the monolayer study of DHPBNS described in Section 3.3 and the discussion in Section 4.5, and has been observed in the literature.[20] Such monolayer destabilisation does affect the morphology of DDPBNS and not of DHPBNS bilayers (because of the much shorter hydrophobic chains that hold the bilayer together), and does affect large vesicles but not small ones (because the small ones cannot respond due to curvature restraints).

Upon addition of calcium chloride to small vesicles of DDPBNS with an oligomerised inner bilayer leaflet, much smaller aggregates were observed. Some aggregates comprise only two or three vesicles that appear to share a common bilayer diaphragm. But most aggregates were considerably larger and denser, with closely packed multilayer rims (Figure 5.6). The spacing of the rims is about 3 nm, as observed in the dense, calcium-induced aggregates of non-oligomerised vesicles. Upon addition of EDTA, the vesicles with an oligomerised inner bilayer leaflet behave very differently compared to the vesicles which are not oligomerised: the calcium-lipid aggregates redisperse slowly into relatively small, *bilamellar* vesicles (Figure 5.6). In addition, networks of thread-like, branched unilamellar vesicles were observed that extend over several microns (Figure 5.6). The width of the threads is variable, but usually no less than about 20 nm, as expected for two bilayers of charged lipids at equilibrium distance.

These observations show that vesicles of DDPBNS fuse into dense aggregates upon addition of calcium chloride, but do so more slowly if they contain an oligomerised inner bilayer leaflet. In that case, fusing vesicles are occasionally trapped in a hemifused intermediate stage, but much less frequently than in the case of DHPBNS vesicles with an oligomerised inner leaflet. It is anticipated that the stability of hemifusion intermediates increases with increasing hydrophobic chain length of the lipid molecules. In addition, the presence of intermediates is strongly dependent on the Ca^{2+}concentration. If the Ca^{2+} concentration is more than 5 mM, no intermediates are observed.

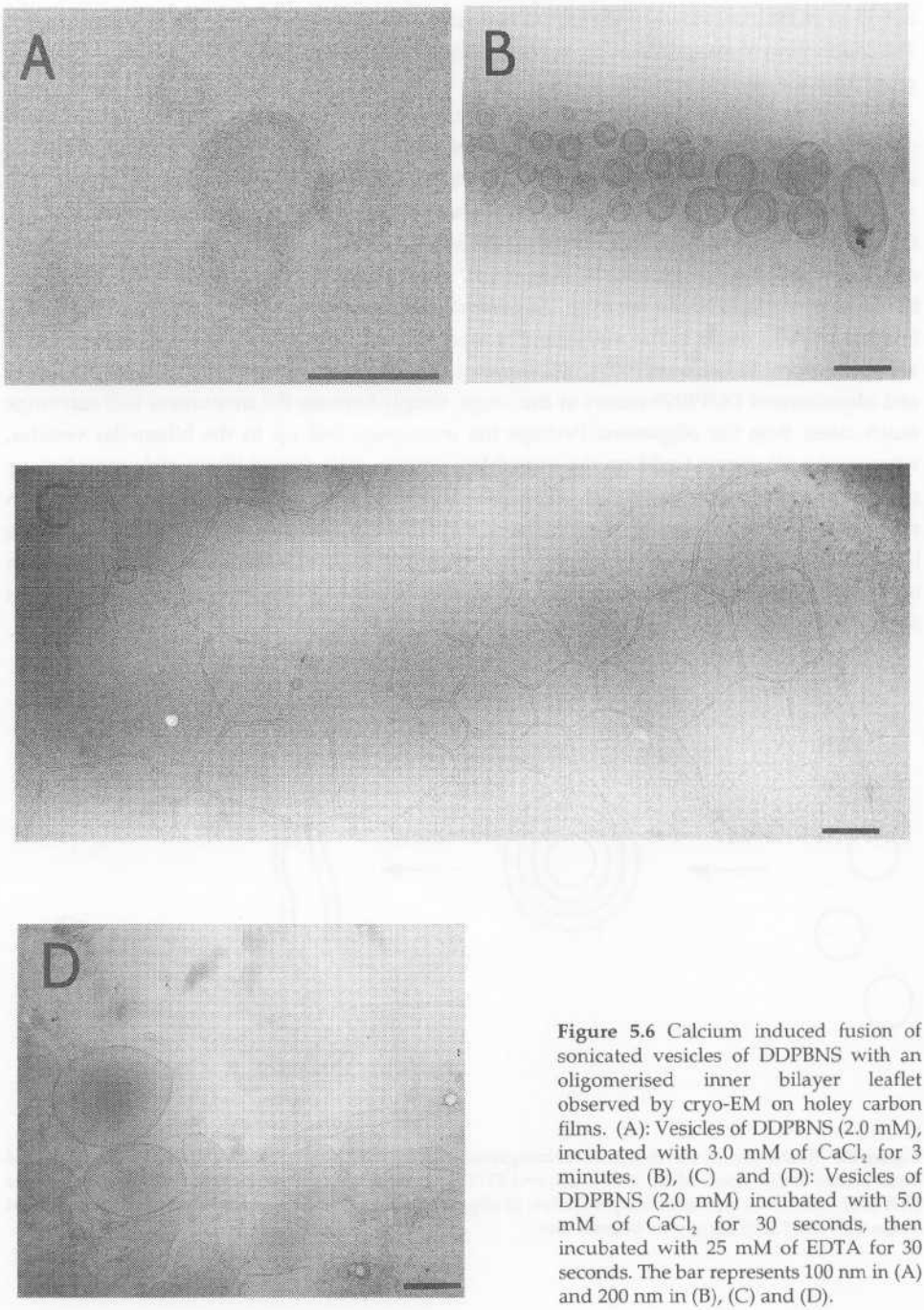

Figure 5.6 Calcium induced fusion of sonicated vesicles of DDPBNS with an oligomerised inner bilayer leaflet observed by cryo-EM on holey carbon films. (A): Vesicles of DDPBNS (2.0 mM), incubated with 3.0 mM of $CaCl_2$ for 3 minutes. (B), (C) and (D): Vesicles of DDPBNS (2.0 mM) incubated with 5.0 mM of $CaCl_2$ for 30 seconds, then incubated with 25 mM of EDTA for 30 seconds. The bar represents 100 nm in (A) and 200 nm in (B), (C) and (D).

The dense calcium-DDPBNS aggregates redisperse upon removal of calcium by EDTA, but do so much more slowly if the parent vesicles contain an oligomerised inner bilayer leaflet. The observation of many bilamellar vesicles is highly intriguing. Thread-like vesicles appear to grow from the aggregates (Figure 5.6).

Figure 5.7 presents a speculative representation of the structural rearrangements which occur when first $CaCl_2$ and next EDTA are added to vesicles of DDPBNS with an oligomerised inner bilayer leaflet. Upon addition of $CaCl_2$, vesicles fuse into multilamellar aggregates. The vesicles fuse faster and more extensively at higher concentrations of $CaCl_2$, in accordance with the results of the lipid mixing assays presented in Chapters 4 and 6. The aggregates are largely dehydrated as a result of efficient binding of Ca^{2+} to the DDPBNS head groups, which is reflected by the close packing of the lamellae. At present, whether or not the asymmetry of the fusing bilayers remains intact in the multilamellar arrangement is uncertain. The aggregates slowly redisperse upon addition of EDTA, and one could imagine that a phase separation of monomer and oligomerised DDPBNS occurs at this stage, simply because the monomers will rearrange much faster than the oligomers. Perhaps the monomers end up in the bilamellar vesicles, whereas the oligomers build up the thread-like vesicles. The thread-like vesicle morphology could be the result of the preference of the linear lipid oligomers for a parallel orientation upon redispersal of the calcium-lipid aggregates. However, the mechanism of formation of the bilamellar vesicles is unclear. In any case, it is likely that these extensive rearrangements upon addition of EDTA to the calcium-lipid aggregates account for the lipid mixing described in Section 4.4.

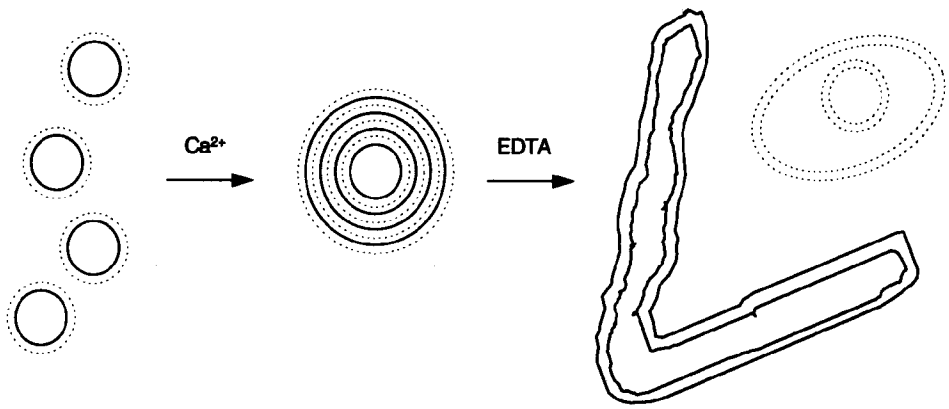

Figure 5.7 Illustration of the structural rearragements of DDPBNS vesicles containing an oligomerised inner bilayer leaflet upon addition of $CaCl_2$ and EDTA. Dotted lines represent bilayer leaflets of monomer DDPBNS, solid lines represent bilayer leaflets of oligomerised DDPBNS. The multilamellar arrangement in the Ca^{2+}-DDPBNS aggregate is uncertain.

5.4 Conclusions

Limited electron microscopic evidence was obtained for calcium-induced hemifusion of DHPBNS vesicles with an oligomerised inner bilayer leaflet. However, vesicles of DHPBNS are flattened, elipsoidal structures and the analysis of their interactions is complicated.

Compared to vesicles which are devoid of oligomerised lipids, vesicles of DDPBNS with an oligomerised inner bilayer leaflet show slow but complicated morphological changes during calcium-induced fusion, as well as upon quenching of the fusion process with EDTA. At present, it is difficult to rationalise these observations. There is no convincing microscopic evidence of calcium-induced hemifusion of vesicles of DDPBNS, which may relate to the relatively short hydrophobic chains of this lipid.

5.5 Experimental section

Materials DDPBNS and DHPBNS were prepared as described in Chapter 2. Cholesterol was obtained from Sigma.

Vesicle preparation Vesicles were prepared by three different methods. Small unilamellar vesicles were prepared by probe sonication and large unilamellar vesicles were prepared by extrusion through a 100 or 200 nm polycarbonate membrane, as described in sections 2.8 and 4.6, respectively. In addition, large unilamellar vesicles of DHPBNS were prepared by detergent dialysis. A clear solution of mixed micelles of 5 mg DHPBNS and 30 mg *n*-octyl *beta*-D-glucopyranoside in 1 mL of 5 mM HEPES/NaAc buffer (pH 7.4) was put in a small dialysis tube and dialysed overnight against 2 x 100 mL buffer kept at 45 °C (the buffer solution was replaced after *ca.* 3 hours). Preparation of DHPBNS vesicles with an oligomerised inner bilayer leaflet was performed as described in section 2.8 (with [DHPBNS] *ca.* 2 mM and pH 12). Preparation of DDPBNS vesicles with an oligomerised inner bilayer leaflet was performed by a selective hydrolysis of the *exo*-vesicular BNS groups at 5 °C with [DDPBNS] *ca.* 2 mM and pH 12 during 75 minutes, followed by photopolymerisation of the *endo*-vesicular BNS groups during 10 minutes. These vesicles were kept at 5 °C to avoid loss of bilayer asymmetry as a result of lipid *flip-flop*, and used for EM on the day of preparation.

Calcium-induced fusion Fusion experiments with vesicles of DHPBNS were performed with a lipid concentration of 1-2 mM in 5 mM HEPES/NaAc (pH 7.4) incubated at 50 °C. Fusion was induced by the addition of 2.5 mM of $CaCl_2$ while the mixture was stirred or vortexed. Samples for EM were taken after an incubation time of 30 seconds to 4 minutes. Fusion experiments with vesicles of DDPBNS *with an oligomerised inner bilayer leaflet* were performed with a lipid concentration of 1-2 mM in 5 mM HEPES/NaAc (pH 7.4) incubated at room temperature. Fusion was induced by the addition of 3.0-5.0 mM of $CaCl_2$ while the mixture was stirred or vortexed. Samples for EM were taken after an incubation time of 0.5-3.0 minutes. Control experiments to study fusion of vesicles of DDPBNS were performed with a lipid concentration of 2 mM in 5 mM HEPES/NaAc (pH 7.4) incubated at room temperature. Fusion was induced by the addition of 10 mM $CaCl_2$ while the mixture was stirred or vortexed. Samples for EM were taken after an

incubation time of 30 seconds. In order to study the effect of EDTA addition after calcium-induced fusion of DDPBNS vesicles, samples that had been incubated with $CaCl_2$ for 30 seconds were incubated a with four-fold excess (relative to calcium) of EDTA.

Electron microscopy Samples for negative staining were prepared as described in Section 2.8. Samples for cryo-EM were brought on a formvar/carbon coated copper grid, or on a holey carbon coated grid (made hydrophilic by glow discharge in air), and a thin film was obtained by gentle blotting with filter paper. Several samples of DHPBNS vesicles were prepared in a Controlled Environment Vitrification System at 50 °C and high relative humidity. The samples were rapidly vitrified by plunging them into liquid ethane. The grids were quickly transferred to Gatan or Philips cryo-holders and examined in JEOL of Philips electron microscopes, operated at 100 or 120 kV. Images were recorded in under low dose conditions.

Acknowledgments

The help and advice of skillful electron microscopists in the Department of Biophysical Chemistry of this University was essential to these investigations and is gratefully acknowledged. Marc Stuart and Jan van Breemen performed most of the cryo-EM experiments, and Prof. Alain Brisson contributed through careful and critical consideration of the results. In addition, Prof. Ishi Talmon and Dr. Dganit Danino at the Technion in Haifa (Israel) are thanked for their efforts to contribute to this project.

References

(1) Burger, K.N.J.; Calder, L.J.; Frederik, P.M.; Verkleij, A.J. Electron microscopy of virus-liposome fusion. *Methods Enzymol.* 1993, 220, 362-379.

(2) Pinto da Silva, P.; Noguira, M.L. Membrane fusion during secretion. *J. Cell Biol.* 1977, 73, 161-181.

(3) Chandler, D.E.; Heuser, J.E. Arrest of membrane fusion events in mast cells by quick-freezing. *J. Cell. Biol.* 1980, 86, 666-674.

(4) Papahadjopoulos, D.; Vail, W.J.; Jacobson, K.; Poste, G. Cochleate lipid cylinders: formation by fusion of unilamellar lipid vesicles. *Biochim. Biophys. Acta* 1975, 394, 483-491.

(5) Kachar, B.; Fuller, N.; Rand, R.P. Morphological responses to calcium-induced interaction of phosphatidylserine-containing vesicles. *Biophys. J.* 1986, 50, 779-788.

(6) Hui, S.W.; Stewart, T.P.; Boni, L.T. Membrane fusion through point defects in bilayers. *Science* 1981, 212, 921-923.

(7) Verkleij, A.J. Lipidic intramembranous particles. *Biochim. Biophys. Acta* 1984, 779, 43-63.

(8) Siegel, D.P. Energetics of intermediates in membrane fusion: comparison of stalk and inverted micellar intermediate mechanisms. *Biophys. J.* 1993, 65, 2124-2140.

(9) Siegel, D.P.; Burns, J.L.; Chestnut, M.H.; Talmon, Y. Intermediates in membrane fusion and bilayer/nonbilayer phase transitions imaged by time-resolved cryo-transmission electron microscopy. *Biophys. J.* 1989, 56, 161-169.

(10) Siegel, D.P.; Green, W.J.; Talmon, Y. The mechanism of lamellar-to-inverted-hexagonal phase transitions: a study using temperature-jump cryo-electron microscopy. *Biophys. J.* 1994, 66, 402-414.

(11) Siegel, D.P.; Epand, R.M. The mechanism of lamellar-to-inverted hexagonal phase transitions in phosphatidylethanolamine: implications for membrane fusion mechanisms. *Biophys. J.* 1997, 73, 3089-3111.

(12) Frederik, P.M.; Stuart, M.C.A.; Verkleij, A.J. Intermediary structures during membrane fusion as observed by cryo-electron microscopy. *Biochim. Biophys. Acta* 1989, 979, 275-278.

(13) Frederik, P.M.; Burger, K.N.; Stuart, M.C.; Verkleij, A.J. Lipid polymorphism as observed by cryo-electron microscopy. *Biochim. Biophys. Acta* 1991, 1062, 133-141.

(14) Kanaseki, T.; Kawasaki, K.; Murata, M.; Ikeuchi, Y.; Ohnishi, S. Structural features of membrane fusion between Influenza virus and liposome as revealed by quick-freezing electron microscopy. *J. Cell Biol.* 1997, 137, 1041-1056.

(15) Spevak, W.; Nagy, J.O.; Charych, D.H.; Schaefer, M.E.; Gilbert, J.H.; Bednarski, M.D. Polymerized liposomes containing C-glycosides of sialic acid: potent inhibitors of Influenza virus in vitro infectivity. *J. Am. Chem. Soc.* 1993, 115, 1146-1147.

(16) Hammarström, L.; Velikian, I.; Karlsson, G.; Edwards, K. Cryo-TEM evidence: sonication of dihexadecyl phosphate does not produce closed bilayers with smooth curvature. *Langmuir* 1995, 11, 408-410.

(17) Zirkzee, H.F. A novel approach to the encapsulation of silica particles. Ph. D. Thesis, Technische Universiteit Eindhoven, 1997.

(18) Bentz, J.; Ellens, H. Membrane fusion: kinetics and mechanisms. *Colloids Surf.* 1988, 30, 65-112.

(19) Lasic, D.D.; Strey, H.; Stuart, M.C.A.; Podgornik, R.; Frederik, P.M. The structure of DNA liposome complexes. *J. Am. Chem. Soc.* 1997,119, 832-833.

(20) Meier, H.; Sprenger, I.; Bärmann, M.; Sackmann, E. Radical polymerization of amphiphiles in a two-dimensional solution (mixed vesicles). *Macromolecules* 1994, 27, 7581-7588.

Chapter 6

Thermodynamics of calcium-induced vesicle fusion[I]

Oligomerisation of the lipid head groups inhibits calcium-induced fusion of small unilamellar vesicles of the lipid sodium 1,2-di-n-dodecyloxypropyl 4-(beta-nitro)styryl phosphate (DDPBNS), but does not influence vesicle aggregation. Addition of a copolymer of lauryl methacrylate and acrylamide (LMPAM) provides the vesicles with a steric shield that prevents both fusion and aggregation. Microcalorimetric determination of the enthalpies of vesicle aggregation and fusion was possible by comparing heats associated with titrations of vesicles to $CaCl_2$ in the absence and presence of LMPAM, both prior to and after oligomerisation of the lipids in the vesicles. Whereas calcium-induced aggregation is associated with an enthalpy of + 2.6 ± 0.1 kJ (mol lipid)$^{-1}$, fusion occurs with minimal endothermic heat. The driving force of membrane fusion must be of entropic origin, and an interpretation is suggested.

6.1 Introduction

A fundamental perspective of membrane fusion that has clearly remained underdeveloped both theoretically and experimentally is a sound thermodynamic analysis of the process. This observation is perhaps even more surprising in view of the extensive thermodynamic descriptions of shape transformations of bilayers,[1] which have been framed in the spontaneous curvature model of Helfrich[2] and the bilayer-coupling model put forward by Svetina and Zeks.[3] The stalk-pore model of membrane fusion is partly based on calculations of the Gibbs energy of formation of hypothetical fusion intermediates from planar lipid bilayers.[4] Thus, the model provides some insight into the activation parameters of membrane fusion, albeit *in vacuo*, but it does not elucidate the thermodynamic driving force(s) of membrane fusion. Papahadjopoulos *c.s.*[5] reported the experimental enthalpy of reaction between phosphatidylserine liposomes and Ca^{2+}, but the recorded heat is a combined result of Ca^{2+}-lipid binding, phase transitions in the bilayer, and liposome aggregation and fusion. Recently, a microcalorimetric analysis of fusion between liposomes and Influenza virus indicated a rather strong endothermic enthalpy of membrane fusion.[6] Unfortunately, the thermodynamic analysis is complicated. Moreover, the authors confuse reaction enthalpies and Gibbs energies of activation, and do not elaborate on the potential entropic driving force for the endothermic process, and on the role of specific protein-lipid interactions.

This chapter reports experiments with the purpose of determining the enthalpy of calcium-induced fusion in a model system composed of vesicles of DDPBNS (which can be oligomerised in the bilayer), either in the absence or presence of a copolymer of lauryl

[I] The research described in this chapter has been submitted for publication in *J. Phys. Chem. B.*

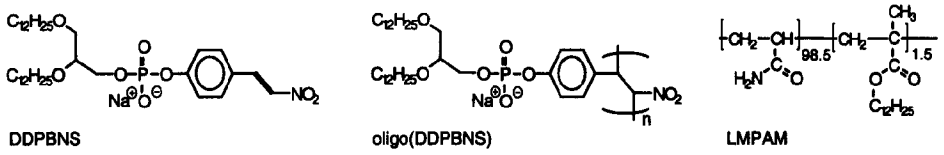

Figure 6.1 Molecular structures of DDPBNS, oligomerised DDPBNS, and the copolymer of lauryl methacrylate and acrylamide (LMPAM).

methacrylate and acrylamide (LMPAM) that efficiently anchors into the hydrophobic interior of the bilayer[7, 8, 9] (Figure 6.1). The interaction of LMPAM and small vesicles of negatively charged lipids has been described.[7] At the low concentrations used in this study (< 0.25 % w/v), depletion interactions can be ignored.

In this model system, the complexities of the biological fusion event have been reduced to three, distinguishable processes: binding of Ca^{2+}, vesicle aggregation, and bilayer fusion. Admittedly, this is a gross simplification of *in vivo* membrane fusion, but the results of this conceptually simple approach have general significance and provide insight into thermodynamics of calcium-induced membrane fusion.

6.2 Separating calcium ion binding, vesicle aggregation, and bilayer fusion

Fusion of small vesicles of DDPBNS was monitored using the *n*-octadecyl rhodamine assay[10] for lipid mixing. The use of this assay (which disagrees with other fusion assays under certain conditions) was warranted in Chapter 4. As can be seen in Figure 6.2, the vesicles fuse readily upon addition of 3-10 mM of $CaCl_2$ at room temperature. After oligomerisation of the lipids, fusion is largely inhibited (Chapter 4). The effect is particularly striking at low Ca^{2+} concentrations. In the presence of a low concentration of LMPAM, no calcium-induced lipid mixing is observed at all. The minimal concentration of LMPAM required to inhibit lipid mixing corresponds to a molar ratio of DDPBNS to LMPAM of 40 to 1. In contrast, poly(acrylamide) (PAM) of comparable molecular weight does not affect fusion at these concentrations.

Aggregation of small vesicles was measured as an increase in turbidity upon addition of $CaCl_2$. The rates of aggregation of the vesicles prior to and after oligomerisation of DDPBNS are equal. Whereas aggregation is not influenced by the non-anchoring PAM, no aggregation was observed if LMPAM was added to the vesicles in a 40 to 1 lipid to polymer ratio (Figure 6.3).

Samples of small vesicles of DDPBNS in the absence and presence of LMPAM and PAM prior to and after addition of $CaCl_2$ were examined using an electron microscope (Figure 6.4). In the absence of polymer, extensive vesicle fusion was evident from an up to tenfold increase in average vesicle diameter upon addition of $CaCl_2$. Similar observations were made in the presence of non-anchoring PAM. However, fusion was blocked in the presence of LMPAM (40 to 1 lipid to polymer ratio).

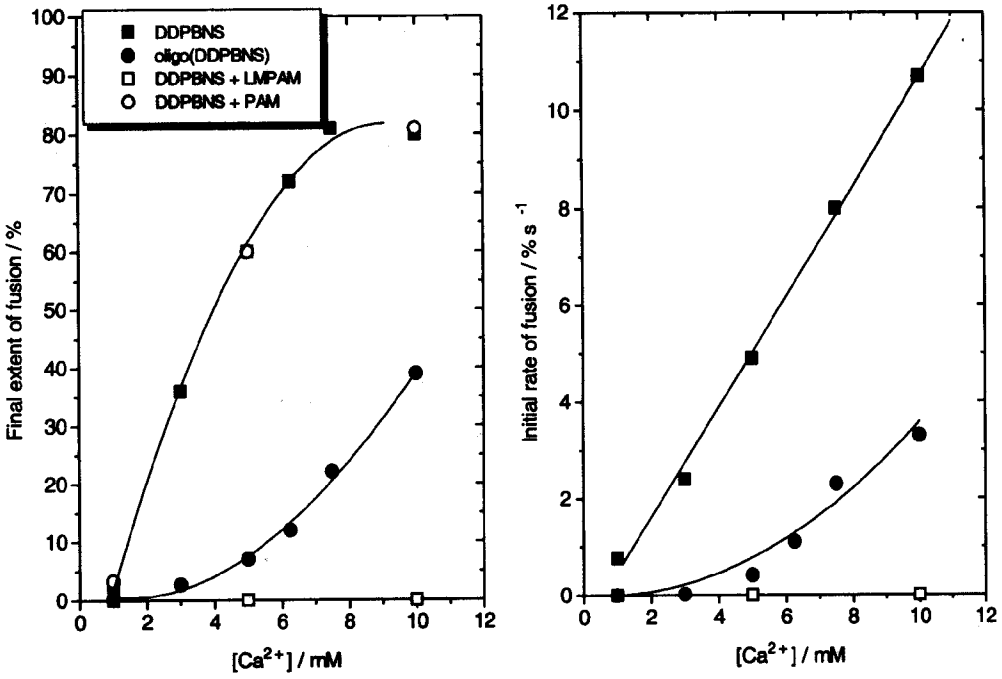

Figure 6.2 (Top) R18 assay of lipid mixing during calcium-induced fusion of small unilamellar vesicles of DDPBNS. The extent of lipid mixing is shown on the left, the initial rate of mixing is shown on the right.

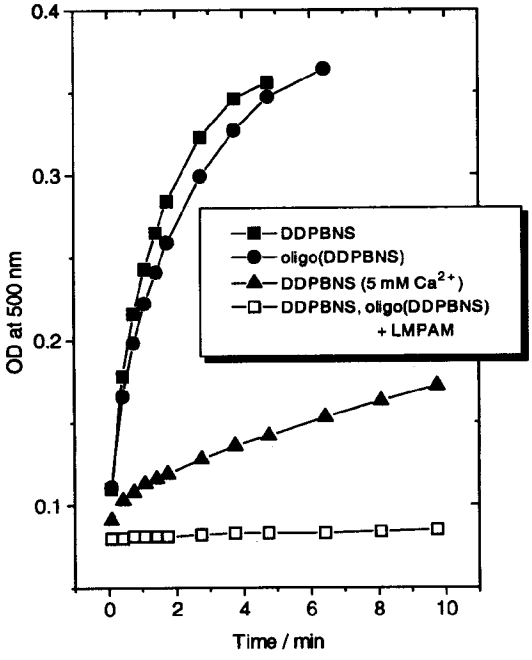

Figure 6.3 (Left) Aggregation of small unilamellar vesicles of DDPBNS (0.1 mM) monitored as an increase in turbidity upon addition of 10 mM of $CaCl_2$.

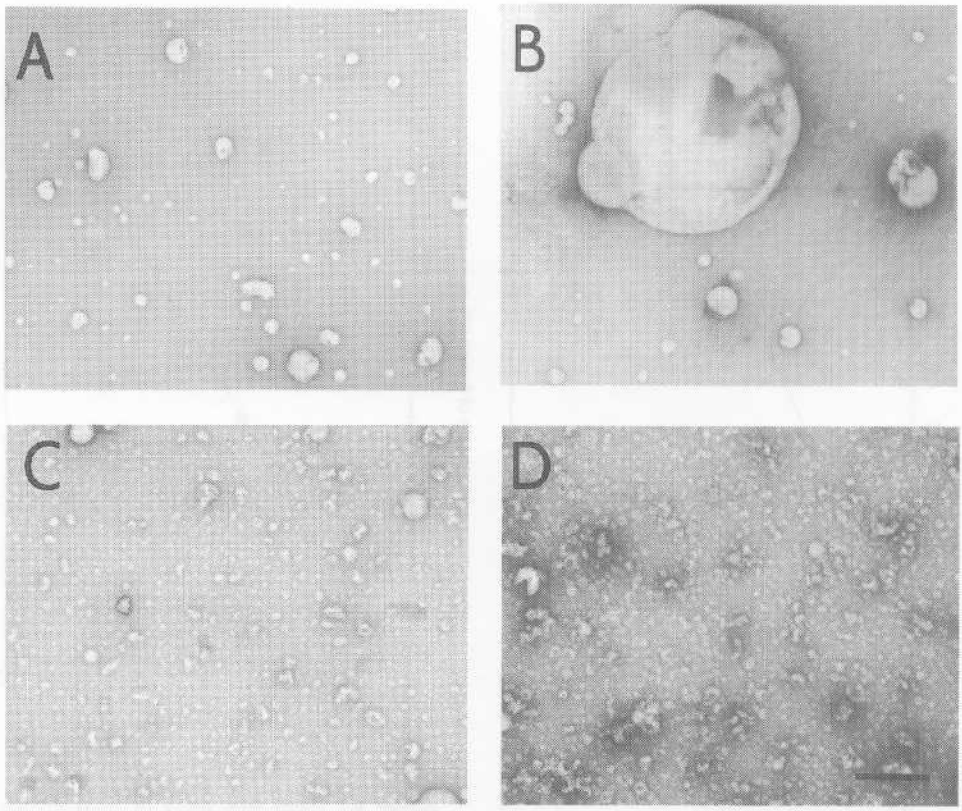

Figure 6.4 Micrographs of vesicles of DDPBNS. Bar represents 250 nm. (A) Small vesicles of DDPBNS (B): Large vesicles of DDPBNS that result from calcium-induced fusion of small vesicles. (C) Small vesicles of DDPBNS in the presence of LMPAM (DDPBNS/LMPAM = 40/1). (D) After addition of LMPAM, calcium-induced aggregation and fusion of the vesicles are completely inhibited.

As described in Chapters 3 and 4, lateral diffusion of the lipid oligomers over the bilayer surface is slow relative to diffusion of the monomers, and fusion is strongly inhibited. In addition, unfavourable curvature effects may play a role (see Section 4.5). However, calcium-induced aggregation of the vesicles is not affected by oligomerisation. LMPAM provides the vesicles with a steric shield that prevents both aggregation and fusion, even at high Ca^{2+} concentrations. Similar observations have been described for liposomes containing a small percentage of poly(ethylene glycol)-derived lipids, as well as lipids substituted with various other water-soluble polymers.[11] PAM has no hydrophobic moiety and is unable to anchor into the vesicle bilayer. Consequently, it lacks the inhibitory effect of LMPAM on aggregation and fusion. The polymer concentration is too low to induce fusion via depletion interaction.[12]

In sum, lipid mixing assays, turbidity measurements and electron microscopy, as well as quasi-elastic light scattering (Section 4.2) provide consistent evidence for a three-step calcium-induced fusion process of small vesicles of DDPBNS, that can be stopped at any of the three successive stages. At room temperature, vesicles of DDPBNS fuse efficiently at a total lipid

concentration of 25-200 μM and Ca^{2+} concentration of 5.0 mM. After oligomerisation of the lipid head groups in the vesicles, the vesicles bind Ca^{2+} and aggregate, but they do not fuse. If the vesicles are coated with LMPAM, the vesicles bind Ca^{2+} but do not aggregate or fuse.

6.3 Titration microcalorimetry and the thermodynamics of membrane fusion

In order to assess the thermodynamics of vesicle aggregation and bilayer fusion, titration experiments were carried out in a high-sensitivity titration microcalorimeter. In the titration experiments, 10 μl aliquots of a sonicated dispersion of small vesicles (5 mM DDPBNS) were injected into 1.37 mL of aqueous $CaCl_2$ (5.0 mM) at 30 °C. Recorded traces of heat flow *vs.* time were integrated to obtain the corresponding enthalpies of reaction. Under these conditions, aggregation and fusion are rapid (*vide supra*). Indeed, in all cases, the baseline was reached before the next aliquot was injected (Figure 6.5). No systematic dependence of the observed enthalpy per injection on the injection number was found (Figure 6.5). As a result, each experiment yields an accurate reaction enthalpy which was taken as the average for 10-12 injections.

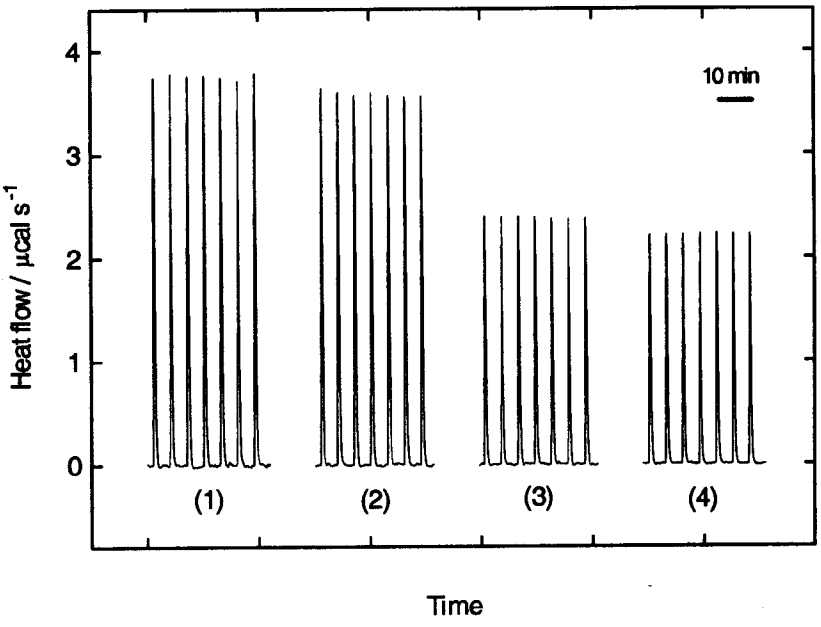

Figure 6.5 Enthalpograms corresponding to the titrations of small unilamellar vesicles of DDPBNS (5.0 mM lipid) into 5.0 mM $CaCl_2$. (1) Monomer lipid vesicles; (2) Oligomerised vesicles; (3) Monomer lipid vesicles coated with LMPAM; (4) Oligomerised vesicles coated with LMPAM.

A ten days' maturing period of the vesicles after sonication is critical to obtain quantitatively reproducible results. If vesicles are used directly after sonication, an exothermic reaction occasionally complicates the enthalpograms in experiments using monomer DDPBNS vesicles. This exothermic reaction is clearly secondary to calcium-induced fusion, and can be attributed to a calcium-induced liquid-crystalline to gel-like phase transition of the bilayer, as described for many negatively charged lipids.[5] Such an exothermic reaction was never observed with vesicles of oligomerised DDPBNS, and it was less significant in the presence of LMPAM. Moreover, the exothermic reaction diminished with time and disappeared if the vesicle solution was left standing for about one week. DDPBNS does not hydrolyse or polymerise during this period. In the presence of 25 mol% of cholesterol, the exothermic reaction was less pronounced and disappeared after two to three days. Indeed, differential scanning calorimetry of a freshly prepared solution of DDPBNS shows a shift of T_m from -1 °C to *ca.* 65 °C upon addition of $CaCl_2$. However, in an old solution no phase transition is observed. In sum, this means that the transition does not occur in an older solution, nor when a 'bilayer lubricant' such as cholesterol is added. Probably, such a calcium-induced ordering of the bilayer is not possible in oligomerised lipid vesicles.

The observed heat effect can be dissected into three well-defined processes: binding of Ca^{2+}, aggregation of the vesicles, and the ultimate merging of the bilayers. In comparison, the thermodynamic analysis of virus-protein-induced membrane fusion is highly complicated.[6] The enthalpy accompanying the titration of vesicles of monomer lipid into the $CaCl_2$ solution not only reflects aggregation and fusion, but also binding of Ca^{2+} to the phosphate headgroups, and any concomitant ion-dehydration effects. Similarly, titration of vesicles of oligomerised lipid into $CaCl_2$ solution yields a reaction enthalpy which solely includes aggregation and binding of Ca^{2+} to the phosphate head groups of the oligomerised lipids. However, binding of Ca^{2+} to oligomerised and monomer lipid bilayers is not thermodynamically equivalent, and simple subtraction of the two heat effects does not yield the true enthalpy of vesicle fusion.

This analytical problem can be solved using the macromolecular hydrophobic anchor LMPAM, which allows for independent measurements of the Ca^{2+} binding effects. In the presence of this polymer, aggregation and fusion are fully blocked for both oligomerised and monomer lipid, and any differences in reaction enthalpies reflect differences in Ca^{2+} binding only. Applying this correction, the enthalpy of fusion can be calculated. This enthalpy does not include enthalpic effects due to dilution of the polymer or Ca^{2+}-LMPAM interactions since the polymer has been added to the contents of both the syringe and the sample cell. The enthalpy of aggregation is obtained by subtracting the heat accompanying the titration of LMPAM-coated oligomerised vesicles into a $CaCl_2$ solution *(binding only)* from the enthalpy for the titration of oligomerised vesicles into a $CaCl_2$ solution of the same molarity *(aggregation + binding)*. This approach is illustrated in Figure 6.6., and Table 6.1 summarises the results.

The data show that binding of Ca^{2+} to the phosphate headgroups is endothermic by 7.0 kJ (mol DDPBNS)$^{-1}$ before oligomerisation, and by 6.5 kJ (mol DDPBNS)$^{-1}$ after oligomerisation. This enthalpy is lower than that accompanying binding of Ca^{2+} to phosphate ions in aqueous solutions which is endothermic by, on average, 11.5 - 13 kJ mol^{-1}.[13] Ca^{2+}-phosphate binding is driven by the release of hydration water,[14] and the difference is accounted for by the fact that the phosphate headgroups are less accessible to bind Ca^{2+} at the vesicle surface, and that they are

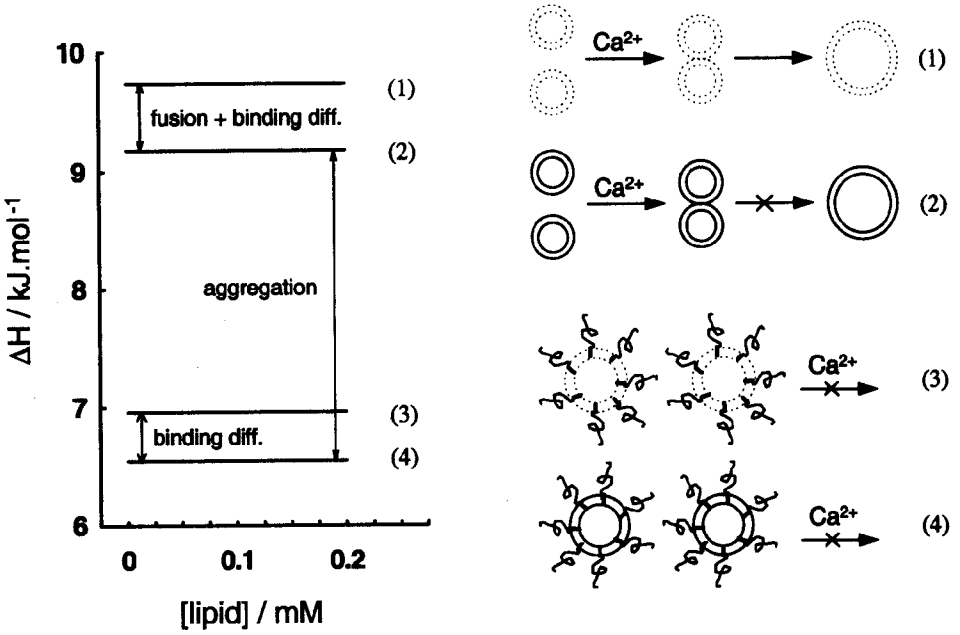

Figure 6.6 Dissecting enthalpies of aggregation and fusion from binding effects: a schematic representation. Monomer lipid bilayers are represented by dashed lines; oligomerised bilayers are represented by solid lines. Numbering corresponds to Table 6.1 (and 6.2) and Figure 6.5 (and 6.7).

Table 6.1 Enthalpies of calcium-induced DDPBNS vesicle aggregation and fusion.

Event*	Description	Enthalpy kJ (mol DDPBNS)$^{-1}$
1	Ca^{2+}-binding to mono(DDPBNS), vesicle aggregation, bilayer fusion	9.74 ± 0.11
2	Ca^{2+}-binding to oligo(DDPBNS), vesicle aggregation	9.18 ± 0.10
3	Ca^{2+}-binding to mono(DDPBNS)	6.96 ± 0.13
4	Ca^{2+}-binding to oligo(DDPBNS)	6.55 ± 0.13
2 - 4	**vesicle aggregation**	**2.6 ± 0.1**
(1 - 2) - (3 - 4)	**bilayer fusion**	**0.15 ± 0.1**

* Numbering corresponds to Figure 6.6.

already partially dehydrated. It is likely that the binding of Ca^{2+} to oligomerised DDPBNS phosphate head groups is slightly less endothermic than the binding to monomer DDPBNS head groups, because the oligomerised head groups are slightly dehydrated relative to the monomer head groups (as indicated by DSC, Section 3.2). Endothermic, entropy-driven binding of Ca^{2+} to mixed liposomes of phosphatidylcholine and phosphatidylglycerol has been reported in the literature.[15]

Vesicle aggregation is endothermic by 2.6 ± 0.1 kJ (mol DDPBNS)$^{-1}$ (Table 6.1). Vesicle aggregation is the result of endothermic but entropically favorable release of hydration water upon close approach of adjacent bilayers. Most likely, increased counterion binding of the lipid head groups contributes to this effect.[16] Since calcium-induced aggregation is a spontaneous process, the driving force is entropic.

Bilayer fusion is associated with an enthalpy of only 0.15 ± 0.1 kJ (mol DDPBNS)$^{-1}$ (Table 6.1). Since the extent of fusion of monomer lipid vesicles is *ca.* 65 % rather than 100 %, and since after oligomerisation it is *ca.* 7 % rather than 0 % (Figure 6.2), the value for *complete* vesicle fusion is 0.25 ± 0.10 kJ (mol DDPBNS)$^{-1}$ rather than 0.15 ± 0.10 kJ (mol DDPBNS)$^{-1}$. Reduction of bilayer curvature promotes formation of larger vesicles from small ones: vesicle fusion proceeds much more readily if the 'reactant' vesicle size remains below 100 nm.[17, 18] Assuming that bilayer curvature becomes negligible, the Gibbs energy of fusion can be estimated as -225 kJ (mol vesicles)$^{-1}$,[19] *i.e.* approximately -0.0225 kJ (mol lipid)$^{-1}$ for bilayer vesicles of 10^4 negatively charged lipids. Vesicle fusion is exergonic since it proceeds spontaneously upon addition of $CaCl_2$. Since bilayer fusion *per se* is associated with a minimal endothermic enthalpy effect ('cold fusion'), *entropy* should provide the driving force for fusion of bilayer membranes. A key question concerns how the relief of curvature strain is expressed at the molecular level. The enthalpy associated with the gel to liquid-crystalline bilayer phase transition becomes more endothermic as the vesicle size increases, indicating a concomitant increase in lateral packing efficiency of lipid molecules.[20] There is further calorimetric evidence that relief of bilayer curvature is exothermic.[21] But if this were the dominant factor in vesicle fusion, formation of large vesicles from smaller ones would be enthalpically favorable. This is not consistent with the present results. Most probably, the entropic driving force for fusion is provided by (1) the increase of the number of (translational, rotational, undulational) modes of freedom of the lipid molecules in going from aggregated clusters of small vesicles to the conformationally less restricted, larger fusion products and (2) a release of hydration water from the lipid head groups as the bilayer curvature is relieved. Finally, the enthalpy loss upon fusion of pure lipid membranes is an order of magnitude smaller than that observed for protein-mediated virus - liposome fusion (2.5-3.0 kJ (mol viral lipid)$^{-1}$).[6] Hence, the enthalpy of mixing of protein-rich viral membrane and pure lipid membrane[22] dominates the thermodynamics of virus - liposome fusion, whereas lipid rearrangements contribute marginally to the overall enthalpy of fusion.

6.4 Influence of cholesterol on the thermodynamics of membrane fusion

In an additional series of titration microcalorimetric experiments, the influence of admixing cholesterol in the vesicle bilayers was investigated. Small vesicles prepared from a 3 to 1 molar mixture of DDPBNS and cholesterol were used in titration experiments as described in Section 6.3. Raw microcalorimetric data are shown in Figure 6.7 and the resulting enthalpies are presented in Table 6.2.

A comparison with the experiments with pure DDPBNS vesicles (Table 6.1) leads to a few striking observations. The enthalpy of binding of Ca^{2+} to the vesicles (prior to lipid oligomerisation) as well as the enthalpy of vesicle aggregation and the enthalpy of bilayer fusion are of similar magnitude in the absence and presence of cholesterol. The enthalpy of binding of Ca^{2+} is almost identical, the enthalpy of aggregation is considerably smaller, and the enthalpy of fusion is slightly higher. However, the difference in binding enthalpy between oligomerised lipid and monomer lipid vesicles is 4.66 kJ (mol DDPBNS)$^{-1}$ in the presence of cholesterol, compared to only 0.41 kJ (mol DDPBNS)$^{-1}$ in its absence. Indeed, the binding of Ca^{2+} to oligomerised vesicles is much less endothermic in the presence of cholesterol (6.55 kJ (mol DDPBNS)$^{-1}$ *vs.* 2.34 kJ (mol DDPBNS)$^{-1}$).

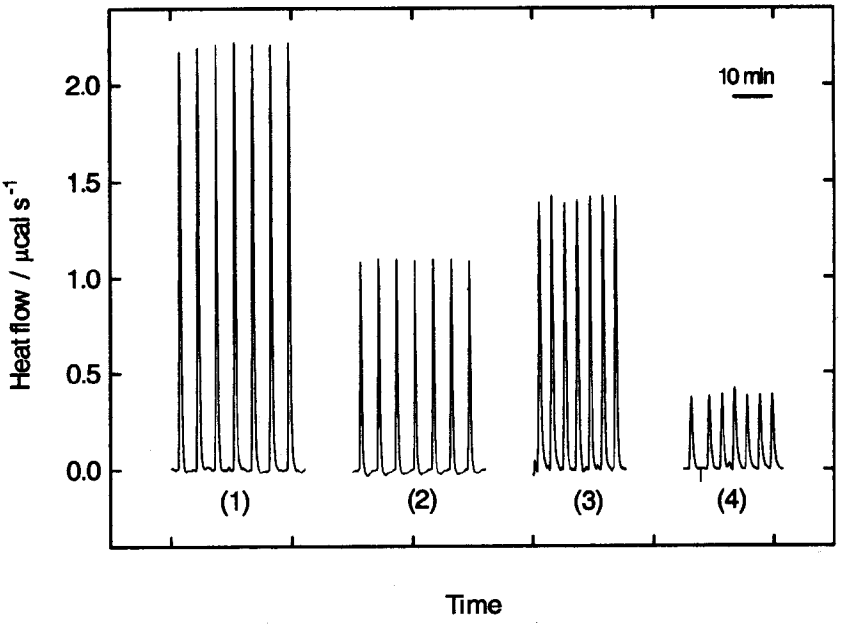

Figure 6.7 Enthalpograms corresponding to the titrations of small unilamellar vesicles of DDPBNS/cholesterol (3/1, 5.0 mM in total) into 5.0 mM $CaCl_2$. (1) Monomer lipid vesicles; (2) Oligomerised vesicles; (3) Monomer lipid vesicles coated with LMPAM; (4) Oligomerised vesicles coated with LMPAM.

Table 6.2 Enthalpies of calcium-induced DDPBNS/cholesterol vesicle aggregation and fusion.

Event*	Description	Enthalpy kJ (mol DDPBNS)$^{-1}$
1	Ca^{2+}-binding to mono(DDPBNS), vesicle aggregation, bilayer fusion	8.56 ± 0.26
2	Ca^{2+}-binding to oligo(DDPBNS), vesicle aggregation	3.59 ± 0.11
3	Ca^{2+}-binding to mono(DDPBNS)	7.00 ± 0.26
4	Ca^{2+}-binding to oligo(DDPBNS)	2.34 ± 0.20
2 - 4	**vesicle aggregation**	**1.25 ± 0.1**
(1 - 2) - (3 - 4)	**bilayer fusion**	**0.31 ± 0.1**

* Numbering corresponds to Figure 6.6.

One may speculate on the possibility of lateral phase separation upon oligomerisation of DDPBNS in vesicles containing cholesterol, and on the extent to which this might prevent efficient binding of Ca^{2+}. If this were the case, this might lead to less extensive vesicle aggregation (hence a lower enthalpy of aggregation) and fusion. Therefore, these data should be considered with care. The enthalpies are reported per mol of DDPBNS, and one could argue that cholesterol should be included (implying that it is the number of vesicles rather than the number of lipid molecules that determines the observed enthalpies). In that case, all enthalpies would be reduced by *ca.* 30 %, which would mean that the enthalpies of all successive stages of the fusion process are lower in the presence of cholesterol. However, this reduced heat effect may be a simple consequence of a reduced efficiency of the fusion process in the presence of cholesterol, which requires experimental verification.

6.5 Conclusions

This chapter describes a simple biomembrane model that provides insight into the thermodynamics of calcium-induced bilayer membrane fusion. Combination of oligomerisable lipids and hydrophobically-modified polymers allows a dissection of the fusion pathway into successive steps of binding of Ca^{2+}, vesicle aggregation, and bilayer fusion. The heat effect accompanying each step can be accurately measured in a titration microcalorimeter. All steps are endothermic, which means that entropy provides the driving force for calcium-induced vesicle fusion. The results shed new light on the enthalpy associated with liposome - Influenza virus fusion,[6] and it appears that in such fusion processes protein-lipid interactions have a much larger enthalpic effect than the lipid rearrangements of membrane fusion *per se*. These considerations are elaborated in Chapter 7.

6.6 Experimental section

Materials and vesicle preparation DDPBNS was synthesised as described in Section 2.8. Poly(acrylamide) (PAM) and the copolymer of lauryl methacrylate and acrylamide (LMPAM) were synthesised according to literature procedures.[7] The molecular weight of LMPAM was estimated as 18,200 (viscosimetry) and the polymer carries an average of four lauryl substituents per molecule (^{1}H-NMR). Small unilamellar vesicles of DDPBNS were prepared by sonication of thin lipid films in 5 mM HEPES/NaAc buffered solutions and polymerisation of DDPBNS vesicles was induced by UV irradiation (Section 2.8). Coating of the DDPBNS vesicles with LMPAM was achieved by 40/1 DDPBNS/polymer molar ratio mixing of appropriate solutions of vesicles and polymer. Hereto, a small aliquot of a concentrated aqueous polymer solution was added to a solution of vesicles in buffer. Prior to microcalorimetric experiments, the vesicles were kept at room temperature for one week (see Section 6.3).

***n*-Octadecyl rhodamine assay of lipid mixing** The R18 assay of lipid mixing was performed as described in Section 4.6. In brief, 5 μM of DDPBNS small unilamellar vesicles with 2 mol% R18 and 20 μM DDPBNS vesicles without fluorescent label were mixed in 2 mL of 5 mM HEPES/NaAc buffer (pH 7.4, 140 mM NaCl added) at 25 °C. LMPAM or PAM were added at a DDPBNS/polymer molar ratio of 40/1. Addition of LMPAM resulted in a small instantaneous increase of fluorescence (3-5 %), presumably reflecting the insertion of the hydrophobic anchor into the vesicle bilayers. PAM had no effect on R18 fluorescence. Addition of either polymer did not result in spontaneous exchange of the R18 probe. Fusion was induced by the addition of 1-10 mM of $CaCl_2$, and quenched by the addition of 4 equivalents of EDTA.

Turbidity assay of vesicle aggregation Aggregation of small unilamellar vesicles of DDPBNS was monitored as an increase in turbidity upon addition of 1-10 mM of $CaCl_2$. The concentration of DDPBNS was 0.1 mM in 5 mM HEPES/NaAc (pH 7.4), and the molar ratio of DDPBNS to polymer was 40 to 1. Turbidities were measured under stirring at 25 °C as the absorbance at 500 nm in 2 mL cells in a Philips PU 8740 UV-VIS spectrophotometer.

Electron microscopy Experiments were carried out as described in Section 2.8.

Isothermal titration microcalorimetry Titration microcalorimetry was performed by injecting 10 μL aliquots of vesicle solution into the sample cell of the microcalorimeter containing a $CaCl_2$ solution (1.37 mL). 10-12 injections were carried out at intervals of 5 minutes. The sample cell was stirred at 350 rpm. Integration of the heat flow *vs.* time yields the enthalpy for each injection. The concentration of DDPBNS in the syringe was 5 mM in 5 mM HEPES/NaAc (pH 7.4) and the concentration of $CaCl_2$ in the sample cell was 5 mM in 5 mM HEPES/NaAc (pH 7.4). Polymers were added to the contents of the syringe as well as to the contents of the sample cell at a 40/1 DDPBNS/polymer molar ratio prior to the titration experiment. The instrument used was an Omega Isothermal Titration Microcalorimeter (Microcal Inc., Northampton, MA, USA), operated at 30 °C.

Acknowledgment

The work described in this chapter was performed in close collaboration with Jan Kevelam, who is gratefully acknowledged for his stimulating as well as critical contributions, and his perseverance in bringing a runaway Friday afternoon experiment to a good end. He synthesised the polymers and performed all microcalorimetric experiments. Also, we are grateful to Prof. Michael Blandamer (University of Leicester, UK) for discussion of the results and to Prof. Alain Brisson and Jan van Breemen for their hospitality in the Laboratory of Electron Microscopy.

6.7 References

(1) Lipowsky, R. The conformation of membranes. *Nature* 1991, 349, 475-481.

(2) Helfrich, W. Elastic properties of lipid bilayers. Theory and possible experiments. *Z. Naturforsch., C* 1973, 28, 693-703.

(3) Svetina, S.; Zeks, B. Bilayer couple as a possible mechanism of biological shape transformation. *Biomed. Biochim. Acta* 1985, 44, 979-986.

(4) Siegel, D.P. Energetics of intermediates in membrane fusion: comparison of stalk and inverted micellar intermediate mechanisms. *Biophys. J.* 1993, 65, 2124-2140.

(5) Rehfeld, S.J.; Düzgünez, N.; Newton, C.; Papahadjopoulos, D.; Eatough, D.J. The exothermic reaction of calcium with unilamellar phosphatidylserine vesicles. *FEBS Letters* 1981, 123, 249-251.

(6) Nebel, S.; Bartoldus, I.; Stegmann, T. Calorimetric detection of influenza virus induced membrane fusion. *Biochemistry* 1995, 34, 5705-5711.

(7) Kevelam, J.; van Breemen, J.F.L.; Blokzijl, W.; Engberts, J.B.F.N. Polymer-surfactant interactions studied by titration microcalorimetry: influence of polymer hydrophobicity, electrostatic forces, and surfactant aggregational state. *Langmuir* 1996, 12, 4709-4717.

(8) Ringsdorf, H.; Sackmann, E.; Simon, J.; Winnik, F.M. Interactions between liposomes and hydrophobically-modified poly-(N-isopropyl acrylamides): an attempt to model the cytoskeleton. *Biochim. Biophys. Acta* 1993, 1153, 335-344.

(9) Simon, J.; Kühner, M.; Ringsdorf, H.; Sackmann, E. Polymer-induced shape changes and capping in giant liposomes. *Chem. Phys. Lipids* 1995, 76, 241-258.

(10) Hoekstra, D.; De Boer, T.; Klappe, K.; Wilschut, J. Fluorescence method for measuring the kinetics of fusion between biological membranes. *Biochemistry* 1984, 23, 5675-5681.

(11) Lasic, D.D. Sterically stabilized vesicles. *Angew. Chem., Int. Ed. Engl.* 1994, 33, 1685-1698.

(12) Lentz, B.R. Polymer-induced membrane fusion: potential mechanism and relation to cell fusion events. *Chem. Phys. Lipids* 1994, 73, 91-106.

(13) The value of 11.5 kJ mol^{-1} was calculated from Kaye, G.W.C.; Laby, T.H. Tables of Physical and Chemical Constants; Longman, New York, 1986. Using the data in the Handbook of Chemistry and Physics, a value of 13 kJ mol^{-1} is obtained.

(14) Irani, R.R.; Callis, C.F. Metal complexing by phosphorus compounds. I. The thermodynamics of association of linear polyphosphates with calcium. *J. Phys. Chem.* 1960, 64, 1398-1407.

(15) Lehrmann, R.; Seelig, J. Adsorption of Ca^{2+} and La^{3+} to bilayer membranes: measurement of the adsorption enthalpy and binding constant with titration calorimetry. *Biochim. Biophys. Acta* 1994, 1189, 89.

(16) Bentz, J.; Ellens, H. Membrane fusion: kinetics and mechanisms. *Coll. Surfaces* 1988, 30, 65-112.

(17) Nir, S.; Wilschut, J.; Bentz, J. The rate of fusion of phospholipid vesicles and the role of bilayer curvature. *Biochim. Biophys. Acta* 1982, 688, 275-278.

(18) Lentz, B.R.; McIntyre, G.F.; Parks, D.J.; Yates, J.C.; Massenburg, D. Bilayer curvature and certain amphipaths promote poly(ethylene glycol)-induced fusion of dipalmitoyl phosphatidylcholine unilamellar vesicles. *Biochemistry* 1992, 31, 2643-2653.

(19) Bergström, M.; Eriksson, J.C. The energetics of forming equilibrated bilayer vesicles. *Langmuir* 1996, 12, 624-635.

(20) Grünewald, B.; Stankowski, S.; Blume, A. Curvature influence on the cooperativity and the phase transition enthalpy of lecithin vesicles. *FEBS Letters* 1979, 102, 227-229.

(21) Epand, R.M.; Epand, R.F. Calorimetric detection of curvature strain in phospholipid bilayers. *Biophys. J.* 1994, 66, 1450-1456.

(22) Seelig, J. Titration calorimetry of lipid-peptide interactions. *Biochim. Biophys. Acta* 1997, 1331, 103-116.

Chapter 7

Fusion of Sendai virus with vesicles of oligomerisable lipids[I]

As shown by lipid mixing assays and electron microscopy, Sendai virus fuses efficiently with small and large vesicles of the lipid 1,2-di-n-hexadecyloxypropyl-4-(beta-nitrostyryl) phosphate (DHPBNS) at pH 7.4 and 37 °C. Fusion is strongly retarded and inhibited by oligomerisation of DHPBNS in the bilayer vesicles. The enthalpy of fusion was measured using titration microcalorimetry. The observed heat of fusion is strongly dependent on the buffer medium, reflecting a charge neutralisation of (part) of the Sendai fusion protein upon insertion into the negatively charged target membrane. No buffer effect was observed with oligomerised vesicles, indicating that inhibition of fusion is a result of inhibition of insertion of the fusion protein into the target membrane. Sendai virus-vesicle fusion is endothermic and entropy-driven. The positive enthalpy term is dominated by protein-lipid mixing interactions rather than the merging of the lipid bilayers per se.

7.1 Introduction

Sendai virus or Hemagglutinating Virus from Japan (HVJ) is a paramyxovirus that infects cells by direct fusion with the cell membrane at neutral pH. Pioneering studies by Shimizu[1] revealed that the virus contains two different spike proteins that protrude from the viral envelope membrane: the HN glycoprotein (with two subunits of 15 kD and 51 kD) with hemagglutinating and neuramidase activity, and a second glycoprotein of 67 kD, also composed of two subunits. One of the subunits of this second spike protein contains a distinct hydrophobic region at its amino terminal end.[2] In later studies, the HN protein was found to be involved in receptor-mediated binding to the cell surface, whereas the second protein mediates fusion with the target membrane. Therefore, the second spike protein is called the fusion or F protein. Many reports of fusion between Sendai virus and liposomes indicate that the physiologically relevant mode of action of Sendai requires a temperature of 37-40 °C and pH 7.4, and a target membrane of phosphatidylcholine and cholesterol that contains a sialic acid receptor (a specific ganglioside) to bind HN.[3,4,5] Fusion involves insertion of the hydrophobic amino terminus of one of the two subunits of the F protein into the target membrane.[6,7] Target membranes that contain negatively charged lipids such as phosphatidylserine or cardiolipin fuse more efficiently.[5,8] It has been suggested that the negatively charged lipids act as aspecific sialic acid substitutes,[8] and/or that the decreased hydration repulsion of charged lipid bilayers favors rapid aggregation and fusion

[I] The research described in this Chapter has been submitted for publication.

between Sendai and liposomes.[5] In addition, an extremely rapid fusion process occurs between Sendai and liposomes containing negatively charged lipids at low pH as a result of aspecific electrostatic interactions between HN (not F) and the target membrane upon protonation of the HN glycoprotein below pH 6 (the isoelectric point of HN is at pH 6.5).[5, 8, 9] This low pH HN-mediated fusion process does not have physiological relevance.

Apparently, the crucial step in Sendai virus fusion is insertion of part of the F protein into the target membrane. In view of the microcalorimetric studies on peptide-lipid interactions by Seelig *c.s.*,[10, 11, 12, 13, 14] this insertion could have drastic influences on the thermodynamic characteristics of the fusion process. Hydrophobic binding of peptides is normally endothermic and driven by an entropically favourable release of hydration water.[15] However, many examples of "non-classical' hydrophobic binding are known in which binding is enthalpy-driven, and the binding entropy is zero or even negative.[10, 12, 14] The thermodynamics of binding are strongly dependent on the internal lateral tension of the lipid membrane (the ease with which it permits insertion of foreign molecules), which is relatively low for very small vesicles, and higher for membranes with less curvature (diameters exceeding 50 nm).[10]

Calcium-induced fusion of small vesicles is slightly endothermic and driven by a gain in entropy of both lipid and water molecules during bilayer merging (Chapter 6). On the other hand, Stegmann *c.s.* reported that fusion of influenza virus and liposomes is highly endothermic (and therefore: entropy-driven, but the authors do not elaborate on this matter).[16] Fusion occurs at pH 5.1 and involves insertion of a hydrophobic part of the influenza hemagglutinin protein into the target membrane. Clearly, the heat effects in protein-mediated fusion are much larger than in calcium-induced fusion of pure lipid vesicles, and it was worthwhile to investigate whether the differences should be attributed to heat effects due to insertion of fusion proteins into the target membrane, due to membrane lipid merging, or because of lipid-protein mixing as a result of fusion between the viral envelope and the target membrane.

A related issue that requires attention is the effect of buffer on the observed enthalpies of fusion, since in several calorimetric studies of peptide-lipid binding, significant buffer dependency has been found.[10, 11, 13, 17] This buffer effect has been interpreted in terms of membrane binding-induced pK_a shifts of residues in the peptide that either binds to the membrane surface or inserts into the membrane interior. Such pK_a shifts can be the result of either transferring of charged aminoacid residues from a polar to a hydrophobic environment, or (in the case of negatively charged bilayers) the local pH near a negatively charged membrane being considerably lower than in bulk solution, leading to protonation of residues.[13] Depending on the aminoacid composition of the peptide, the membrane binding-induced pK_a shift(s) may lead to either a net uptake or a net release of protons upon binding, which causes a heat effect that is directly correlated to the ionisation enthalpy of the buffer. Therefore, common practice measures the heat effect of peptide-lipid interactions in several buffers of known ionisation enthalpy, and determines the *intrinsic heat effect* by extrapolation to zero buffer ionisation enthalpy. Unfortunately, this practice has been ignored in the calorimetric study of influenza virus-liposome fusion.[16]

This chapter describes an investigation of the fusion of vesicles of the negatively charged, oligomerisable lipid *1,2*-di-*n*-hexadecyloxypropyl-4-(*beta*-nitrostyryl) phosphate (DHPBNS) with Sendai virus. Three main questions are addressed. (1) Since fusion requires insertion of (part of)

the F protein into the target membrane, is fusion inhibited upon oligomerisation of the lipids in the target membrane, because this could inhibit insertion of the F protein? (2) Is it possible to measure the heat effect that accompanies fusion of Sendai virus and DHPBNS vesicles with titration microcalorimetry? (3) Is it possible to account for the differences that are anticipated for the enthalpy of interaction of Sendai virus with vesicles of DHPBNS prior to and after lipid oligomerisation?

7.2 Lipid mixing assays and electron microscopy of Sendai virus-vesicle fusion

Lipid mixing in the course of fusion between Sendai virus and vesicles of DHPBNS was monitored by the *n*-octadecyl rhodamine (R18) assay.[18] The virus was labeled with R18 according to standard literature procedures.[5] Although this assay is known to disagree with other fusion assays in some cases, it has recently been verified again that the dequenching of R18 gives an accurate measure of membrane fusion of Sendai virus, particularly in the first minutes of the fusion process.[19] Aspecific probe transfer occurs at a much longer time scale.

The extent and the initial rate of fusion of Sendai virus and *small* (50-100 nm) vesicles of DHPBNS are shown in Figure 7.1. The data are reported as a function of DHPBNS concentration at four temperatures. Fusion becomes faster and more extensive as the concentration of target membrane and/or the temperature are increased. Since the virus was added at a concentration of 5 μg viral protein/mL, which is equivalent to 2.0 μM viral lipid (Sendai virus contains *ca.* 400 nmol of lipid (including cholesterol) per mg of viral protein),[20] efficient fusion requires a large excess of target membrane. Fusion is very slow and inefficient at 21 °C, but it occurs more readily at 30 °C, and it is quite efficient at 37 °C and 44 °C. Remarkably, Sendai can fuse with DHPBNS vesicles below their main phase transition temperature (T_m is 40 °C, see Chapter 2).

Figure 7.2 illustrates the effect of lipid oligomerisation in the DHPBNS vesicles on the extent and rate of fusion with Sendai virus at 37 °C. Clearly, fusion is strongly inhibited and retarded. Inhibition and retardation of fusion diminish as the concentration of target membrane is increased, but even at a 25-fold excess of target membrane (50 μM DHPBNS) oligomerisation still results in a 70-75 % lower extent and rate of fusion.

The results of a lipid mixing assay of fusion of Sendai virus and *large* (200 nm) vesicles of DHPBNS at 37 °C are also presented in Figure 7.2. Large vesicles fuse with Sendai equally efficiently as small vesicles (Figure 7.1). The initial rate of fusion tends to be somewhat smaller, but the extent of fusion is slightly higher. Fusion becomes more efficient at higher temperature (43 °C), *i.e.* well above the T_m of DHPBNS (data not shown). Oligomerisation of DHPBNS leads to a strong inhibition and retardation of fusion. As for the small vesicles, inhibition and retardation of fusion diminish as the concentration of target membrane is increased.

Electron microscopy of samples of Sendai virus and DHPBNS vesicles incubated under various conditions confirmed the results from the R18 fusion assays. Incubation of Sendai and small DHPBNS vesicles at 40 °C results in large fusion products (Figure 7.3). However, if Sendai is incubated at 40 °C with small vesicles of oligomerised DHPBNS, hardly any fusion products are observed, and the majority of virus and vesicles persist. Similar observations were made for Sendai virus and vesicles incubated at 4 °C. At this temperature, Sendai is not fusogenic.

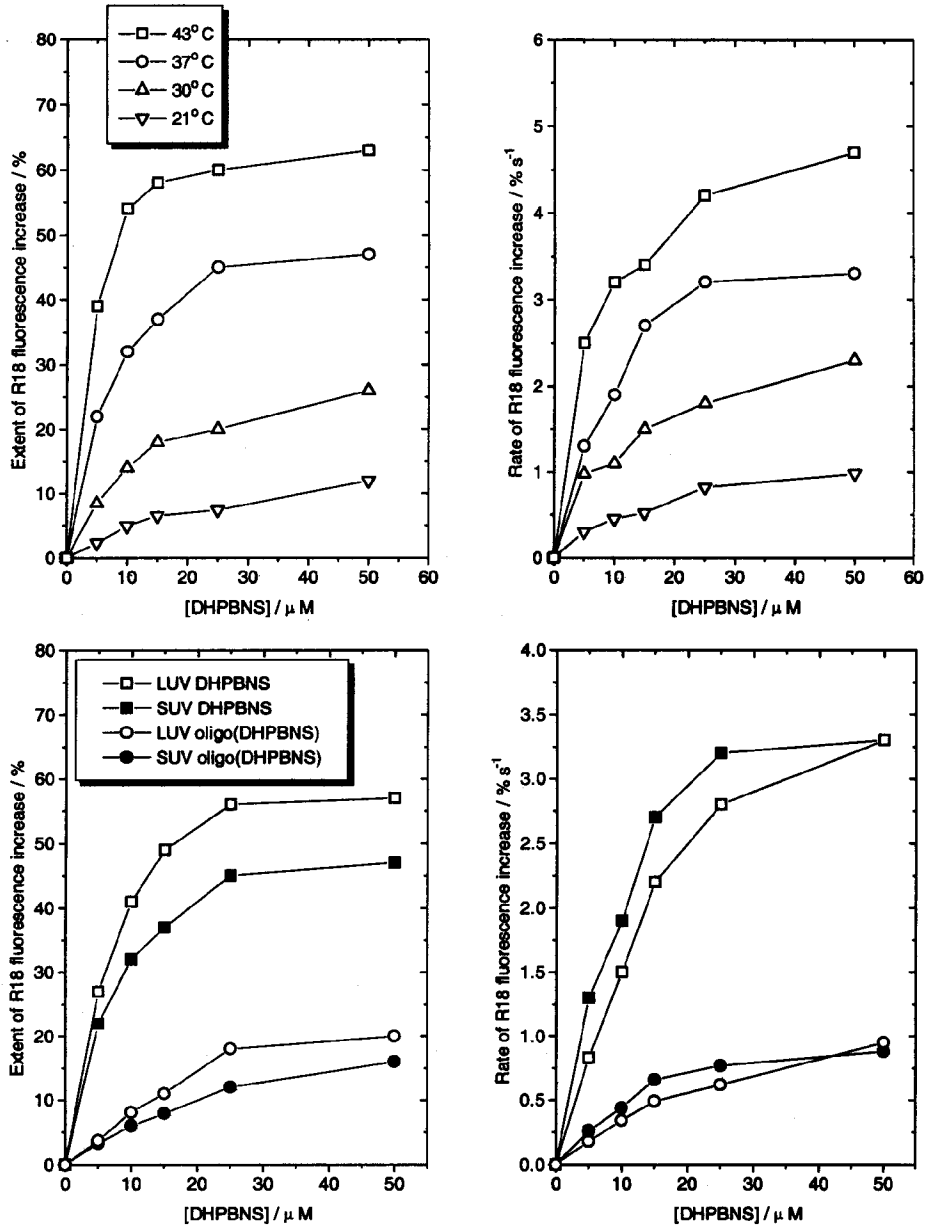

Figure 7.1 (Top) Temperature dependence of lipid mixing during fusion of Sendai virus and *small vesicles* of DHPBNS as a function of DHPBNS concentration. Left: extent of fusion, right: initial rate of fusion.
Figure 7.2 (Bottom) Lipid mixing during fusion of Sendai virus (5 μg/mL) and *small* and *large vesicles* of DHPBNS at 37 °C as a function of DHPBNS concentration before and after oligomerisation of DHPBNS. Left: extent of fusion, right: initial rate of fusion.

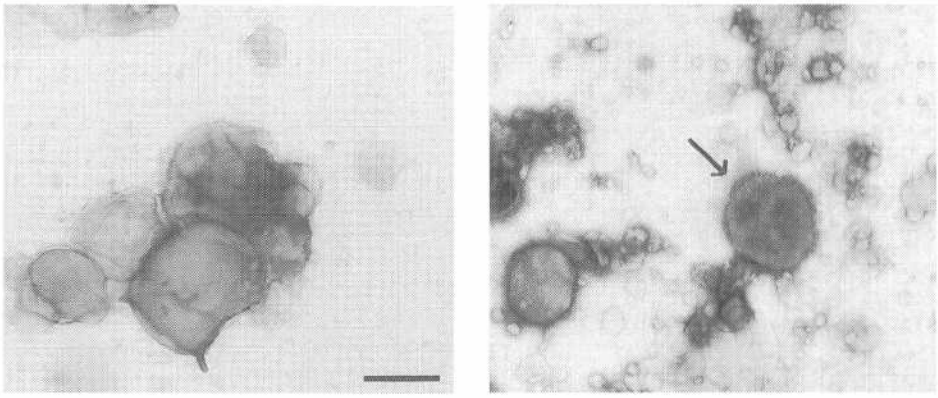

Figure 7.3 Electron micrographs of mixtures of Sendai virus and small vesicles of DHPBNS. Left: virus and vesicles incubated at 40 °C. Right: virus and vesicles of oligomerised DHPBNS incubated at 40 °C. The arrow indicates an intact virion, easily identified because of its spike coating. Bar represents 200 nm.

7.3 Microcalorimetry of Sendai virus-vesicle fusion

The enthalpy of the interaction between Sendai virus and small vesicles of DHPBNS was measured using isothermal titration microcalorimetry (compare Section 6.3). Ten to twelve 10 µL aliquots of a suspension of Sendai virus (2.0 mg viral protein/mL, *i.e.* approximately 0.80 mM viral lipid) were injected into the sample cell containing 1.37 mL of a solution of small (50-100 nm) vesicles of DHPBNS (0.5 mM lipid) at 37 °C. Hence, in the course of the titration experiment, *ca.* 100 nmol of viral lipid was added to 680 nmol of DHPBNS. Upon each injection, endothermic heat effects were observed over a timescale of about one minute. Typical plots of the heat flow *vs* time are presented in Figure 7.4. The experiment was repeated in four different buffers (phosphate, PIPES, HEPES and TRIS) of identical concentration and pH (7.40). The intensity of the observed heat effect is strongly dependent on the buffer medium. As the ionisation enthalpy of the buffer increases, the reaction becomes more endothermic. As illustrated in Figure 7.5, a linear correlation ($r = 0.95$) relates the observed heat and the ionisation enthalpy of the buffer. Extrapolation of the linear fit to zero buffer ionisation enthalpy yields an intrinsic heat effect for the interaction of Sendai virus with small vesicles of DHPBNS of $+4.3\pm1.1$ kJ (mol viral lipid)$^{-1}$. The positive slope of the plot of the observed heat *vs* the buffer ionisation enthalpy implies that buffer dissociates during the interaction of Sendai and the vesicles, which indicates an uptake of protons in the course of the fusion process. The slope is a quantitative measure for the number of protons that are taken up, and it amounts to 0.15 ± 0.04 mol protons (mol viral lipid)$^{-1}$.

Similar titration experiments of Sendai virus and small vesicles of oligomerised DHPBNS yielded much smaller endothermic heat effects. Most interestingly, experiments in four different buffers yielded identical heat effects of $+2.8\pm0.2$ kJ (mol viral lipid)$^{-1}$. This pattern implies that

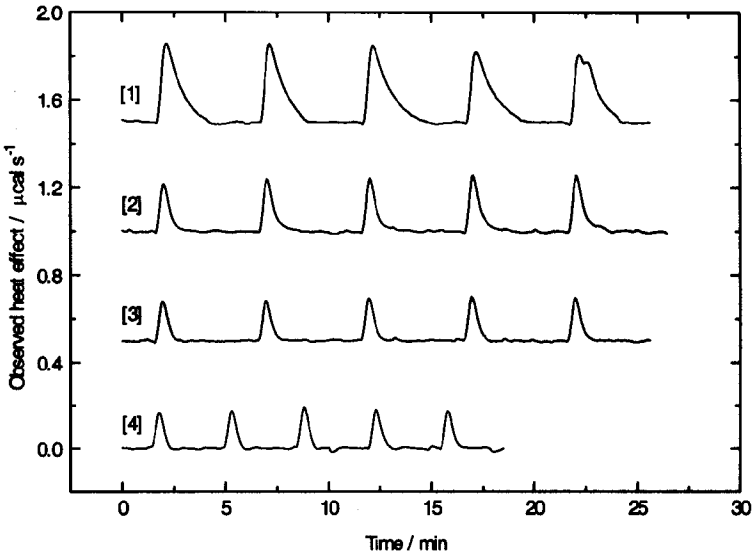

Figure 7.4 Heat flow *vs* time during a titration of Sendai virus to small vesicles of DHPBNS at 37 °C. (1) DHPBNS and virus in HEPES buffer. (2) DHPBNS and virus in phosphate buffer. (3) Oligomerised DHPBNS and virus in HEPES buffer. (4) Oligomerised DHPBNS and virus in phosphate buffer.

no protons are taken up (or released) during the interaction of Sendai virus with small vesicles of oligomerised DHPBNS. Control experiments in which Sendai virus was titrated into various buffer solutions in the absence of vesicles revealed that the enthalpy of dilution of the concentrated virus suspension amounts to +2.1±0.2 kJ (mol viral lipid)$^{-1}$, and therefore accounts for most of the heat that is observed in the titration of Sendai virus to oligomerised DHPBNS vesicles. Most likely, a small extent of fusion (Figure 7.1) is responsible for the additional heat effect, but any buffer dependence is lost in the error margins of the experiments.

The buffer dependence of the heat observed upon fusion of Sendai virus and vesicles of DHPBNS can be explained by the insertion of the F protein of Sendai into the target membrane. The amino terminal part of the subunit of the F protein that is believed to insert into the target membrane contains 20 hydrophobic residues,[2, 21] which cannot possibly be protonated or deprotonated. In addition, the amino terminal part contains three threonine residues which are not hydrophobic, but possess a pK_a far outside the range that could be influenced by insertion into the membrane. The only residue that contains a pH sensitive group is the amino terminal phenylalanine, with the terminal NH_2 with a pK_a of *ca.* 8. This implies that the NH_2 of this phenylalanine residue is only partially protonated at pH 7.4. The microcalorimetric data suggest that the NH_2 is protonated, which is probably the result of the low local pH near the surface of the negatively charged membrane (rather than deprotonated, which would imply a charge neutralisation that favours membrane insertion). Similar effects have been described in a calorimetric study of binding between a model peptide and liposomes.[10]

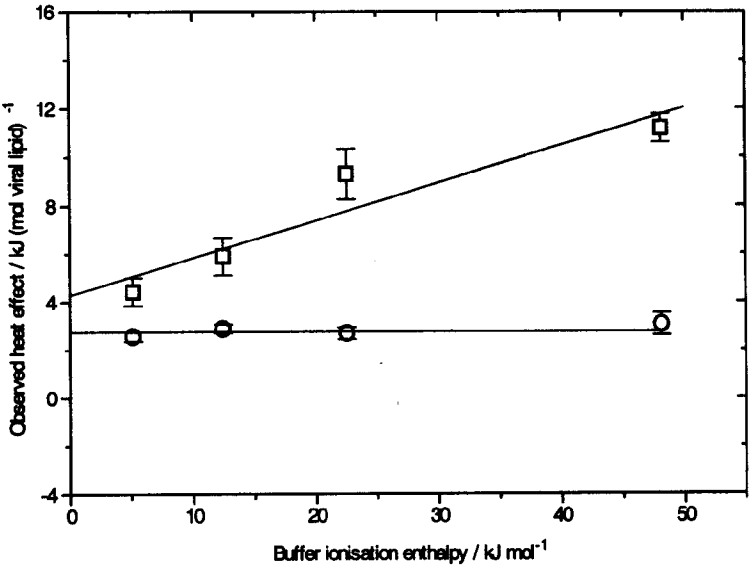

Figure 7.5 Plot of the observed heat effect of titration of Sendai virus to DHPBNS vesicles in various buffers *vs* the enthalpy of ionisation of the buffers. Legend: squares: DHPBNS vesicles, circles: Oligomerised DHPBNS vesicles.

However, it would be a gross oversimplification to suggest that only the residues in the amino terminal part of the F protein are affected during fusion with the target membrane. Certainly, in the course of fusion, a considerable part of the F protein as well as the HN protein approach closely to the negatively charged membrane. The F and HN proteins have their isoelectric point at pH 4.9 and pH 6.5, respectively, which means that they are negatively charged at pH 7.4. Upon close association with the negatively charged membrane (with low local pH), they will be protonated to some extent. Ultimately, fusion of Sendai and the target membrane results in mixing of the viral envelope and the target membrane (as evidenced by the lipid mixing assay), implying a transfer of the viral spike proteins from a neutral to a negatively charged membrane. Most certainly, the F and HN proteins will be protonated to some extent. Unfortunately, these effects are difficult to quantify in terms of which aminoacid residues are effected and to what extent. The viral envelope contains about 1600 nmol of lipid (including cholesterol) per mg of spike protein (F and HN, both of molecular weight around 66 kD),[20] which means about 100 lipid molecules per protein molecule. According to the plot of the observed heat effect against the buffer ionisation enthalpy, about 0.15 protons are taken up per viral lipid molecule, which means about 15 protons should be taken up per protein molecule. This may appear a large number, but both F and HN are composed of *ca.* 500 aminoacids, many of which are potential proton acceptors.[2] Assuming an equimolar ratio of HN and F, it is obvious that protonation effects specifically related to insertion of the amino terminal part of the F protein (max. 0.5 proton/protein) are very modest compared to protonation of F and HN as a result of membrane merging (almost 15 protons/protein).

The data in Section 7.2 lead to the conclusion that fusion of Sendai virus and small (as well as large) vesicles of DHPBNS is inhibited by oligomerisation of DHPBNS. Since no buffer effect is observed for the titration of Sendai virus to vesicles of oligomerised DHPBNS, the F protein does not insert into this target membrane (presumably because the lipid molecules have been covalently linked into oligomers). Hence, fusion is inhibited as observed in the lipid mixing assays and in the electron microscopic experiments.

Individual injections into the titration microcalorimeter can be compared to successive fusion experiments with a high ratio of target membrane to virus, and indeed the time scale of the heat effect matches the rapid fusion observed in the lipid mixing assay. Therefore, the difference in the heat effect that is observed when comparing the titration of Sendai virus to DHPBNS vesicles prior to and after oligomerisation can be attributed to heat effects associated with the membrane fusion process that occurs between Sendai and the DHPBNS vesicles (and *not* with the oligomerised DHPBNS vesicles). Therefore, the enthalpy of the fusion process is 4.3±1.1 - 2.8±0.2 kJ (mol viral lipid)$^{-1}$ = 1.5±1.3 kJ (mol viral lipid)$^{-1}$. Hence, fusion is an endothermic process which is entropy-driven.

Calcium-induced lipid bilayer merging of vesicles of the C12 analogue of DHPBNS is associated with an endothermic heat of 0.15-0.25 kJ (mol lipid)$^{-1}$ (Chapter 6). Therefore, it is likely that most of the enthalpy cost of Sendai virus-vesicle fusion is a result of mixing of the viral envelope and the target membrane, rather than merging of the lipid bilayers *per se*. Mixing is accompanied by protonation of some of the protein residues in the viral envelope proteins, which is expected to be *exothermic*. The enthalpy of this protonation is difficult to estimate, since we do not know which residues are involved, and to what extent they are protonated. In any case, the intrinsic enthalpy of the fusion process must be even larger than 1.5 kJ (mol viral lipid)$^{-1}$, and, consequently, a strong entropic driving force is required. A significant entropy gain can result from the liberation of hydration water upon insertion of (part of) the F protein into the target membrane, as expected for a hydrophobic binding process. In addition, the thermodynamics of the fusion process may be interpreted in terms of the model proposed by Seelig.[10] According to this model, binding of the viral envelope proteins and the target membrane is endothermic, because it requires enthalpy input to insert a protein into the target membrane. Provided the bilayer membrane is not exceedingly curved (the vesicle diameter should be 50 nm or more, which is the case for these vesicles), the internal tension in a lipid membrane is high, and any gain in Van der Waals energy upon inserting a foreign molecule is overruled by the energy required to make room for it. On the other hand, mixing of a protein-rich and a protein-free membrane entails a large entropy gain because of a large increase in continuous membrane surface area, which results in an increased degree of freedom of the lipid and protein molecules.

7.4 Conclusions

Sendai virus fuses efficiently with vesicles of DHPBNS, and fusion is strongly inhibited by lipid oligomerisation. Fusion is triggered by insertion of part of the F protein into the target membrane, which is inhibited upon oligomerisation of the lipids in the target membrane. Fusion is accompanied by an endothermic heat effect of at least 1.5 kJ (mol viral lipid)$^{-1}$. This heat effect is dependent on the buffer ionisation enthalpy, reflecting (partial) charge neutralisation of the viral spike proteins as the viral envelope merges with the negatively charged target membrane. The enthalpy of fusion of Sendai virus and DHPBNS vesicles is ten times larger than the enthalpy of fusion of pure lipid bilayers. Apparently, the loss of enthalpy during fusion is a result of protein-lipid mixing interactions, rather than merging of the lipid bilayers. Fusion is driven by a gain of entropy of lipid and water molecules.

7.5 Experimental section

Materials DHPBNS was prepared according to the procedures described in Chapter 2. R18 was generously provided by the Laboratory of Physiological Chemistry at this University. NaH_2PO_4 and PIPES were purchased from Merck, Germany, HEPES from Calbiochem Co., USA, and TRIS from Aristar BHD Chemicals Ltd., England.

Vesicle preparation Small vesicles were prepared by brief probe sonication and large vesicles were prepared by extrusion through 200 nm polycarbonate membranes, as described in Section 2.8 and Section 4.6, respectively. Oligomerisation of DHPBNS in vesicles was performed as described in Section 2.8.

Virus The Z strain of Sendai virus was kindly provided by Karin Klappe at the Laboratory of Physiological Chemistry at this university. It was grown, isolated and stored as described.[5] R18 labeling was performed according to the literature.[5] The concentration of Sendai virus was determined by protein measurement against an albumine standard, and is reported as such in the text (unless indicated otherwise). For the calorimetric experiments in different buffers, the virus was twice pelleted by centrifugation and resuspended in the appropriate buffer.

***n*-Octadecyl rhodamine assay of lipid mixing** The R18 lipid mixing assay was performed as described in the literature.[5] Fusion assays were performed with R18 labeled Sendai virus at 5 μg protein/mL and 5-50 μM of DHPBNS in 5 mM HEPES/NaAc buffer (140 mM NaCl, pH 7.4).

Electron microscopy Experiments were performed as described in Section 2.8.

Isothermal titration microcalorimetry Titration microcalorimetry was performed by injecting 10 μL aliquots of Sendai virus suspension into the sample cell containing a solution of DHPBNS vesicles (1.37 mL). 10-12 injections were done at 5 minute intervals. The sample cell was stirred at 350 rpm. Integration of the heat flow *vs.* time yields the enthalpy for each injection. The concentration of Sendai virus in the syringe was 2.0 mg protein/mL and the concentration of

DHPBNS in the sample cell was 0.5 mM . The instrument was an Omega Isothermal Titration Microcalorimeter (Microcal Inc., Northampton, MA, USA), operated at 37 °C. Both the Sendai virus and the DHPBNS vesicles were suspended/prepared in four different buffers (phosphate, PIPES, HEPES and TRIS) with [buffer] = 10.0 mM, 140 mM NaCl and pH 7.40. The values of the buffer ionisation enthalpies were taken from the best available literature data. Unfortunately, not all ionisation enthalpies have been measured at 37 °C, but for those that have been measured as a function of temperature (PIPES, HEPES and several others)[22] the heat capacity is rather small, and the value at 25 °C can safely be used for the extrapolation. We used 5.10 kJ $(mol)^{-1}$ for phosphate,[13] 12.4 kJ $(mol)^{-1}$ for PIPES,[22] 22.5 kJ $(mol)^{-1}$ for HEPES[22] and 48.1 kJ $(mol)^{-1}$ for TRIS.[13]

Acknowledgments

Karin Klappe and Prof. Dick Hoekstra at the Laboratory of Physiological Chemistry at this University are gratefully acknowledged for generous supply of Sendai virus, help in the R18 labeling of Sendai, and critical discussion of the results. Jaap Klijn performed the titration microcalorimetric experiments.

7.6 References

(1) Shimizu, K.; Shimizu, Y.K.; Kohama, T.; Ishida, N. Isolation and characterization of two distinct types of HVJ (Sendai virus) Spikes. *Virology* 1974, 62, 90-101.

(2) Gething, M.J.; White, J.M.; Waterfield, M.D. Purification of the fusion protein of Sendai virus: analysis of the NH_2 terminal sequence generated during precursor activation. *Proc. Natl. Acad. Sci. USA* 1978, 75, 2737-2740.

(3) Haywood, A.M.; Boyer, B.P. Sendai virus membrane fusion: time course and effect of temperature, pH, calcium, and receptor concentration. *Biochemistry* 1982, 21, 6041-6046.

(4) Citovsky, V.; Blumenthal, R.; Loyter, A. Fusion of Sendai virions with phosphatidylcholine-cholesterol liposomes reflects the viral activity for fusion with biological membranes. *FEBS Letters* 1985, 193, 135-140.

(5) Klappe, K.; Wilschut, J.; Nir, S.; Hoekstra, D. Parameters affecting fusion between Sendai virus and liposomes. Role of viral proteins, liposome composition, and pH. *Biochemistry* 1986, 25, 8252-8260.

(6) Hsu, M.; Scheid, A.; Choppin, P.W. Activation of the Sendai virus fusion protein (F) involves a conformational change with exposure of a new hydrophobic region. *J. Biol. Chem.* 1981, 256, 3557-3563.

(7) Novick, S.L.; Hoekstra, D. Membrane penetration of Sendai virus glycoproteins during the early stages of fusion with liposomes as determined by hydrophobic photoaffinity labeling. *Proc. Natl. Acad. Sci. USA* 1988, 85, 7433-7437.

(8) Haywood, A.M.; Boyer, B.P. Effect of lipid composition upon fusion of liposomes with Sendai virus membranes. *Biochemistry* 1984, 23, 4161-4166.

(9) Chejanowsky, N.; Zakai, N.; Amselem, S.; Barenholz, Y.; Loyter, A. Membrane vesicles containing the Sendai virus binding glycoprotein, but not the viral fusion protein, fuse with phosphatidylserine liposomes at low pH. *Biochemistry* 1986, 25, 4810-4817.

(10) Beschiaschvili, G.; Seelig, J. Peptide binding to lipid bilayers. Nonclassical hydrophobic effect and membrane-induced pK shifts. *Biochemistry* 1992, 31, 10044-10053.

(11) Seelig, J.; Nebel, S.; Ganz, P.; Bruns, C. Electrostatic and nonpolar peptide-membrane interactions. Lipid binding and functional properties of somatostatin analogues of charge z = +1 to z = +3. *Biochemistry* 1993, 32, 9714-9721.

(12) Thomas, P.G.; Seelig, J. Binding of the calcium antagonist flunarizine to phosphatidylcholine bilayers: charge effects and thermodynamics. *Biochem. J.* 1993, 291, 397-402.

(13) Seelig, J. Titration microcalorimetry of lipid peptide interactions. *Biochim. Biophys. Acta* 1997, 1331, 103-116.

(14) Wenk, M.R.; Seelig, J. Magainin 2 amide interaction with lipid membranes: calorimetric detection of peptide binding and pore formation. *Biochemistry* 1998, 37, 3909-3916.

(15) Russel, C.J.; Thorgeirsson, T.E.; Shin, Y. Temperature dependence of polypeptide partitioning between water and phospholipid bilayers. *Biochemistry* 1996, 35, 9526-9532.

(16) Nebel, S.; Bartoldus, I.; Stegmann, T. Calorimetric detection of influenza virus induced membrane fusion. *Biochemistry* 1995, 34, 5705-5711.

(17) Baker, B.M.; Murphy, K.P. Evaluation of linked protonation effects in protein binding reactions using isothermal titration calorimetry. *Biophys. J.* 1996, 71, 2049-2055.

(18) Hoekstra, D.; de Boer, T.; Klappe, K.; Wilschut, J. Fluorescence method for measuring the kinetics of fusion between biological membranes. *Biochemistry* 1984, 23, 5675-5681.

(19) Ohki, S.; Flanagan, T.D.; Hoekstra, D. Probe transfer with and without membrane fusion in a fluorescence fusion assay. *Biochemistry* 1998, 37, 7496-7503.

(20) Loyter, A.; Volsky, D.J. Reconstituted Sendai virus envelopes as carriers for the introduction of biological material into animal cells. *Cell Surf. Rev.* 1982, 8, 215-266.

(21) White, J.; Kielian, M.; Helenius, A. Membrane fusion proteins of enveloped animal viruses. *Q. Rev. Biophys.* 1983, 16, 151-195.

(22) Roig, T.; Bäckman, P.; Olofsson, G. Ionization enthalpies of some common zwitterionic hydrogen-ion buffers (HEPES, PIPES, HEPPS and BES) for biological research. *Acta Chem. Scand.* 1993, 47, 899-901.

Chapter 8

Epilogue

This chapter presents a brief evaluation of the results of the experimental work described in this thesis, and summarises the main achievements with respect to a better understanding of the process of bilayer membrane fusion. Furthermore, experiments are suggested in which the beta-nitrostyrene lipids are used as a tool, rather than a model system to study membrane fusion.

8.1 Aims and achievements

This chapter evaluates the results of the experimental work described in this thesis and estimates its contribution to a better understanding of bilayer membrane fusion. Current ideas about the mechanism of bilayer membrane fusion have been briefly reviewed in Chapter 1, and serve as a basis for the interpretation of the data. Employing a novel membrane mimetic system of oligomerisable lipid molecules, three important issues were addressed: (1) Does the current model of membrane fusion apply to a calcium-induced fusion process? (2) Is it possible to characterise membrane fusion intermediate structures? (3) Which are the thermodynamic driving forces of fusion?

The use of a sophisticated membrane mimetic system has validated itself in the course of the work described in this thesis. The strength of this approach rests in the structural (chemical) modifications of lipid components of the membrane, which can be used to steer the properties of the entire bilayer membrane in a predictable manner. Admittedly, the novel lipid molecules that contain a *beta*-nitrostyrene moiety covalently linked to their phosphate head group are synthetic molecules. This fact alone may render the results unhelpful in understanding natural phenomena in the critical eye of the biochemist or cell biologist. But these lipid molecules definitely are a versatile tool for obtaining kinetic, structural and thermodynamic data on the properties of bilayer membranes, and on bilayer membrane fusion in particular. All biological lipid bilayer membranes are transversely asymmetric, which is immediately obvious from their asymmetric composition, and can be understood from the fact that each side of the membrane faces a different environment. This thesis describes the first synthetic lipid bilayer with a comparable degree of functional asymmetry. The model system provides membrane vesicles with outer membrane leaflets of lipid monomers, and inner membrane leaflets of oligomerised lipids. We contend that particularly this strict asymmetry will inspire future studies. The lateral diffusion of lipid oligomers is much slower than the lateral diffusion of lipid monomers, and lipid oligomers most likely have an increased negative curvature compared to lipid monomers, because of the closer packing of the head groups. In addition, membranes of oligomerised lipids are less permeable than membranes of lipid monomers.

Chapters 3 and 4 show that the inhibiting effect of lipid oligomerisation on calcium-induced membrane fusion can be readily interpreted in terms of the stalk-pore model. Membrane

leaflets composed of oligomerised lipids resist formation of local defects that would trigger calcium-induced fusion in membranes of monomer lipids. In cases where the inner leaflet is oligomerised, it is anticipated that fusion is retarded because pore formation is strongly inhibited. Many observations indicate that lipid oligomerisation poses a kinetic barrier to membrane fusion, rather than making it structurally impossible. If less oligomerised lipid is involved, if more fusogenic agent is applied, or if the temperature is raised, the inhibiting effect diminishes. One would expect that a completely polymerised lipid bilayer leaflet is not able to fuse under any circumstances.

Unfortunately, the electron microscopic investigations described in Chapter 5 did not provide the unambiguous structural information that was hoped for. According to the stalk-pore model, asymmetric bilayer membranes with an oligomerised inner bilayer leaflet should form lipid stalks and engage in hemifusion, but would not, or only very slowly, form pores in the hemifusion bilayer diaphragm (leading to complete fusion). Despite many attempts, we could not prove that calcium-induced hemifusion of these membranes occurs. One the one hand, experimental difficulties make the quest for bilayer fusion intermediates a demanding task. On the other hand, we cannot conclude that these fragile structures do not exist simply because they were never observed. Suggestions for further investigations are presented in Section 8.2.

This thesis has lead to significant progress in understanding the thermodynamic charateristics of membrane fusion. Titration microcalorimetry had not been applied succesfully to this problem before, and the experimental results descibed in Chapters 6 and 7 shed new light on the driving force for membrane fusion. Exploiting the oligomerisable lipids, and, in addition, coating the vesicles with a hydrophobically-modified poly(acrylamide), it was possible to dissect calcium-induced vesicle fusion into successive steps of binding of calcium ion, aggregation of vesicles, and bilayer fusion. Isothermal titration calorimetry was used to determine the enthalpies associated with each of these processes, and it was possible to suggest a likely interpretation of the thermodynamic data. By far most of the heat effect accompanying calcium-induce vesicle fusion is caused by binding of Ca^{2+} to lipid head groups, and aggregation of vesicles. Fusion of bilayer membranes *per se* is endothermic and driven by a gain in entropy. Dehydration of the lipid head groups dominates the enthalpy of vesicle fusion. Although the model system presents a gross simplification of biological fusion events, its serves as an illustration of the powerful combination of sophisticated membrane mimics and ultrasensitive calorimetry.

The latter approach was taken one step further in Chapter 7, which describes fusion of Sendai virus and vesicles of oligomerisable lipids. Fusion between Sendai virus and vesicles is mediated by the viral membrane proteins. Fusion is strongly inhibited by lipid oligomerisation, most likely because the fusion peptide on the membrane protein of the virus cannot insert into the oligomerised lipid bilayer. Isothermal titration microcalorimetry shows that fusion of Sendai virus with these vesicles is endothermic, but most of the enthalpy cost resides is the insertion of the fusion protein into the vesicle membrane, and concomitant dehydration and protonation effects. As with calcium-induced vesicle fusion, fusion between Sendai virus and vesicles is entropy-driven. We suggest that all membrane fusion processes are entropy-driven (and not enthalpy-driven).

The temperature dependence of the enthalpy associated with calcium-induced vesicle fusion as well as Sendai virus - vesicle fusion would be informative, since a significant heat capacity is expected if indeed the fusion process is primarly governed by a release of hydration water. However, such an analysis should be performed with care since both the extent and the rate of fusion are very temperature dependent.

8.2 Prospects

In most experiments described in this thesis, membrane vesicles were used that are exclusively composed of *beta*-nitrostyrene lipids, which have negatively charged head groups. However, one can imagine a multitude of relevant experiments using a mixture of these synthetic lipids and a natural phospholipid such as phosphatidylcholine, perhaps in combination with cholesterol. The most obvious advantage of such mixed membranes would be that they are more like biological membranes, which always contain mixtures of several lipids, and only a relatively modest amount of negatively charged lipids (depending on the location and function of the membrane). Such mixed membranes generally show slower fusion kinetics than membranes exclusively composed of negatively charged lipids. Generally, the mixed membranes respond slower to addition of fusogenic agent, or require more fusogenic agent, which probably relates to the lower degree of hydration of the charged lipids relative to the neutral lipids. In addition, several negatively charged lipids undergo phase transitions upon complexation of fusogenic metal ions, and they are susceptible to aspecific (electrostatic) interactions with proteins, which complicate the analysis of their fusion behaviour. Fortunately, the *beta*-nitrostyrene lipids seem relatively well-behaved, even though they manifest surprisingly complicated behaviour in some cases, as illustrated in Sections 5.2, 5.3 and 6.3. All of these complications, as well as the perpetual comment of 'biological irrelevance', could be bypassed by admixing the *beta*-nitrostyrene lipids to other lipids (perhaps in combination with cholesterol) and using them as a true tool instead of a realistic, but rather exotic membrane mimetic system.

Some preliminary experiments investigated the properties of mixed bilayer membranes of *beta*-nitrostyrene lipids and other lipids. Figure 8.1 illustrates the selective *exo*-vesicular hydrolysis of the BNS group in vesicles of a mixture of DHPBNS and dipalmitoyl phosphatidylcholine and dipalmitoyl phosphatidylglycerol in a 2/7/1 ratio. Clearly, the BNS groups can be cleaved at the outer bilayer leaflet, while the BNS groups at the inner bilayer leaflet remain intact.

Consequently, it should be possible to oligomerise the BNS groups, either in both membrane leaflets, or (after selective *exo*-vesicular hydrolysis) exclusively in the inner bilayer leaflet. It would be worthwhile to investigate whether the rate and degree of oligomerisation are affected by the composition of the membrane. Another issue that requires attention is the possibility of phase separation upon oligomerisation of the BNS lipids, as has been observed in mixed vesicles of polymerisable and nonpolymerisable lipids (see the references in Section 3.1). An indication of such a phase separation was found in the titration microcalorimetric experiments of a 3/1 mixture of DDPBNS and cholesterol, for which a very different enthalpy of binding of Ca^{2+} was measured before and after oligomerisation of the head groups of DDPBNS (see Sections 6.3 and 6.4). A straightforward method to predict the phase behaviour of mixed

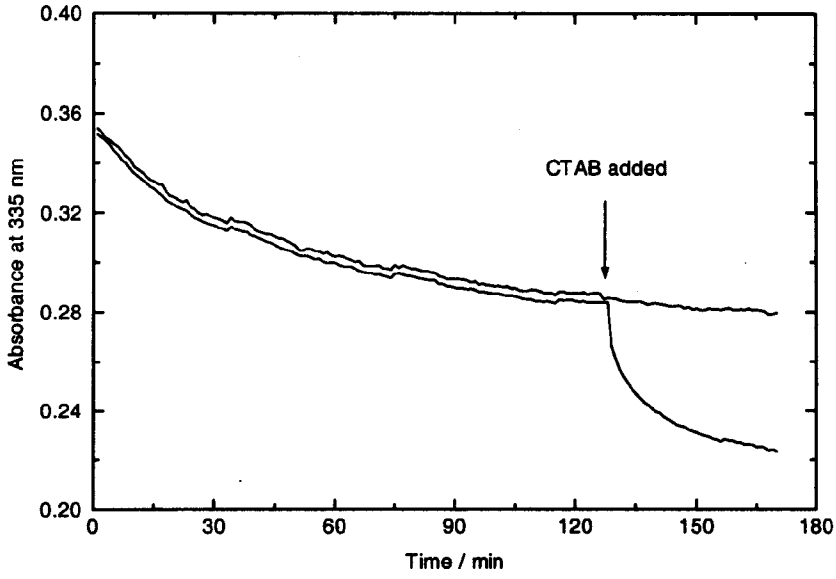

Figure 8.1 Selective hydrolysis of BNS at the *exo*-vesicular leaflet of mixed vesicles of 2/7/1 DHPBNS/DPPC/DPPG. The total lipid concentration was 0.20 mM, the temperature was 25 °C, and the external pH was 11.5.

bilayer leaflets upon lipid oligomerisation could be fluorescence microscopy of a monolayer on the air-water interface, as described in Section 3.3. Finally, it should be established which is the minimal amount of oligomerisable lipid required to obtain a significant inhibition of membrane fusion.

If these experiments are successful, the electron microscopic and microcalorimetric studies of the fusion process could be continued along the lines set out in this thesis. Mixtures of the BNS lipids and other lipids would be expected to yield spherical vesicles which are well suited for cryo-electron microscopic investigation of calcium-induced vesicle fusion, or fusion with viruses. In view of the increased hydration repulsion of the mixed membranes, a detrimental collapse into dense calcium-lipid aggregates (as observed for DDPBNS vesicles) is not expected. Using titration microcalorimetry, it should be possible to determine the influence of membrane composition on calcium-induced vesicle fusion, as well as fusion between Sendai virus and vesicles. Since it was observed that (de)hydration effects play a primordial role in the thermodynamics of membrane fusion, significant effects of a changing membrane composition are anticipated. Perhaps a correlation can be established between the enthalpy of (de)hydration of lipid head groups and the propensity to fusion of the lipid membrane.

Summary

Fusion of lipid bilayer membranes is a ubiquitous event in all eukaryotic cells. Membrane fusion provides an essential cross-membrane transport pathway for a myriad of substances. It is involved in uptake and secretion by cells (endocytosis and exocytosis), in intracellular transport, in cell-cell fusion (*e.g.* fertilisation) and in infection of cells by enveloped viruses. *In vivo* membrane fusion is controled by an intricate protein machinery, of which we only have a rudimentary understanding sofar. The complexities of biological membrane fusion have been successfully mimicked in model membrane systems of increasing sophistication, and the techniques to investigate membrane fusion have advanced along. Although biological membrane fusion is a protein-mediated process, the molecular mechanism of membrane fusion appears to be a delicate lipid rearrangement, best described by the 'stalk-pore' model (see Figure 1.6 in Section 1.4). According to this hypothesis, adjacent bilayer membranes first establish contact through a narrow stalk of lipid molecules. Consequently, the contact bilayer leaflets can merge, but the distal bilayer leaflet remain intact and separate the two fusing membrane compartments by a mutual bilayer diaphragm (hemifusion). A small pore opens in the hemifusion diaphragm, and as it widens, the lipids of the distal bilayer leaflets merge, and the contents of the compartments mix. Complete fusion is achieved once the pore has widened irreversibly, and the bilayer relaxes.

This thesis aimed to support the current model of membrane fusion by (1) providing an avenue towards ultrastructural characterisation of hypothetical membrane fusion intermediates, such as the stalk (2) extending the model to calcium-induced membrane fusion and (3) analysing the thermodynamic characteristics of membrane fusion. A membrane model system of novel synthetic lipid molecules was used as a tool to obtain kinetic, structural and thermodynamic data on fusion of bilayer membranes.

Chapter 2 describes the synthesis and characterisation of four phospholipid derivatives containing a *beta*-nitrostyrene unit linked to the phosphate head group (Figure 1). Vesicles of these lipids were characterised by transmission electron microscopy, quasi-elastic light scattering and differential scanning calorimetry. The *beta*-nitrostyrene units can be polymerised by UV irradiation when the lipids are arranged in a bilayer, yielding vesicles with bilayer leaflets in which the lipid head groups have been linked into linear oligomers of at least 4 lipid molecules. Furthermore, under alkaline conditions and at temperatures below the main phase transition temperature of the lipid bilayer, the *beta*-nitrostyrene unit can be cleaved specifically at the outer surface of the vesicles ('*exo*-vesicularly'). The cleavage process was analysed in terms of a kinetic model providing independent rates of hydrolysis of the *beta*-nitrostyrene groups at the *exo*-vesicular leaflet of the vesicle and lipid *flip-flop* between the inner and outer bilayer leaflets. *Exo*-vesicular cleavage of the *beta*-nitrostyrene groups followed by polymerisation of the remaining '*endo*-vesicular' *beta*-nitrostyrene units results in surface-differentiated vesicles containing lipid oligomers in the inner bilayer leaflet and lipid monomers in the outer bilayer leaflet. This is an extreme case of asymmetry of the two membrane leaflets, which has not been reported before.

The effect of lipid oligomerisation on the bilayer properties of small unilamellar vesicles of lipids that contain a *beta*-nitrostyrene unit has been examined in Chapter 3. Differential scanning microcalorimetry, ^{31}P-NMR spectroscopy, compression experiments of a monolayer on

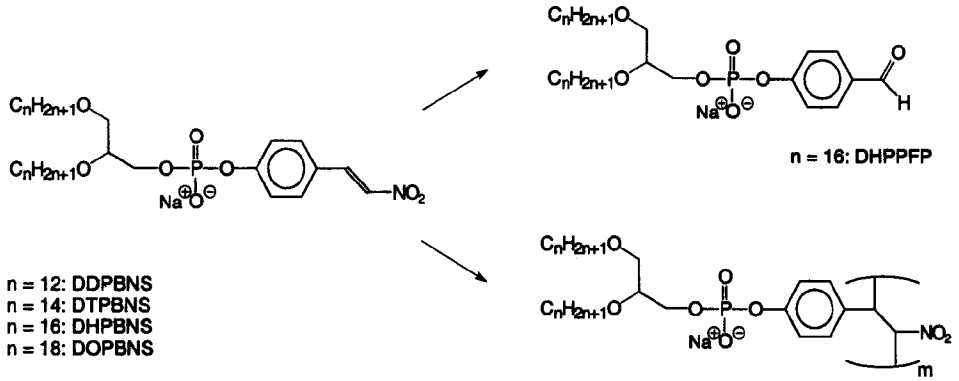

Figure 1 Molecular structures of the synthetic lipids described in this thesis, and the products that result from alkaline hydrolysis and photopolymerisation.

the air-water interface, contents leakage assays and vesicle solubilisation studies provided insight into the phase behaviour, the molecular mobility and the permeability of the lipid bilayer prior to and after oligomerisation of the lipid head groups. Oligomerisation leads to a denser lipid head group packing without affecting the flexibilty of the hydrocarbon chains of the lipid molecules. As a result, the rate of lateral diffusion of the lipid molecules and the permeability of the membrane are strongly reduced.

Membrane fusion induced by divalent calcium ions has been examined in a model system of small unilamellar vesicles, as described in Chapter 4. Although calcium-induced aggregation of the vesicles is not affected, a combination of lipid mixing assays, electron microscopy and light scattering measurements indicate that calcium-induced fusion of the bilayer vesicles is strongly retarded and inhibited by the oligomerisation. Remarkably, oligomerisation of only the inner leaflet of the bilayer is already sufficient to affect fusion. The efficiency of inhibition and retardation of fusion critically depends on the relative amount of oligomerised lipid present, on the concentration of calcium ions, and on temperature. Knowing that lipid oligomerisation leads to closer packing of the lipid head groups and to a reduction of the lateral diffusion rate, the inhibition of fusion can interpreted in terms of the stalk-pore model. Fusion is much less efficient if one or two of the fusing bilayer leaflets are oligomerised due to a reduced mobility of the lipid molecules and an unfavourable curvature tendency of the lipid oligomers.

In Chapter 5, calcium-induced fusion of vesicles of the lipids DHPBNS and DDPBNS was investigated by cryo-electron microscopy. According to the stalk-pore model, vesicles with an oligomerised inner bilayer leaflet would be expected to show hemifusion, but not complete fusion. Surprisingly, DHPBNS vesicles are not spherical but flattened, ellipsoid structures. Although some indications were obtained for calcium-induced hemifusion of DHPBNS vesicles with an oligomerised inner bilayer leaflet, it is extremely difficult to provide unambiguous microscopic proof due to the irregular morphology of the fusing vesicles. On the other hand, DDPBNS vesicles do show the expected spherical morphology. Upon addition of excess calcium ions, DDPBNS vesicles fuse into dense aggregates that show a regular spacing corresponding to the bilayer width. Upon addition of EDTA, the aggregates readily disperse into large unilamellar vesicles. At low concentration of calcium, DDPBNS vesicles with an oligomerised

inner bilayer leaflet from small multilamellar aggregates, in which a spacing corresponding to the bilayer width appears. Addition of excess EDTA results in slow redispersal of the calcium-DDPBNS aggregates into a heterogeneous mixture of mostly bilamellar, spherical vesicles and networks of thread-like vesicles. It is not easy to rationalise these phenomena, and future studies will be required to elucidate the structural characteristics of calcium-induced fusion of vesicles with an oligomerised inner bilayer leaflet.

Chapter 6 presents a microcalorimetric study of the thermodynamic characteristics of calcium-induced fusion of small vesicles of DDPBNS. Oligomerisation of the lipid head groups inhibits calcium-induced fusion of small unilamellar vesicles of DDPBNS, but does not influence vesicle aggregation. Addition of a copolymer of lauryl methacrylate and acrylamide (LMPAM) provides the vesicles with a 'steric shield' that prevents both fusion and aggregation. Accurate microcalorimetric determination of the enthalpies of vesicle aggregation and fusion was possible by comparison of titrations of vesicles to $CaCl_2$ in the absence and presence of LMPAM, both prior to and after oligomerisation of the lipids in the vesicles. Whereas binding of Ca^{2+} to the phosphate head groups is associated with an enthalpy of + 7.0 ± 0.1 kJ (mol lipid)$^{-1}$ and calcium-induced aggregation is associated with an enthalpy of + 2.6 ± 0.1 kJ (mol lipid)$^{-1}$, fusion occurs with a endothermic heat effect of only + 0.15 ± 0.1 kJ (mol lipid)$^{-1}$. Calcium binding and vesicle aggregation are endothermic processes which are driven by an entropically favourable release of hydration water from the lipid head groups as well as Ca^{2+}. The driving force of membrane fusion must also be of entropic origin, and most likely resides in a increase in degrees of freedom of the lipid molecules in going from a cluster of aggregated small vesicles to a continuous membrane, as well as an additional release of hydration water that occurs when highly curved membranes fuse into larger, less curved fusion products.

As evidenced by lipid mixing assays and electron microscopy (Chapter 7), Sendai virus fuses efficiently with small and large vesicles of the lipid DHPBNS. Fusion is strongly retarded and inhibited by oligomerisation of DHPBNS in the bilayer vesicles. The enthalpy of the fusion process was measured by comparison of microcalorimetric titrations of the virus to vesicles of DHPBNS (which fuse with Sendai virus) and vesicles of oligomerised DHPBNS (which do not fuse with Sendai virus). The observed heat effect of fusion is strongly dependent on the buffer medium that was used, reflecting a charge neutralisation of (part) of the Sendai fusion protein upon insertion into the negatively charged target membrane. No buffer effect was observed with oligomerised vesicles, indicating that inhibition of fusion is a result of inhibition of insertion of the fusion protein into the target membrane. Fusion of Sendai virus with vesicles is endothermic by + 1.5 ± 1.3 kJ (mol viral lipid)$^{-1}$. The enthalpy cost largely resides in the mixing of the proteins in the viral envelope with the negatively charged vesicle membrane, rather than in the lipid rearrangement of fusion itself. Fusion is most likely driven by a gain of entropy as a result of a release of hydration water from the viral proteins, and a gain in degrees of freedom of both the lipid molecules and the proteins upon merging of the viral and vesicle membranes.

Finally, Chapter 8 presents an evaluation of the results of the experimental work described in the preceding chapters, and summarises the main achievements with respect to a better understanding of the process of bilayer membrane fusion. Furthermore, several experiments are suggested in which the *beta*-nitrostyrene lipids are used as a tool, rather than a model system to study membrane fusion.

Samenvatting

Alle levende cellen worden omsloten door een membraan van lipidemoleculen. Deze membranen vormen ook talrijke compartimenten binnenin de cellen, die de organellen ('celorganen') afscheiden van de waterige inhoud van de cel. Membranen vormen een barrière, die de cel en zijn onderdelen beschermt tegen het weglekken van kostbaarheden zoals voedingsstoffen, energiedragers en erfelijk materiaal, en tegen het binnendringen van giftige stoffen, vreemd erfelijk materiaal, en dergelijke. Het membraan is opgebouwd uit een bont mengsel van lipidemoleculen, die gekenmerkt worden door hun ambivalente karakter: vrijwel allemaal zijn het langwerpige, cilindervormige moleculen met een 'kop' die graag in water oplost, en twee 'staarten' die juist niet in water, maar liever in olie oplossen. In water, het natuurlijke milieu van iedere cel, vormen de lipidemoleculen uitgestrekte dubbele lagen waarin de moleculen kop-staart-staart-kop, als in een soort sandwich, geordend zijn. Op deze manier bevinden de koppen van de lipidemoleculen zich zoveel mogelijk in contact met water, terwijl de olie-achtige staarten opeengepakt zijn en door de koppen vrijwel volledig van het water worden afgeschermd (Figuur 1). Zo bezien is het membraan dus eigenlijk een flinterdunne film van olie, en precies hierop berust de beschermende werking: wateroplosbare verbindingen die zich aan een van beide zijden van het membraan bevinden, kunnen niet door het membraan dringen, omdat ze volstrekt niet in olie oplosbaar zijn.

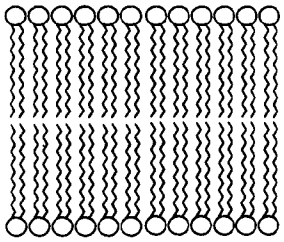

Figuur 1 Kop-staart-staart-kop rangschikking van de lipidemoleculen in een membraan

Anderzijds zou geen enkele cel een lang leven beschoren zijn als hij geen stoffen uit kon wisselen met zijn omgeving, en tussen de verschillende organellen onderling. Voedingsstoffen moeten efficiënt worden opgenomen, en afvalstoffen moeten verwijderd worden. Bouwstenen die in het ene organel geproduceerd worden, worden in een ander organel gebruikt. In ieder levende cel is dus een druk verkeer van stoffen door het membraan noodzakelijk. Hiervoor zijn twee belangrijke routes beschikbaar. In de eerste plaats bevatten alle membranen naast lipidemoleculen ook allerlei eiwitmoleculen, die transport van stoffen door het membraan verzorgen. Deze grote, complexe moleculen vormen vaak letterlijk een minuscule tunnel in het membraan, die naar behoefte open of gesloten kan worden. Deze tunnels zijn bovendien zo gevormd dat in de meeste gevallen slechts één bepaalde stof de tunnel kan passeren, en dan ook nog maar in één bepaalde richting. Honderden verschillende eiwitmoleculen zorgen er zo voor dat een cel exact die stoffen binnen kan laten die hij nodig heeft, en precies die stoffen kan lozen die hij graag kwijt wil. Op precies dezelfde manier verzorgen dergelijke eiwitmoleculen het transport over de organel membranen van een veelvoud stoffen binnenin de cel. Er is echter niet een specifiek eiwit molecuul voor iedere denkbare stof, en in sommige gevallen gaat het vervoer van stoffen op deze manier te traag. Veel stoffen zijn domweg te groot om ooit in dergelijke tunnels te passen. Daarom is er nog een andere wijze van transport van materialen door het membraan: membraanfusie. Kortgezegd betekent dit bijvoorbeeld dat twee membranen, die ieder een compartiment omsluiten, samensmelten, zodat de inhoud van de beide

compartimenten bijeen komt. In een andere variatie van hetzelfde proces wordt een klein stukje membraan afgesnoerd van een groter membraan, waarna het membraan met zichzelf fuseert, en een klein compartimentje afstoot (inclusief de inhoud). In weer een andere variatie kan zo'n compartiment fuseren met het membraan dat de cel omsluit, waarbij de inhoud van het compartiment geloosd wordt buiten de cel. Alle denkbare variaties van ditzelfde proces zijn geïllustreerd in Figuur 2. Ze komen allemaal voor in het dagelijkse leven van de cel, en ook op bijzondere momenten. Fusie van een eicel en een zaadcel ('bevruchting') kunnen we gerust een hoogtepunt in het celleven noemen, terwijl fusie van een virus met een cel ('virus infectie') vaak een voortijdig einde van het celleven inluidt.

Wanneer we twee nabijgelegen membranen op moleculaire schaal beschouwen, dan is het fascinerend om te constateren dat ze zo efficient kunnen fuseren, terwijl eigenlijk niemand precies weet hoe dit in zijn werk gaat. Er is wel een hypothese over de manier waarop de lipidemoleculen in de dubbellaag zich moeten herschikken om membraanfusie mogelijk te maken. Centraal daarbij staat de vereiste dat de koppen van de lipidemoleculen zoveel mogelijk in contact met water moeten blijven, terwijl ieder contact van de staarten met water juist vermeden dient te worden. De hypothese heet in het engels 'stalk-pore model', een term die zich helaas niet beter laat vertalen dan met 'steel-porie model'. Volgens dit model (zie Figuur 3) gedragen de beide helften van het membraan zich feitelijk onafhankelijk van elkaar tijdens het fusieproces. De buitenste twee helften van twee membranen die met elkaar in contact komen vormen een klein steeltje van lipidemoleculen, dat zich vervolgens in het vlak van het membraan uitbreidt. Zo ontstaat een 'hemifusiediafragma', een stuk membraan dat bestaat uit alleen de binnenste helften van de twee fuserende membranen. In dit diafragma ontstaat een kleine porie,

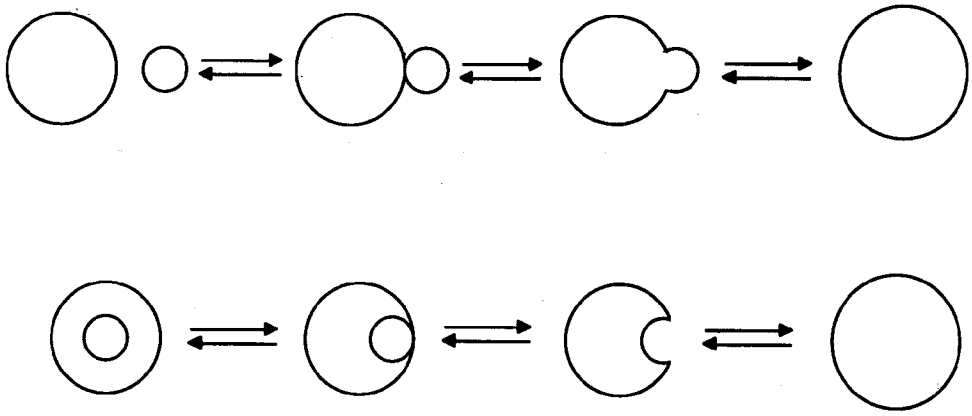

Figuur 2 Alle denkbare varianten van fusie tussen membranen van lipidemoleculen. De processen van links naar rechts leiden tot samensmelting van twee membranen, waarbij boven ook de inhoud van de beide compartimenten vermengt raakt, terwijl beneden juist de inhoud van het kleine compartiment uitgescheiden wordt. De processen van rechts naar links leiden tot afsplitsing van een klein membraancompartiment van een groter membraan, waarbij in de bovenste situatie twee afzonderlijk membraanomsloten compartimenten onstaan, terwijl beneden materiaal van buiten het oorspronkelijke compartiment ingekapseld wordt.

die snel groter wordt, en uiteindelijk net zo groot is als het oorsponkelijke diafragma. Nu is de fusie in feite voltooid, en kunnen de membranen zich ontspannen naar een minder gebogen vorm.

Deze hypothese klinkt aannemelijk en er zijn ook veel indirecte aanwijzingen dat membraanfusie op deze manier plaats vindt. Maar er is geen experimenteel bewijs dat fusie op deze manier plaats vindt, alhoewel het bijvoorbeeld mogelijk is om met behulp van electronenmicroscopie de beide helften van het membraan te onderscheiden. Niemand heeft onomstotelijk kunnen aantonen dat steeltjes tussen en porieën in fuserende membranen echt bestaan. Bovendien is de hypothese gebaseerd op berekeningen aan membranen van lipidemoleculen waarvan de koppen geen electrische lading hebben. Dit betekent dat electrostatische interacties tussen de lipidemoleculen onderling, en tussen lipidemoleculen en andere stoffen in of in de buurt van het membraan (zowel afstotende krachten tussen gelijke ladingen (+ + of - -), als aantrekkende krachten tussen ongelijke ladingen (+ -)) niet in beschouwing genomen worden, terwijl die in alle biologische membranen een grote rol spelen. Tenslotte zijn is er nauwelijks experimentele gegevens over de thermodynamische eigenschappen van het fusieproces. Het is onbekend of membranen fuseren vanwege een gunstige balans van aantrekkende krachten tussen de lipidemoleculen en eventuele andere moleculen die bij fusie een rol spelen (*enthalpie*winst), of vanwege de grotere mate van bewegingsvrijheid die de lipidemoleculen en hun directe buren (met name: water) verkrijgen als gevolg van membraanfusie (*entropie*winst).

Er zijn dus veel vragen over de manier waarop membraanfusie precies plaats vindt, en wat de drijvende krachten hiervoor zijn. Het onderzoek dat beschreven is in dit proefschrift poogt op een aantal van deze vragen een antwoord te geven. Afgezien van het feit dat het van fundamenteel wetenschappelijk belang is om een dergelijk essentieel biologisch proces tot in detail te begrijpen, is het wel zeker dat de medische wetenschap baat zal hebben bij een goed begrip van transportprocessen in de cel, en dus ook van transport door middel van

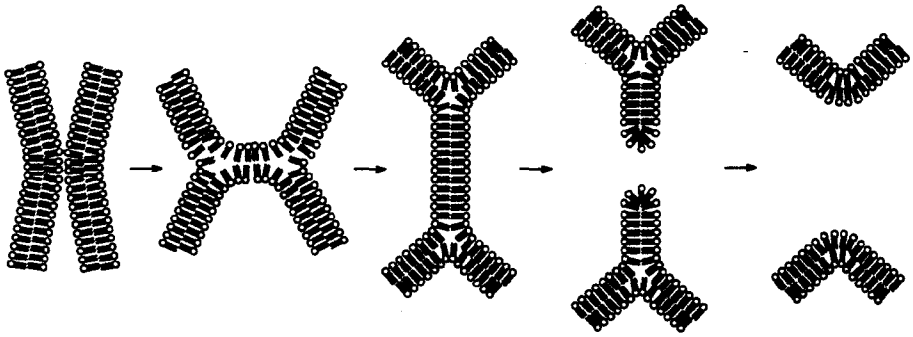

Figuur 3 Illustratie van het steel-porie model voor membraanfusie. Van links naar rechts: twee membranen die plaatselijk dicht opeen gebracht zijn, vormen een steeltje van lipidemoleculen. Het steeltje dijt uit tot een hemifusiediafragma (midden), waarin een porie ontstaat. Wanneer de porie groot genoeg is, kan het membraan ontspannen naar een minder gebogen vorm en is het fusieproces compleet.

membraanfusie. Veel huidige en toekomstige therapieën zijn immers alleen dan effectief wanneer medicijnen op de juist plaats in de juist cellen terechtkomen. Veel ziektes (griep, AIDS, hondsdolheid, enz.) worden door virussen veroorzaakt, die middels membraanfusie de cel infiltreren. En ook het functioneren van het zenuwstelsel valt of staat met een razendsnel membraanfusieproces aan het uiteinde van zenuwcellen. Overigens is het goed hier op te merken dat een zeer intrigerend aspect van biologische membraanfusie buiten het bestek van dit onderzoek valt: de 'regulering' van fusie. Met andere woorden: hoe komt het dat het ene membraan specifiek met het andere membraan fuseert, en alleen onder bepaalde voorwaarden, en op een bepaald tijdstip? Hierover zijn veel creatieve ideeen naar voren gebracht, en maar weinig harde gegevens, en hier ligt zonder meer een van de grote uitdagingen in de biologische wetenschappen van de nabije toekomst.

Het onderzoek aan membraanfusie dat beschreven wordt in dit proefschrift is niet uitgevoerd met levende cellen, maar met een sterk versimpeld modelsysteem van kleine membraanblaasjes ('vesicles' of 'liposomen') die los van elkaar in water rondzweven. Onder bepaalde omstandigheden is het mogelijk de membraanblaasjes te laten fuseren: in dit fusieproces versmelten de membranen en mengt de inhoud van de blaasjes. Uit een flink aantal kleine blaasjes kan zo één 'groot blaasje' ontstaan. Zulke modelsystemen worden al meer dan twintig jaar gebruikt voor onderzoek aan membraanfusie in cellen, en ze zijn bijzonder populair omdat (1) ze in vergelijking met levende cellen eenvoudig te bereiden, te hanteren en te bestuderen zijn, (2) in tegenstelling tot levende cellen de samenstelling van de lipidemoleculen en andere componenten (zoals eiwitmoleculen) volledig naar wens van de onderzoeker gevarieerd kan worden, en (3) herhaaldelijk gebleken is dat ze weliswaar een versimpeld, maar zeker geen onrealistisch beeld van echte celprocessen bieden.

Het unieke van de membraanblaasjes die zijn gebruikt in dit proefschrift, is dat ze zijn opgebouwd uit nieuwe lipidemoleculen, die speciaal voor dit onderzoek gesynthetiseerd zijn, en in de natuur *niet* voorkomen. De structuur van de lipidemoleculen staat afgebeeld in Figuur 4. Deze lipidemoleculen kunnen *gepolymeriseerd* worden: door middel van bestraling met ultraviolet licht ontstaat een chemische binding tussen de koppen van naburige lipidemoleculen. Door middel van een simpele chemische reactie kunnen bovendien de polymeriseerbare koppen van de lipidemoleculen in de buitenkant van het membraanblaasje desgewenst verwijderd worden, zodat alleen de lipidemoleculen aan de binnenkant door bestraling gepolymeriseerd worden. Zo onstaan blaasjes van 'asymmetrische' membranen, die aan de buitenkant en aan de binnenkant een andere structuur hebben. Bijna alle natuurlijk membranen vertonen dergelijke asymmetrie, wat logisch is, omdat de beide zijden van het membraan met een verschillend milieu in contact staan, en dus feitelijk in een andere omgeving moeten functioneren. De membranen die in dit proefschrift zijn beschreven vormen eigenlijk de eerste nabootsing van deze natuurlijke asymmetrie.

Gemiddeld worden er tengevolge van de bestraling minimaal vier lipidemoleculen 'aaneengeknoopt'. Dit lijkt misschien weinig, maar uit het onderzoek blijkt dat dit een dramatisch effect heeft op het gedrag van de membranen. Een belangrijk effect van de polymerisatie is een enorme afname van de vrijheid die de lipidemoleculen normaliter hebben om te bewegen in het vlak van het membraan (de *laterale diffusie snelheid*). Dit kan men zich misschien het gemakkelijkste voorstellen als een drukke winkelstraat op zaterdagmiddag,

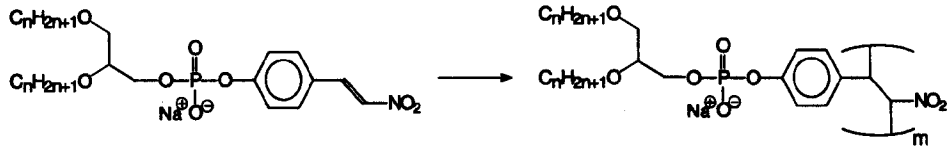

Figuur 4 Structuur van de nieuwe synthetische lipidemoleculen beschreven in dit proefschrift. De waarde van n is 12, 14, 16 of 18. De waarde van m is ongeveer 4.

waarin ieder voor zich zijn weg naar de gewenste aanbieding nog vinden kan, maar die al snel volledig geblokkeerd zou raken als iedereen op zeker moment vier-aan-vier zijn/haar toevallige buurman de hand zou geven, en vasthouden. Een tweede effect schuilt in het feit dat de koppen van de lipidemoleculen door de chemische binding iets dichter op elkaar komen te zitten, waardoor de lipidemoleculen netto de vorm van een afgeplatte kegel in plaats van een rechte cilinder krijgen. Ze passen daarom niet meer goed in een vlak membraan, en neigen naar in- en uitstulpingen van het membraan. Een derde effect is dat de koppen van de lipiden door de chemische binding duidelijk sterker aaneenhechten, waardoor vreemde moleculen veel moeilijker in het membraan door kunnen dringen dan vóór de polymerisatie.

Een belangrijk deel van het onderzoek is gewijd aan fusie van membraanblaasjes van de nieuwe lipidemoleculen onder invloed van calciumionen. De positief geladen calciumionen binden sterk aan de negatief geladen koppen van de lipidemoleculen. Zo neutraliseren ze de electrostatische afstoting tussen de membranen, en verwijderen bovendien veel watermoleculen die normaal gesproken de koppen van de lipidemoleculen omringen. Daardoor wordt het mogelijk dat de blaasjes elkaar zeer dicht naderen, zo dicht dat ze samenklonteren en uiteindelijk fuseren tot grotere blaasjes. In het proefschrift wordt beschreven hoe dit fusieproces enorm vertraagd wordt, wanneer de lipidemoleculen worden gepolymeriseerd. Met een aantal verschillende technieken is aangetoond dat de blaasjes wel samenklonteren wanneer ze in aanraking komen met calciumionen, maar dat ze niet of heel langzaam fuseren. Het maakt daarbij nauwelijks uit of de lipidemoleculen in beide helften van het membraan, of alleen die in de binnenkant van het membraan worden gepolymeriseerd. Deze waarnemingen stroken met het 'steel-porie model': het is weliswaar denkbaar dat steeltjes tussen de buitenkanten van de gepolymeriseerde lipide membranen gevormd worden, maar wanneer de binnenkant van het membraan gepolymeriseerd is, is het vrijwel onmogelijk om een porie te vormen in het hemifusiediafragma. Het lag vervolgens in de lijn der verwachting dat blaasjes met alleen een gepolymeriseerde binnenkant op grote schaal 'hemifusie' zouden vertonen omdat ze wel een steeltje tussen de buitenkanten kunnen vormen, dat uit kan dijen tot een hemifusiediafragma, maar geen porie, zodat geen volledige fusie op kan treden. Met verschillende electronenmicroscopische technieken is geprobeerd dit daadwerkelijk zichtbaar te maken, maar helaas stellen de resultaten teleur. Er werden weliswaar enige bemoedigende aanwijzingen voor hemifusie gevonden (zie Figuur 4.3 in Hoofdstuk 4), maar experimentele en technische complicaties maken het moeilijk hieruit harde conclusies te trekken. Een van de verrassende bevindingen was dat sommige membraanblaasje helemaal niet (zoals verwacht) bolvormig, maar sterk afgeplat zijn. Dit maakt het nog gecompliceerder om het fusieproces eenduidig in beeld te brengen.

Het laatste deel van het proefschrift is met name gewijd aan een thermodynamische analyse van membraanfusie. Hiertoe werd de fusie van membraanblaasjes onder invloed van calciumionen bestudeerd in een microcalorimeter. Dit apparaat is in staat uiterst geringe warmte-effecten (enthalpieverschillen) zeer nauwkeurig te meten. Deze geraffineerde techniek was nog niet eerder gebruikt om een membraanfusieproces in detail te analyseren. In het kort bestaat het experiment uit een titratie van een oplossing met membraanblaasjes aan een oplossing van calciumchloride, waarbij de microcalorimeter de warmte meet die vrijkomt of opgenomen wordt tengevolge van de interactie tussen de membraanblaasjes en de calciumionen. Dit zijn achtereenvolgens: (1) binding van calciumionen aan de koppen van de lipidemoleculen, (2) samenklontering van de membraanblaasjes, (3) fusie van de membraanblaasjes. De relatieve bijdrage van deze drie opeenvolgende processes werd bepaald door titraties te vergelijken van 'normale' membraanblaasjes (blaasjes die calciumionen binden, samenklonteren, en fuseren), van membraanblaasjes waarin de lipidemoleculen gepolymeriseerd zijn (blaasjes die calciumionen binden en samenklonteren, maar niet fuseren), en van membraanblaasjes die beschermd werden met een speciale 'jas' van polymeermoleculen, die er voor zorgt dat de membraanblaasjes nog wel calciumionen kunnen binden, maar niet kunnen samenklonteren, laat staan fuseren. Uit de vergelijking blijkt dat alle drie de stappen in het fusieproces van de membraanblaasje gepaard gaan met een opname van warmte (alle stappen zijn *endotherm*). De binding van calciumionen en de samenklontering van de blaasjes kosten echter bijna 50 keer zoveel warmte-energie (enthalpie) als de uiteindelijke fusie van de membraanblaasjes. Deze hoge 'energierekening' wordt vermoedelijk betaald door het vrijkomen van grote hoeveelheden watermoleculen, die normaal gesproken gebonden zijn aan de koppen van de lipidemoleculen, maar die vrijkomen wanneer calciumionen gebonden worden en de blaasjes samenklonteren. Ook tijdens de daadwerkelijke fusie van de membranen van de blaasjes kan nog water bevrijd worden van de koppen van de lipidemoleculen. Bovendien krijgen de lipidemoleculen netto meer bewegingsvrijheid wanneer verschillende, samengeklonterde kleine blaasjes fuseren tot een groot membraan. Zo bezien wordt membraanfusie dus gedreven door een forse *entropiewinst* (toenemende bewegingsvrijheid) van zowel de lipidemoleculen als van het omringende water. Water speelt een onverwacht belangrijke rol in de energiehuishouding van de herschikking van de lipidemoleculen tijdens membraanfusie.

Tenslotte is het onderzoek uitgebreid naar de fusie die optreedt tussen membraanblaasjes van de nieuwe synthetische lipiden en het Sendaivirus. Dit virus is een kippenvirus afkomstig uit Japan. Het wordt omsloten door een membraan dat is opgebouwd uit lipide- en eiwitmoleculen, dat met verschillende membranen kan fuseren. Het virus dringt op deze manier door in kippencellen, en buit de verschillende organellen van de cel uit om zichzelf te reproduceren. Het fusieproces wordt in gang gezet door twee eiwitmoleculen aan het oppervlak van het virus membraan. Uit dit onderzoek blijkt dat het Sendaivirus uitstekend met de membraanblaasjes van de nieuwe lipidemoleculen fuseert, maar dat dit fusieproces sterk belemmerd wordt wanneer de lipidemoleculen worden gepolymeriseerd. Dit is waarschijnlijk te wijten aan het feit dat de eiwitmoleculen van het Sendaivirus die fusie induceren niet door kunnen dringen in het oppervlak van de membraanblaasjes wanneer de lipidemoleculen gepolymeriseerd zijn. Ook dit proces werd bestudeerd in de microcalorimeter, en het bleek dat het fusieproces warmte *kost* (net als voor fusie van membraanblaasje onder invloed van

calciumionen) , wat gecompenseerd wordt door een toename van de bewegingsvrijheid van zowel lipide, als eiwit, als watermoleculen wanneer de membranen van het virus en de blaasjes fuseren. Uit de analyse bleek dat er ook een aantal andere processes zijn die tijdens fusie een fors warmte-effect veroorzaken, terwijl deze processen niet met het fuseren van de membranen op zich te maken hebben. Deze effecten zijn over het hoofd gezien in de enige eerdere studie over dit onderwerp.

In retrospectief is het duidelijk dat de nieuwe lipidemoleculen een fraai stuk gereedschap vormen om membraanfusieprocessen op een voorspelbare manier te beinvloeden, en te bestuderen. De meeste resultaten zijn goed te verklaren aan de hand van het steel-porie model voor membraanfusie, maar helaas is het nog niet mogelijk gebleken om de voorgestelde intermediaire membraanstructuren ook echt aan te tonen. Het gebruik van de microcalorimeter om membraanfusie te bestuderen levert verrassende inzichten op, en verdient navolging. Dit onderzoek zou een vruchtbaar vervolg kunnen krijgen door de nieuwe lipidemoleculen te mengen met natuurlijke lipidemoleculen, en zo het realiteitsgehalte van het modelsysteem nog te verhogen.